INVESTIGATION OF FACTORS AFFECTING RESILIENT MODULUS FOR HOT MIX ASPHALT

a thesis submitted in partial fulfilment of the requirements for the degree of

Master of Engineering in Transportation Engineering (MET)

at the University of Canterbury

By

Su Jian Ji

Supervisors:

Dr. Mofreh Saleh

Associate Professor Alan Nicholson

Department of Civil Engineering

University of Canterbury

Christchurch, New Zealand

2006

Abstract

Resilient modulus is an important property for asphalt concrete design and for mechanistic analysis of pavement response under traffic loading. This study investigates the different factors affecting the resilient modulus of hot mix asphalt. A fractional factorial design of experiment was carried out to investigate six factors each factor was studied at two levels. These factors are: the maximum nominal aggregate size, specimen diameter and thickness, the load pulse form and duration, and the compaction method. Two types of hot mix asphalts with different maximum aggregate sizes (10 mm and 14 mm) were studied. Gyratory and Marshall compaction methods were used to prepare the specimens. Sinusoidal and triangular load pulse forms were used in the measurement of the resilient modulus. This study attempts to examine how the different factors interrelate to affect the resilient modulus. In addition to this, two other investigations will be carried out. The first is the comparison of the strain backcalculated using the resilient modulus test results with the strain measured using strain gages and strain values obtained from finite element modelling (FEM), and determine whether the FEM or the closed form equation is the more accurate method for determining strain. The second is the investigation of the relationship between the flexural, complex and resilient modulus.

Analysis of the factorial experimental design showed that the maximum nominal aggregate size is the most important factor affecting the resilient modulus, followed by the load duration, the specimen geometry represented by the thickness and diameter then the interactions between the different factors.

The strain comparison suggested that the closed form equations were indeed a suitable approach to determine maximum horizontal strain during a resilient modulus test. The modulus comparison suggested that it is possible to predict either resilient, complex and flexural modulus given that only one of them is known, but only for AC10 specimens.

Acknowledgement

I would like to thank all the people whose patience, advice, encouragement and support have helped me complete this thesis.

My deepest gratitude goes to my supervisor, Dr. Mofreh Saleh, who has provided me with the knowledge and supervision in the laboratory work, and the amount of time and energy to comment on my writing while he was on holiday.

Thanks also go to Mr. Frank Greenslade who has helped me with a tremendous amount of laboratory work.

I would also like to thank Fulton Hogan for providing the funding for this research, especially Mr. John Forest, who provided all the asphalt mix.

Thank you also to the academic members of the Transportation Programme, Assoc. Prof. Alan Nicholson, Dr. Andre Dantas and Mr. Glen Koorey who provided a lot of knowledge during my year in the masters programme.

Finally, I would like to thank my family for supporting my study, and Denise for all the encouragement.

Table of Contents

1. Introduction 1

1.1 Background 1

1.2 Objectives 2

1.3 Report Structure 3

2. Literature Review 4

2.1 Definition of Resilient Modulus 4

2.2 Resilient Modulus Test 5

2.2.1 Preconditioning and test setting determination 5

2.2.2 Resilient modulus determination 6

2.3 Investigating Factors 7

2.3.1 Geometric Factors and Maximum Nominal Aggregate Size 7

2.3.1.1 Diameter of Specimen 7

2.3.1.2 Thickness of Specimen 9

2.3.1.3 Maximum Nominal Aggregate Size 10

2.3.2 Experimental Factors 11

2.3.3 Compaction Methods 12

2.3.3.1 Gyropac compactor 12

2.3.3.2 Marshall Compaction Hammer 16

2.4 Factorial Experimental Design 17

3. Research Methodology 20

3.1 Source of materials 20

3.2 Mix Preparation 22

3.2.1 Determining the Optimum Compaction Temperature 23

3.2.2 Sample preparation 27

3.2.3 Determination of Air Voids Percentage 30
3.2.4 Determination of the Bulk Specific Gravity, G_{mb} 30
3.2.5 Determination of the Maximum Specific Gravity, G_{mm} 31
3.2.6 Generating Compaction curves 34
3.3 Design of experiment 37
3.4 Laboratory Measurements of Complex, Flexural and Resilient modulus relationship .. 39
3.4.1 Complex modulus test 39
3.4.2 Flexural test 41
3.4.3 Resilient modulus test 44
4. Analysis of the Experimental Results 45
4.1 Factorial experimental design 45
4.2 Strain Comparison 61
4.3 Modulus Comparison 66
5. Conclusions and Recommendations 68
References 69
Appendix 1 1
Determination of the Compacting Temperature A1
Determination of the Maximum Specific Gravity, G_{mm} A3
Using ABAQUS A5
Appendix 2 ..... A10
Compaction Curves Results A10
Specimen properties for Factorial Experimental Design A21
Specimen properties for the Strain Comparison investigation A23
Specimen properties for the Modulus Comparison investigation A25

List of Figures

Figure 2.1 Strains under repeated load 4

Figure 2.2 Gyropac produced by Industrial Process Controls LTD 13

Figure 2.3 Gyropac with displacement transducer and height indicator 15

Figure 2.4: Marshall compaction hammers for 100 mm diameter specimen (left) and for the 150 mm diameter specimen (right) 16

Figure 3.1 Particle size distribution for the AC10 asphalt mixtures 21

Figure 3.2 Particle size distribution for the AC14 asphalt mixtures 22

Figure 3.3 Brookfield Thermosel Apparatus; from the left, the sample chamber, the Brookfield viscometer, and the temperature controller 23

Figure 3.4 Schematic of the Brookfield Thermosel Apparatus 24

Figure 3.5 The temperature-viscosity curve with the viscosity axis transformed to a logarithmic scale 26

Figure 3.6 Manual hydraulic jack for extracting Gyropac and Marshall hammer Specimens 28

Figure 3.7 A pycnometer used to measure the maximum specific gravity, G_{mm} 32

Figure 3.8 The complex modulus test setup 40

Figure 3.9 AC14 asphalt beams 41

Figure 3.10 Cut surfaces of the asphalt beams, with AC14 on the left and AC10 on the right 42

Figure 3.11 Flexural modulus testing apparatus in a temperature-controlled cabinet 42

Figure 4.1 Normal probability plot of the standardised effects 48

Figure 4.2 Pareto chart which displays the significant interactions at a 0.05 significance level 49

Figure 4.3 Effect of maximum nominal aggregate size on the resilient modulus 50

Figure 4.4 Effect of load duration on the resilient modulus 51

Figure 4.5 Effect of specimen thickness on the resilient modulus 52
Figure 4.6 Effect of specimen diameter on the resilient modulus 53
Figure 4.7 Effect of interaction between aggregate size and specimen diameter on the resilient modulus 54
Figure 4.8 Effect of interaction between aggregate size and compaction method on the resilient modulus 55
Figure 4.9 Effect of interaction between aggregate size and compaction method on the resilient modulus 56
Figure 4.10 Cube plot of the 3-way interaction of specimen diameter, thickness and aggregate size 57
Figure 4.11 Effect of interaction between specimen diameter and compaction method on the resilient modulus 58
Figure 4.12 Effect of interaction between specimen thickness and aggregate size on the resilient modulus 59
Figure 4.13: Effect of compaction method on the resilient modulus 60
Figure 4.14 Half cylindrical model representation of the cylindrical sample, with the boundary conditions highlighted in red 63
Figure 4.15 Comparison plot of the three strain derived from closed form equations, FEM and strain gages 65
Figure 4.16 Modulus comparison for AC10 aggregate gradation 67
Figure 4.17 Modulus comparison for AC14 aggregate gradation 67

Appendices

Figure A1.1 Placing the sample container into the thermo-container A1
Figure A1.2 Inserting the spindle A2
Figure A1.3 Placing the lid to avoid bitumen splashing A2

Figure A1.4 Sample are separated out so that the finer aggregate portions are not larger than 6mm A3
Figure A1.5 Using a mallet, gently tap on the pycnometer to help with the air bubbles removal A3
Figure A1.6 Inverting the pycnometer several times until no more bubbles can be observed A4
Figure A1.7 Measuring the mass of the pycnometer, lid, sample and water A4
Figure A1.8 Creating the model by first specifying the cross-section of the model..... A6
Figure A1.9 Shape of model A6
Figure A1.10 Model with partitioned curved face for loading and boundary condition A7
Figure A1.11 Boundary conditions are highlighted in red..... A7
Figure A1.12 Hexagonal meshing of the model A8
Figure A1.13 Visualisation of the deformed model..... A8
Figure A1.14 Deformed contour displaying the path highlighted in red A9
Figure A1.15 Plot showing the maximum tensile strain along the path A9
Figure A2.1 Compaction curve as plotted from Table A1.1 and Table A1.2 for Gyropac compacted specimens A12
Figure A2.2 Compaction curve as plotted from Table A1.3 and Table A1.4 for Gyropac compacted specimens A22
Figure A2.3 Compaction curve as plotted from Table A1.5 and Table A1.6 for Gyropac compacted specimens A15
Figure A2.4 Compaction curve as plotted from Table A1.7and Table A1.8 for Gyropac compacted specimens A15
Figure A2.5 Compaction curve as plotted from Table A1.7 for Gyropac compacted specimens..... A17

Figure A2.6 Compaction curve as plotted from Table A1.8 for Gyropac compacted specimens..... A17

Figure A2.7 Compaction curve as plotted from Table A1.9 for Gyropac compacted specimens..... A19

Figure A2.8 Compaction curve as plotted from Table A1.10 for Gyropac compacted specimens..... A19

List of Tables

Table 2.1 Specifications of Gyropac..... 14

Table 2.2 Example of constructing a 2^{3-1} factorial of resolution III design..... 18

Table 3.1 Viscosities for the two asphalt binder samples at different temperatures 26

Table 3.2 Maximum specific gravity calculations for aggregate gradation AC10 for each of the three batches of asphalt mix. 34

Table 3.3 Maximum specific gravity calculations for aggregate gradation AC14 for each of the three batches of asphalt mix. 34

Table 3.4 Factors for determining the compaction curves..... 35

Table 3.5 Alias structure for the one half fractional factorial design 38

Table 4.1 Factors considered in the factorial analysis 46

Table 4.2 Analysis of Variance of the significant factors..... 47

Table 4.3 Comparison of the cored and moulded samples. 61

Table 4.4 Percentage error of closed form solution and FEM compared with strain gage measurement 65

Appendices

Table A2.1 Compaction curve values for AC10 aggregate gradation Gyropac compacted samples A10

Table A2.2 Compaction curve values for AC10 aggregate gradation Marshall hammer compacted samples A10

Table A2.3 Compaction curve values for AC14 aggregate gradation Gyropac compacted samples A11

Table A2.4 Compaction curve values for AC14 aggregate gradation Gyropac compacted samples A11

Table A2.5 Compaction curve values for AC10 aggregate gradation Gyropac compacted samples A13
Table A2.6 Compaction curve values for AC10 aggregate gradation Marshall hammer compacted samples A13
Table A2.7 Compaction curve values for AC14 aggregate gradation Gyropac compacted samples A14
Table A2.8 Compaction curve values for AC14 aggregate gradation Marshall hammer compacted samples A14
Table A2.9 Compaction curve values for AC10 aggregate gradation Gyropac compacted samples A16
Table A2.10 Compaction curve values for AC14 aggregate gradation Gyropac compacted samples A16
Table A2.11 Compaction curve values for AC10 aggregate gradation Gyropac compacted A18
Table A2.12 Compaction curve values for AC14 aggregate gradation Gyropac compacted A18
Table A2.13 Specimen properties for factorial experimental design A20
Table A2.14 Specimen properties for strain comparison samples prepared in laboratory. A22
Table A2.15 Strain results using FEM A23
Table A2.16 Properties for specimens used in Modulus comparison A24
Table A2.17 Percentage air voids determination for specimens used in Modulus Comparison..... A24

List of Equations

Equation 1 Estimated Peak Load 5

Equation 2 Recovered Horizontal Strain 6

Equation 3 Resilient Modulus 6

Equation 4 Percentage Air Voids 30

Equation 5 Bulk Specific Gravity 31

Equation 6 Maximum Specific Gravity 33

Equation 7 Tensile Stress 43

Equation 8 Tensile Strain 43

Equation 9 Flexural Stiffness 43

Equation 10 Maximum Tensile Stress 61

Equation 11 Maximum Tensile Strain 61

Chapter 1

Introduction

1.1 Background

The resilient modulus is an important parameter that is used in the mechanistic pavement design as it is being used as an input to the multilayer layer elastic theories or finite elements models to compute pavement response under traffic loading. These responses can be used through transfer functions to calculate the optimum thickness design for new pavement or to estimate the remaining life of an existing pavement. This makes the resilient modulus one of the most important parameters in pavement design and analysis.

Due to the simplicity and ease of application to test laboratory compacted specimens and field cores, the indirect tensile test is the most common repeated load test to measure the resilient modulus of bituminous mixture. This involves preparing a compacted cylindrical asphalt mixture subjected to diametrical repeated loading. This test is standardised as the Australian standard AS 2891.13.1-1995. However, there are a lot of factors affecting resilient modulus of asphalt subjected to indirect tensile test. These include the geometric factors of the test specimens, maximum nominal size of aggregates, the load waveforms and pulse durations applied to the test specimens, the preset strain measurement that is to be met during the test, and the type of compaction of the test specimen. This research is to study the effects of these factors, their interactions, and their significance on the resilient modulus through a fractional factorial design of experiment.

In addition to the factorial experimental design, two other separate investigations are conducted. The first is on the comparison of the maximum tensile strain measured for several cylindrical samples made at different thicknesses during an indirect tensile test using strain gauges and the predicted strains from the closed form equation used in the indirect tensile test, and those predicted by finite elements modelling using ABAQUS. This is to determine the range of specimen thicknesses that the closed form equation can be used correctly to calculate the resilient modulus. This is because the closed form equations are widely used for resilient or stiffness modulus determination.

The second investigation is on the determination of relationships among the resilient modulus, the flexural modulus, and the complex modulus. These will all be discussed in Section 2.2 in Chapter 2.

1.2 Objectives

This research, in general, was carried out to investigate the effect of several factors on the resilient modulus of a bituminous mix subjected to resilient modulus testing by the indirect tensile method. The relationship between the resilient modulus, flexural and complex modulus was also investigated. The specific objectives of this research can be summarised as the following points:

- To determine the extent of the effect of the geometric factors (thickness and diameter of specimen, and the maximum nominal aggregate size) on the resilient modulus of a bituminous material,
- To determine the extent of the effect of the load factors (load waveform and load duration) on the resilient modulus of a bituminous material,

- To determine the extent of the effect of the preset strain level (50με) as recommended in standard test procedure on the resilient modulus,
- To determine the extent of the effect of the method of compaction on the resilient modulus. Two methods of compaction has been used in this study, namely, Gyropac and Marshall compaction hammer,
- To examine the range of specimen thicknesses within which the closed form equation for the indirect tensile is valid by comparing the calculated strains using finite element modelling, closed form equation with the measured strains from the resilient modulus test using strain gages,
- Investigating the relationships between the flexural, complex, and resilient moduli.

1.3 Report Structure

There are five chapters following this introductory part. Chapter 2 is a review of the resilient modulus test, the factors affecting the resilient modulus test, and a general principle behind the half fractional factorial design of experiment. Chapter 3 and 4 explain the source of materials used in this research, the mix preparation methodology and the research methodology for the design of experiment, strain comparison and modulus comparison. Chapter 5 present the laboratory results with discussions, and Chapter 6 include a summary, conclusions, recommendations and some ideas for further studies.

Chapter 2

Literature Review

2.1 Definition of Resilient Modulus

The resilient modulus is defined as the ratio of the deviator stress to the recoverable strain. It is known that the bituminous material is not elastic, but experiences some permanent deformation after each load application. However, if the load is small compared to the strength of the material and is repeated for a large number of times, the deformation under each load repetition is nearly completely recoverable and proportional to the load and can be considered as being elastic (Huang, 1993).

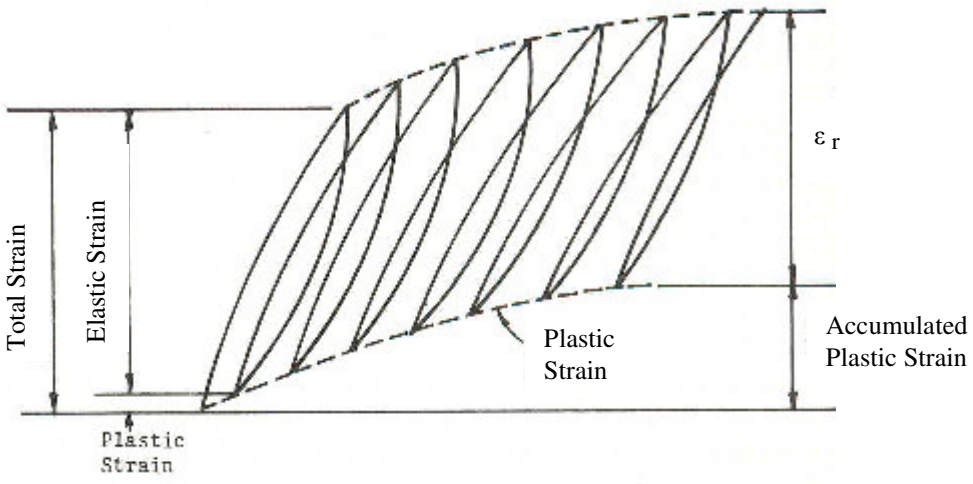

Figure 2.1 Strains under repeated load

Under a repeated load test which strains the asphaltic specimen, as shown in Figure 2.1 above, there is considerable plastic strain at the initial stage of load applications. As the number of load repetition increases, the plastic strain due to each load repetition decreases. After 100 to 200 repetitions, the strain is almost all recoverable, as indicated by ε_r in the figure. Hence, the

elastic modulus based on the recoverable strain is defined as the resilient modulus, which is the deviator or axial stress over the recoverable strain."

2.2 Resilient Modulus Test

The resilient modulus test has become popular with many laboratories due to its simplicity and applicability to test field cores, and is the most common method of determining the stiffness modulus for hot mix asphalt (Roberts, 1996). It involves preparing a compacted cylindrical asphalt mixture that is subjected to a diametrical repeated loading. There are two parts to the testing procedures; the preconditioning and test setting determination, and the resilient modulus determination.

2.2.1 Preconditioning and test setting determination

For the preconditioning and test setting determination, the range of the recovered horizontal strain must be specified, and the peak load that is required to deform the specimen within that range of recovered horizontal strain is determined by Equation 1.

$$P_e = \frac{ED\varepsilon h_c}{(\upsilon + 0.27)x10^6} \qquad \text{Equation 1}$$

Where P_e = estimated peak load (N)

E = estimated resilient modulus of the specimen (MPa)

D = average diameter of the cylindrical specimen (mm)

h_c = average height of the specimen (mm)

ε = recovered horizontal strain (με)

υ = Poisson ratio (estimated as 0.4)

A single pulse within a specified rise time is applied to the estimated peak load calculated above, and removed. The recovered horizontal deformation at the end of the pulse is then measured and the recovered horizontal strain is then calculated from the Equation 2.

$$\varepsilon = \frac{H}{D} \qquad \text{Equation 2}$$

Where ε = recovered horizontal strain

H = recovered horizontal deformation (mm)

D = average diameter of the cylindrical specimen (mm)

If the recovered horizontal strain is within the specified range apply further preconditioning pulses at the same estimated peak load until five pulses of preconditioning have been completed. If the recovered horizontal strain is not within the specified range, adjust the estimated peak load so that the recovered horizontal strain will fall within the specified ranges.

2.2.2 Resilient modulus determination

Following the preconditioning procedures above, apply five load pulses with the specified rise time to the peak load determined from before. The recovered horizontal deformation after each pulse is measured and recorded. The resilient modulus is determined by the Equation 3.

$$E = \frac{P(\upsilon + 0.27)}{Hh_c} \qquad \text{Equation 3}$$

Where E = resilient modulus (MPa)

P = peak load (N)

υ = Poisson ratio (assumed as 0.4)

H = recovered horizontal deformation of specimen (mm)

h_c = height of specimen (mm)

2.3 Investigating Factors

In this section, literature reviews of the factors are separated into geometric factors, experimental factors and compaction methods. The literature reviews of the flexural and complex modulus will also be included in this section.

2.3.1 Geometric Factors and Maximum Nominal Aggregate Size

The geometric factors to be taken into account in this research are the diameter and thickness of the cylindrical specimen. The maximum nominal aggregate size used in the bituminous mix is also investigated. These factors are discussed in the following subsections.

2.3.1.1 Diameter of Specimen

The standard for determining the resilient modulus of an asphalt mix using the indirect tensile testing method specifies that the diameter of the specimen to be either 100 mm or 150 mm. However, it is not known the extent of the effect of the specimen diameter and whether a larger diameter will increase or decrease the resilient modulus compared to a smaller diameter cylindrical specimen.

A study was conducted on the comparative evaluation of 4 inch and 6 inch diameter specimens for testing of large stone asphalt mixes (Kandhal and Brown 1990). This study

compared the mix properties such as the Marshall stability and flow, indirect tensile strength, and permanent deformation obtained on 4 inch and 6 inch diameter specimens. However, since this study is concerned only with the resilient modulus by indirect tensile test, only the indirect tensile strength will be discussed. Kandhal found that the tensile strength of the 6 inch specimens were always lower than the 4 inch specimen. This is due to the fact that although the loading rate was the same for both sets of experiments, the strain rate for the 6 inch specimens was lower than that for the 4 inch specimens. Therefore a lower loading rate should produce a lower tensile strength in the 6 inch specimens.

Another study that concerned resilient modulus was by Lim, who conducted the study to evaluate the specimen size effects on the results of diametrical mechanical testing methods, namely the resilient modulus test and the indirect tension test (Lim, Tan et al. 1995). Specimens of diameters 4, 5 and 6 inch were prepared, keeping the diameter/height ratio constant at 1.6. It was observed that within the same mix, the resilient modulus decreased as the diameter of the specimen increased, therefore Lim concluded that specimen size does affect the resilient modulus. The resilient modulus decreases as the size of the specimen increases.

These results indicated that the diameter of the specimens do affect the resilient modulus obtained by diametrical testing. Therefore, the hypothesis of this thesis on the effect of the diameter of the specimen will be the decreasing of resilient modulus with increasing diameter of the cylindrical specimen.

2.3.1.2 Thickness of Specimen

Standard AS 2891.13.1 (1995) for determining the resilient modulus of an asphalt mix using the indirect tensile testing method specifies that the thickness of the specimen to be between 70 and 35mm for the 100 mm diameter specimen, and 75 ± 15 mm for the 150 mm diameter specimen. However, considering one diameter size, it is not known whether the resilient modulus obtained from a thinner specimen will differ from a thicker specimen.

A previous study was conducted by Hugo and Schreuder to evaluate the influence of the specimen thickness on the tensile strength and related engineering properties for different asphalt mixes using static indirect tensile test (Hugo and Schreuder 1993). The effect of specimen thickness on stiffness was also evaluated, but to a lesser extent.

The motivation behind the research of Hugo and Schreuder was that the interpretation of the indirect tensile test results is subjected to a fair amount of criticism due to the assumption of the test being conducted under a state of plane stress when it really is a three-dimensional stress field, and the assumption of linear elasticity. Therefore, Hugo and Schreuder conducted the structure of the research to provide an answer to this.

Hugo and Schreuder found that in general, the indirect tensile strength increases with increased specimen thickness. A 64 mm long sample may overestimate a 20 mm long sample by 36 percent. At 40 mm the overestimation would on average be 13 percent. Therefore it was apparent that account had to be taken of the thickness of the specimen. Specimens thicker than 20 mm would experience stress concentrations at the top and bottom contact points. The stress along the remainder of the vertical diameter would be reduced far below the average calculated stress level. This could be the cause of the increase in tensile strength as the sample becomes thicker due to the fact that the unequal stress distribution caused the specimen

strength to be stress dependent. This means the middle portion of the specimen only commences once the top and bottom contact points (highly stressed points) on the outside had started to fail, resulting in an increase in required failure load.

2.3.1.3 Maximum Nominal Aggregate Size

The Australian Standard AS2891.13.1 states that test specimens containing maximum particle size of up to 40 mm can be used for the resilient modulus test. However, the interaction of the aggregate size with other factors is not known.

Lim et al (1995) also investigated the effect of specimen diameter to maximum nominal stone size ratio on the resilient modulus in the same study. It was found that the resilient modulus decreases as the diameter/maximum nominal size ratio increased. This means that if a small diameter was used to test large top stone size, which means a smaller diameter/top stone size ratio, a higher resilient modulus would be obtained.

Brown conducted a research on the determination of the relationship between asphalt mixture properties and maximum aggregate size (Brown and Basset, 1990). Aggregate gradations chosen in the study contain maximum aggregate size of 9.5 mm, 12.7 mm, 19 mm and 38 mm. The resilient modulus was measured for all mixes and evaluated for the effects of aggregate size. It was found that there is a good correlation between the resilient modulus and the maximum aggregate size, with R^2 ranging from 0.53 to 0.87. As the aggregate size increased from 12.7 mm to 38 mm, the resilient modulus increased as well. In addition, taking account of testing temperature at 5°C, 25°C and 40°C, there was a resilient modulus increased of 53%, 107% and 93% respectively.

Although many studies considered the effect of aggregate size on the resilient modulus, nothing could be found to show the effect of the interaction between the aggregate size and other factors such as specimen diameter, thickness, loading waveform, loading duration, preset strain level and compaction method which will be covered thoroughly in this research.

2.3.2 Experimental Factors

The experimental factors considered in this thesis are the load duration, load waveforms and the strain level. In a resilient modulus test, the standard values for the load duration and the strain level is 100ms and 50 microstrain respectively. Since the effects of each of these factors on the resilient modulus are unknown to a certain extent, this thesis included the investigation of these three experimental factors.

For load duration, it is expected that the higher the duration, the bigger the plastic strain, hence the smaller the resilient modulus.

For load waveforms, the standard did not specify the waveform to be used in the test. Therefore this thesis included the haversine and triangular shaped waveforms and deduces whether load waveform has any significant effect either by itself or with other factors on resilient modulus.

For the strain level, the standard states that the recovered horizontal strain has to be 50 ± 20 microstrain. This thesis investigates the effect of a low (20 microstrain) and high (60 microstrain) recovered horizontal strain on the resilient modulus.

2.3.3 Compaction Methods

This section describes the two compaction methods taken into under consideration in this research, specifically the Gyropac compactor, which uses a kneading effort to compact specimens, and Marshall compaction hammer, which uses impact weight to compact specimens.

The purpose of compaction is to decrease the air void content to ensure that friction between the aggregate particles and bond between the bitumen and the aggregates can be achieved. Previous studies (Harvey, Eriksen et al. 1994) had shown that different compaction method produce specimens with significantly different permanent deformation responses to repeated shear loading, which indicated each method of compaction gives a particular type of aggregate orientation and binder-aggregate film. The literature reviews on the Gyropac compactor and the Marshall compaction hammer are separated into two subsections described in Section 2.3.3.1 and Section 2.3.3.2 respectively.

2.3.3.1 Gyropac compactor

Gyropac is a gyratory compactor that uses a kneading process that simulates the roller action during construction. It has the ability to vary the vertical pressure, gyration angle, and the number of gyrations to simulate field compaction equipment (Roberts, 1996). A picture of Gyropac, which is produced by Industrial Process Controls LTD, is shown in Figure 2.2. The specifications of Gyropac are shown in Table 2.1 (Industrial Process Control LTD).

Figure 2.2 Gyropac produced by Industrial Process Controls LTD

Table 2.1 Specifications of Gyropac

Specification	**Description**
Gyration angle	0 - 3° with defined angles of 2° and 3° ± 0.1°
Gyratory speed	Fixed 60 cycles per minute
Specimen diameter	100 mm and 150 mm ± 0.1 mm
Compactive force	100 mm specimen 0 – 310 kPa 150 mm specimen 0 – 700 kPa
Specimen height	65 mm and 85 mm for 100 and 150 mm samples respectively
Height indicator	Between 50 and 170 mm
Gyration counter	0 – 10,000 cycles
Dimensions	470 mm wide x 460 mm deep x 760 mm height
Power and air supplies	240 volts 50 Hz @ 1.2 amps 700 kPa (minimum 600 kPa)

The Gyropac can compact asphalt samples by two modes of operation. The first mode is that it can produce samples that are compacted to a predetermined height; 65 mm for 100 mm samples and 85 mm for 150 mm samples. The density of the sample is controlled by measuring the mass of the material to be compacted. The second mode is that it can produce samples that are compacted for a preset number of gyrations. The density is now controlled by the number of gyrations given the mass of the material.

During compaction, a compressive force is applied to a specimen via the top platen to a specimen while the mould containing the asphalt mix is tilted from side to side in a gyrating movement, with the mould fixed to the mould carrier. Gyropacs that are fitted with

displacement transducer and height indicator allows the number of gyrations and the height of the sample to be monitored. This is shown in Figure 2.3.

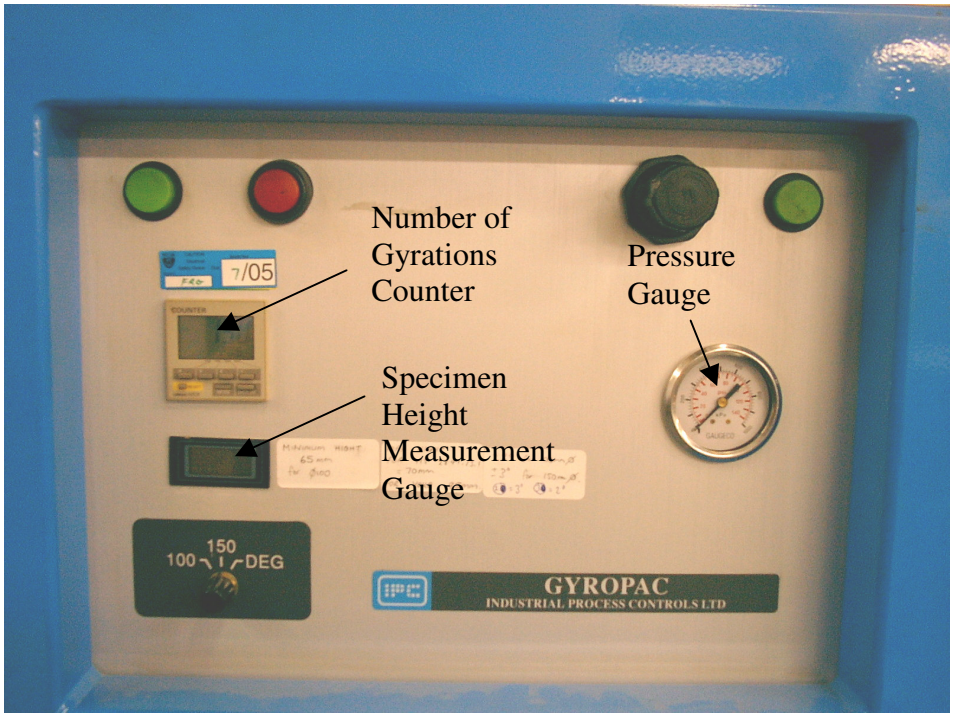

Figure 2.3 Gyropac with displacement transducer and height indicator

One problem with a kneading compactor is that it does not produce a Marshall-sized specimen that has a uniform density profile. Fwa (1993) conducted a research in evaluating of the density profile of asphalt mixtures specimens compacted by four compaction methods for laboratory testing; drop hammer compactor, kneading compactor, single plunger compression and double plunger compression (Fwa, Low et al. 1993). The density is measured using a laboratory twin-probe gamma-ray gage. Test results show that the kneading compactor does not produce uniform density profiles for 64 mm-tall samples. The density is between 2.35 and 2.4 t/m^3 for the top half of the sample and between 2.35 and 2.25 t/m^3 for the lower half of the sample. This non-uniform density profile will probably produce a resilient modulus that is

different to the same sample produced by other means of compaction. In this research, the comparison will be carried out by gyratory compaction by Marshall compaction hammer.

2.3.3.2 Marshall Compaction Hammer

The Marshall compaction hammer is still the most frequently used compaction method for preparing cylindrical specimens (Hartman, Gilchrist et al. 2001). It uses the impact of a 4536 g hammer falling from a height of 457 mm to achieve compaction. Figure 2.4 shows the Marshall compaction hammer for preparing the 100 mm diameter specimen and 150 mm diameter specimen. The standard number of blows for a 65 mm tall specimen is 50 blows per side for medium traffic and 75 blows per face for heavy traffic.

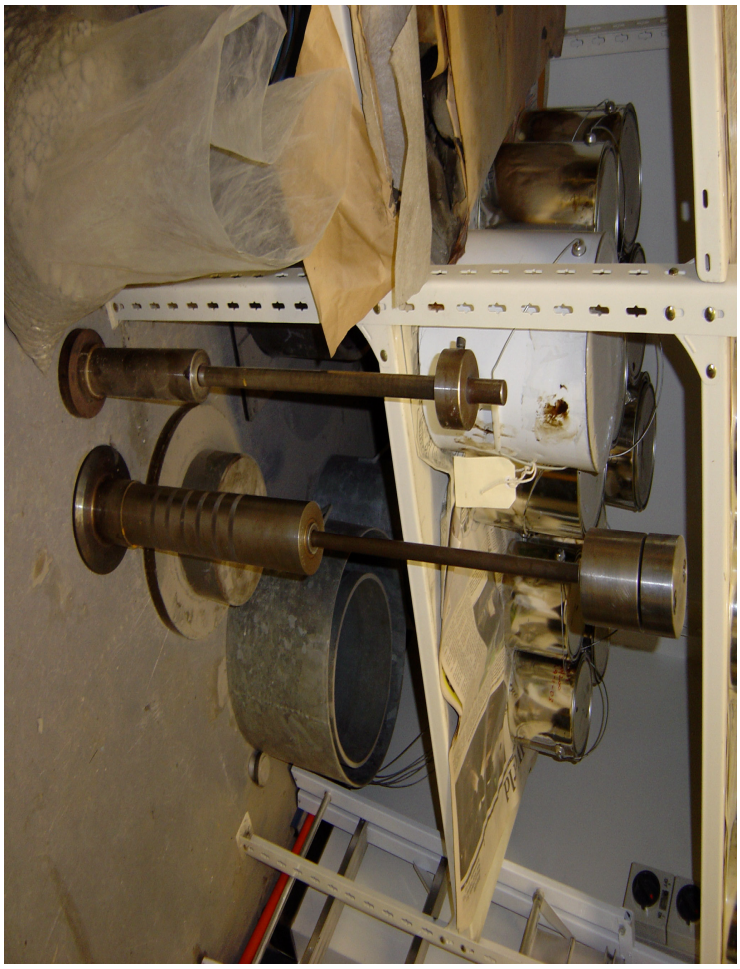

Figure 2.4: Marshall compaction hammers for 100 mm diameter specimen (left) and for the 150 mm diameter specimen (right)

Although the Marshall compactor is widely used, it produces samples considerably different than insitu compaction (Button, Little et al. 1994). It uses impact forces which degrade aggregates, instead of a kneading action to reorientate the aggregates (Hartman, Gilchrist et al. 2001). During the static compression test, high pressures must be applied to achieve the required density, which leads to the crushing of aggregates and squeezing of binder film, resulting in a microstructure different to that of insitu material. The reproducibility of the compaction method is also poor. Therefore Marshall specimens should not be used for the determination of mechanical properties if the height to diameter ratio is not close to 0.6 (Bonnot, 1997).

2.4 Factorial Experimental Design

The normal procedure when investigating the effect of factors is the one-factor-at-a-time strategy. However, this fails to consider the interaction between factors. Therefore, when dealing with multiple factors such as the factors in Section 2.3, the best approach is to conduct a factorial experiment (Montgomery, 2001). Factorial experiment is the only way to discover whether interactions are present between variables (Montgomery, 2003).

The most basic factorial design is the 2^k factorial design, where the 2 denotes the two levels of experiment (high and low) and k denotes the number of factors. For this thesis, there are in total seven factors. Therefore, if the 2^k factorial design is used, there will be in total 2^7 tests, which is 128. Furthermore, three replicates will be considered in this thesis, bringing the total to 384 tests. This is too great a number of tests to be ran, therefore, by assuming that high-order interactions are negligible, the next most sensible design of experiment option is the 2^{k-1}

one-half fractional factorial experimental design(OHFFED), which resulted in 192 number of tests including three replicates.

The 2^{k-1} OHFFED is ideal because its objective is to identify those factors in a many-factors experiment that have significant effects. However, because of the use of fractional factorial design rather than the full factorial design, one effect is confounded with another effect. These are called aliases. Therefore, the results from this type of experimental design are slightly compromised, but by neglecting interactions higher than three-factor interactions, the effects estimated are more reliable.

To construct a one-half fraction of the 2^k design, first all the runs for a full 2^{k-1} factorial design are computed. Then the *k*th factor is added by identifying its plus and minus levels with the plus and minus signs of the highest-order interaction ABC···(K-1). For example, a 2^{3-1} fractional factorial of resolution III is obtained first by writing down the full 2^2 factorial design, then factor C is equated to the AB interaction. This is illustrated in Table 2.2. (Montgomery, 2003)

Table 2.2 Example of constructing a 2^{3-1} factorial of resolution III design

	Full 2^2 factorial		2^{3-1} resolution III		
Run	A	B	A	B	C=AB
1	-	-	-	-	+
2	+	-	+	-	-
3	-	+	-	+	-
4	+	+	+	+	+

In this research, MINITAB®, a programme specialising in Statistical Process Control and Design of Experiment is used to generate the OHFFED. By inputting the factors with their high and low level and the number of replicates, all the runs required for analysis are generated. After the response are gathered and inputted into the worksheet, MINITAB® will run statistical analysis to determine the effect estimates and to determine the significant effects.

Ideally, screening designs often lead to further experimentation once the dominant factors are identified. However, in this thesis, no further exploration of the dominant factors will be carried out due to time constraint and other investigations.

Chapter 3

Research Methodology

This section describes the materials used for sample preparation, the methods used to determine the mix design parameters (such as the optimum temperature range for compaction, the percentage of air voids, the bulk specific gravity and the maximum theoretical specific gravity of the mix) including the respective results, and the main investigations.

Section 3.1 describes the source of materials that is used to produce all the testing samples. Section 3.2 describes the mix preparation steps used to create the testing samples at specific level and also to generate compaction curves that shows the compaction effort required to achieve certain percentage of air voids in the total mix. Section 3.3 describes the procedures used to compute the one-half fractional factorial design. Section 3.4 describes the procedures of conducting the complex, flexural and resilient modulus tests and the analysis of the results.

3.1 Source of materials

The asphalt mixtures were supplied by Fulton Hogan Ltd (Canterbury). The AC10 and AC14 mixtures were ready-mixed and came in paper bags of roughly 10 kg each.

The aggregates used in the asphalt mixtures were 95% crushed Canterbury greywacke extracted from the Pound Road Quarry located in near Christchurch, South Island, New Zealand. The bitumen used was 80/100 penetration grade and was produced at the Fulton Hogan Canterbury asphalt plant.

Three lots of asphalt mixtures were ordered from three different batches, resulting in slightly different mixtures. However, the maximum specific gravity from each batch was tested using Rice test (AS2891.7.1 – 1993) in the University of Canterbury Transportation Laboratory and found to be all consistent.

Since the three samples of the asphalt mixtures were extracted from big asphalt mix batch, the proportion of the aggregate sizes in each bag was likely to be inconsistent. The particle size distribution for AC10 and AC14 for the whole batch is illustrated in Figure 3.1 and Figure 3.2 respectively.

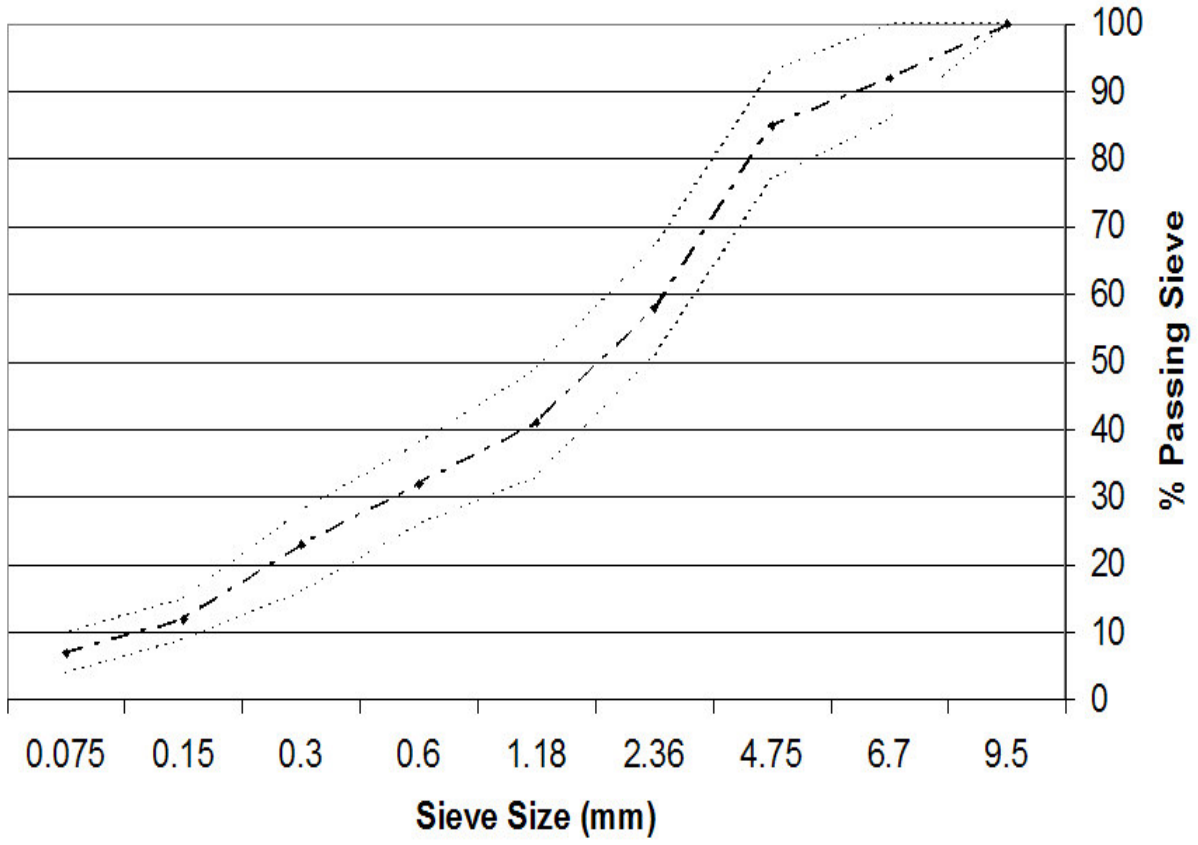

Figure 3.1 Particle size distribution for the AC10 asphalt mixtures

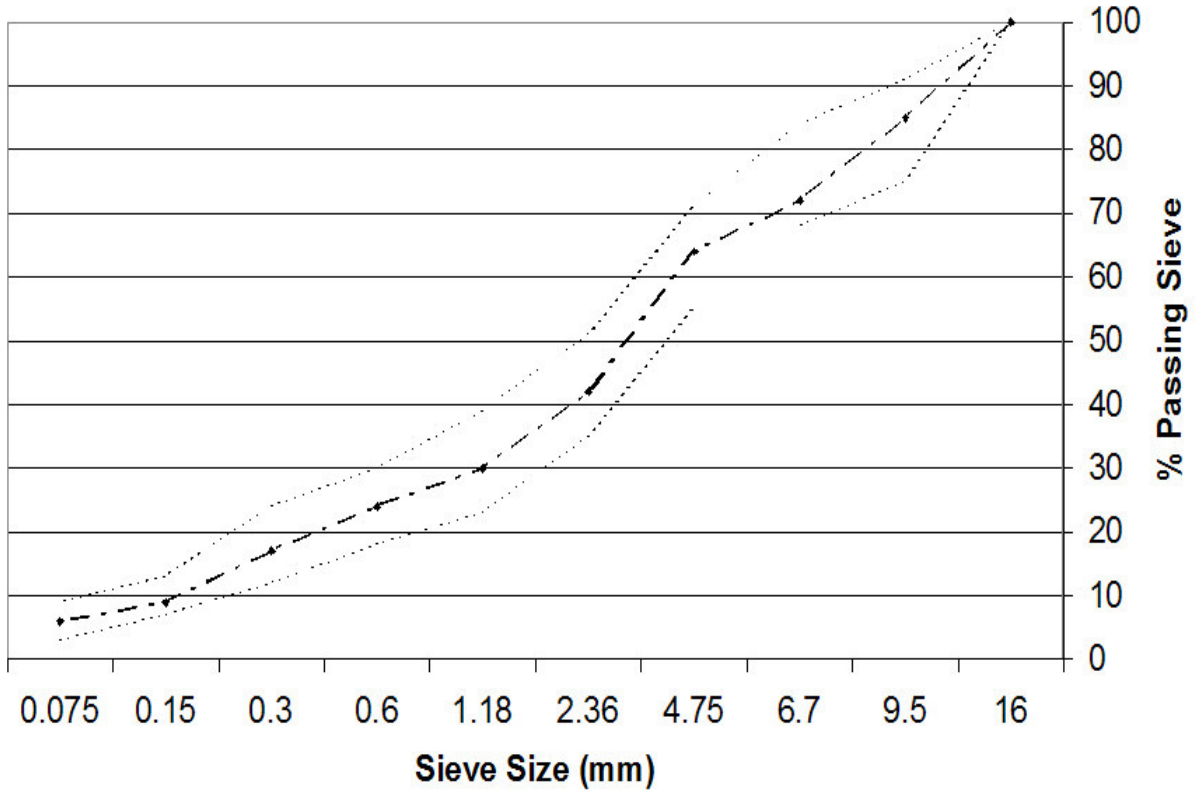

Figure 3.2 Particle size distribution for the AC14 asphalt mixtures

After the determination of the maximum theoretical specific gravity for AC10 and AC14, the next step is to prepare asphalt samples.

3.2 Mix Preparation

In order to prepare the asphalt samples which maintain certain volumetric properties such as certain percentage of air voids, several parameters were needed to be measured. The maximum theoretical specific gravity, the optimum compaction temperature, and the bulk specific gravity of the compacted mix were measured first. In this research the percentage of air voids was maintained at 5% ± 0.5% for all specimens regardless of the geometry or the compaction method. Section 3.2.1 describes the procedure to determine the optimum compacting temperature for the asphalt mix, leading to the preparation of specimen in Section 3.2.2. Section 3.2.3 to Section 3.2.5 describes the methods used to determine the bulk specific

gravity and maximum specific gravity needed for percentage air voids determination. This is used for generating the compaction curves, described in Section 3.2.6

3.2.1 Determining the Optimum Compaction Temperature

Determination of the mixing and compacting temperatures is a crucial laboratory task to be done. This is because a certain level of viscosity is needed to ensure that the asphalt binder is sufficiently fluid for mixing and compacting. Since the asphalt mix were ready-mix when received, only the compaction temperature was to be determined. This is done using a rotational viscometer, specifically the Brookfield Thermosel Apparatus, shown in Figure 3.3. The Brookfield Thermosel Apparatus consists of a sample chamber, a thermo-container, a spindle, a digital readout, and a temperature controller, shown as a schematic in Figure 3.4.

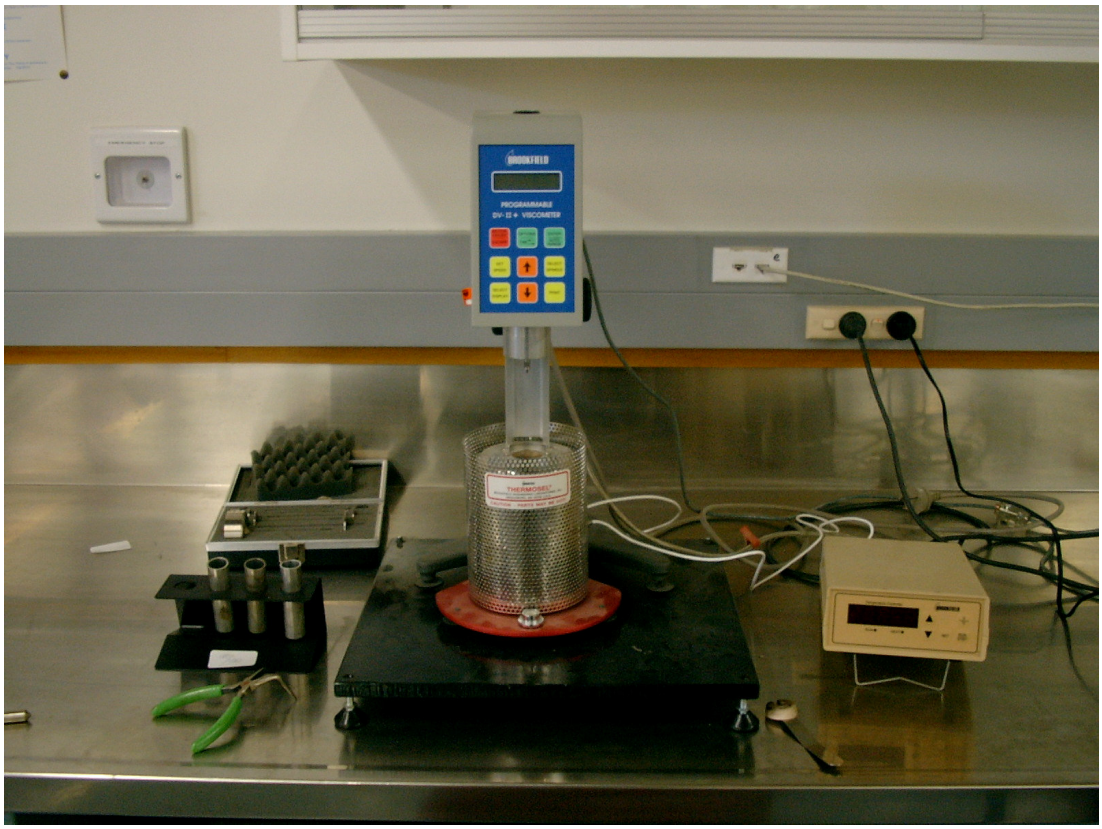

Figure 3.3 Brookfield Thermosel Apparatus; from the left, the sample chamber, the Brookfield viscometer, and the temperature controller

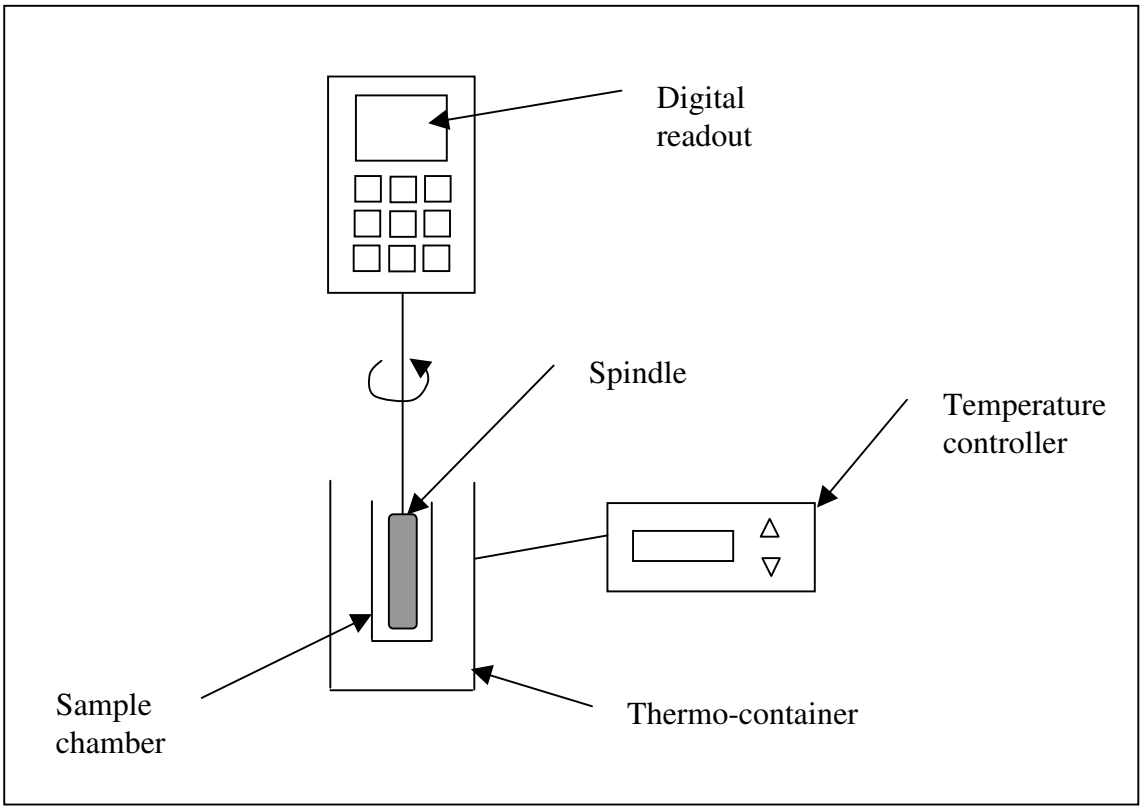

Figure 3.4 Schematic of the Brookfield Thermosel Apparatus

The principle behind the Brookfield viscometer is that the rotational viscosity is determined by measuring the torque required to maintain a constant rotational speed of 20 RPM of a cylindrical spindle number 27 while submerged in an asphalt binder at a constant temperature (Roberts, 1996). The torque is directly related to the viscosity of the sample and is determined automatically by the viscometer.

The details of the test can be found in ASTM D4402. A brief summary of the test procedure is given in the following section. The bitumen is heated in an oven of 100ºC. Then 10ml of the hot bitumen is poured into the sample chamber, and placed into the 100ºC thermo-container (Figure A1.1 in the appendix). The thermo-container keeps the asphalt binder at the temperature desired for testing via the temperature controller. The number 27 spindle is then mounted (Figure A1.2) and the lid placed (Figure A1.3). When the sample temperature is

stable, the viscometer is turned on at 20 RPM. The digital readout then displays the viscosity of the bitumen at that particular temperature in centipoises or mPa.s.

Repeating the above test at different temperatures and collecting the necessary data points, a temperature-viscosity relationship can be constructed. The temperature-viscosity curve is needed to determine the correct range of compacting temperature. To plot the temperature viscosity curve, the viscosities at the temperatures between 100ºC to 140ºC were recorded for two replicates of asphalt binder 80/100 penetration grade. Using the average of the two replicates, the temperature-viscosity curve was plotted on a semi-logarithmic chart with the viscosity on the logarithmic axis and the temperature on the arithmetic axis. The compaction temperature of the asphalt mixture is therefore traced using the temperature-viscosity curve given that the compaction viscosity needed to be between 250 and 310 m.Pa.s.

Following the method described above, the viscosities at the temperatures range from 100°C to 140°C are shown in Table 3.1. The last column displays the model fitted to approximate the viscosities at the appropriate temperatures, and is shown as the solid line in Figure 3.5. Extrapolating the fitted model to obtain the compaction temperature range for the viscosities at 250 and 310 m.Pa.s determines that the optimum compacting temperature should be between 140°C and 144°C.

Table 3.1 Viscosities for the two asphalt binder samples at different temperatures

	Viscosity (m.Pa.s)			
Temperature (°C)	Sample 1	Sample 2	Average	Fitted Line (CurveExpert)
100	3340	3420	3380	3147.6
110	1683	1722	1702.5	1769.7
120	912.5	940.3	926.4	995
130	545	545	545	559
140	335	336.2	335.6	314.5

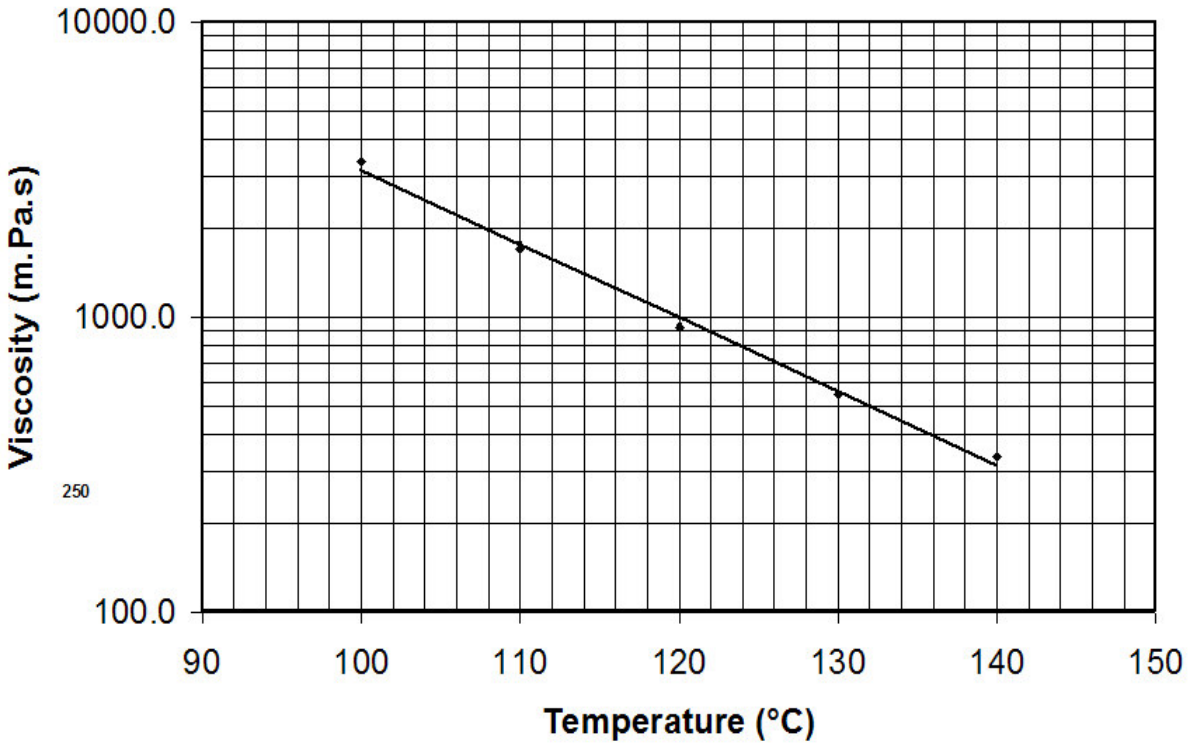

Figure 3.5 The temperature-viscosity curve with the viscosity axis transformed to a logarithmic scale

With the determination of the compacting temperature, samples for generating the compaction curves can now be done.

3.2.2 Sample preparation

This subsection discusses the number of the samples needed to be prepared and the mix design for each sample.

The method of sample preparation using Gyropac gyratory compactor for both the 100 mm and 150 mm diameter samples follows AS 2891.2.2-1995 Sample preparation – compaction of asphalt test specimens using a gyratory compactor. Asphalt mix was heated to the compacting temperature (Section 3.2.2) and placed in heated mould with the paper disc, steel disc and top and bottom platen and compacted at desired number of gyrations. Samples were extracted from the mould with the use of a hydraulic jack shown in Figure 3.6 when the sample was sufficiently cooled to avoid distortion.

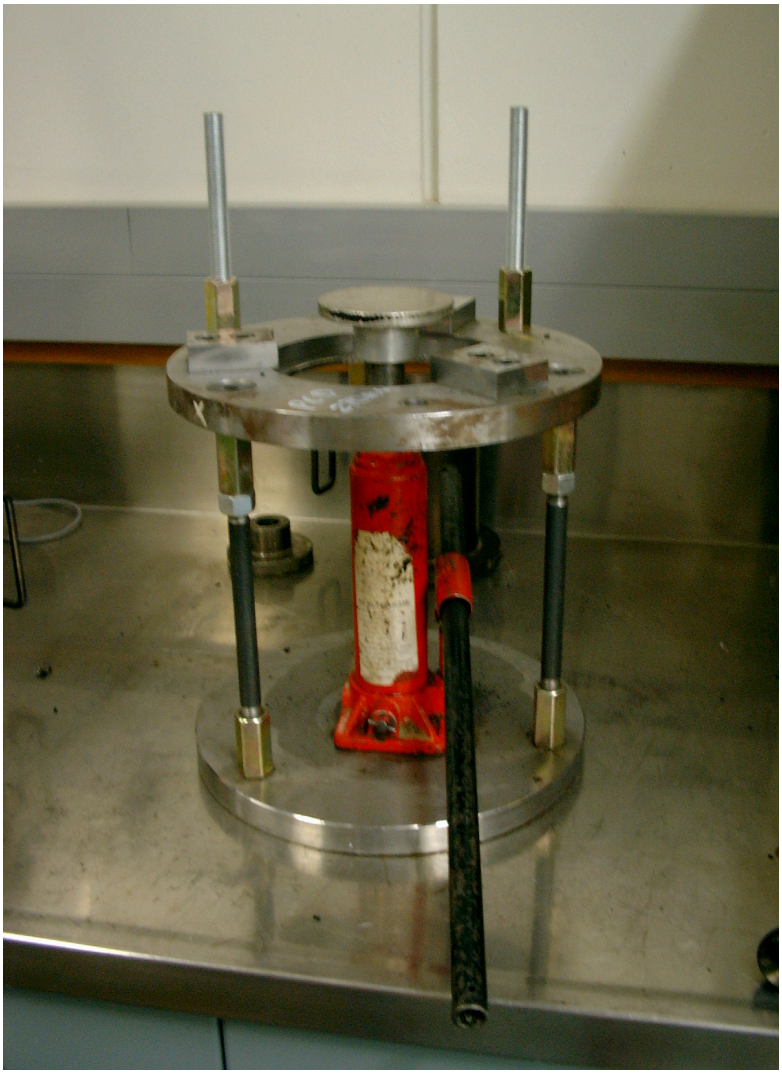

Figure 3.6 Manual hydraulic jack for extracting Gyropac and Marshall hammer specimens

Compaction of samples using the Marshall compaction hammer for the 100 mm samples follows ASTM D1559-89 Standard test method for resistance to plastic flow of bituminous mixtures using Marshall apparatus. However, for the 150 mm diameter, Modified Marshall procedures were adopted and the bigger hammer was built by the University of Canterbury machining department. A manual hammer with 10.2 kg weight and 457.2mm drop height was made. Figure 2.4 from Section 2.3.4 already depicts the two hammers used for compaction.

In the fractional factorial analysis the required number of runs was determined as 192, however, the required number of specimens was reduced to 48 specimens. The reason for this is resilient modulus test is non-destructive test and the same sample could be tested at different time duration or pulse shape. Therefore, the 48 specimens are those with different geometry (that is, diameter and thickness) and different gradation AC10 or AC14.

In this research, the controlled variable for the preparation of all specimens is the percentage of the air voids. The criterion for computing the equivalent compaction energy for the different specimen geometries, aggregate gradations and compction methods is by maintaining the same percentage of air voids in all specimens. Because the maximum theoretical specific gravities for both mixes are almost the same, therefore, all specimens have very similar bulk densities. This means that any differences in the value of the resilient modulus test of the specimens prepared by either the Gyropac or Marshall Compaction Hammer can be attributed to the different orientation of the aggregate particles during compaction or aggregate size or other factors excluding the degree of compaction. Therefore, compaction energy can be eliminated as a factor that will influence the resilient modulus. The air void percentage is fixed at 5±0.5 % which is recommended value by Australian Specification AS 29891.2.2.

[I82]

To determine the required number of blows for Marshall compaction hammer specimens and the number of gyrations for Gyropac specimens for a given air void percentage, compaction effort compaction curves will be needed. This is a chart that shows the compaction effort needed (number of blows for Marshall and number of gyrations for Gyropac) to achieve a certain percentage air voids.

To generate the compaction curves, firstly the bulk specific gravity and maximum specific gravity which are needed for the percentage air voids determination are measured. These are described in Section 3.2.3, 3.2.4 and 3.2.5. Section 3.2.6 displays the compaction curves generated using bulk specific gravity, maximum specific gravity and percentage air voids.

3.2.3 Determination of Air Voids Percentage

Determination of air voids percentage follows American standard ASTM D3203-94. To determine the air voids percentage, Equation 4 is used.

$$\%VA = (1 - \frac{G_{mb}}{G_{mm}})100\% \qquad \text{Equation 4}$$

Where $\%VA$ = Percentage air voids

G_{mb} = Bulk specific gravity

G_{mm} = Maximum specific gravity

The bulk specific gravity (G_{mb}) and maximum specific gravity were both determined experimentally in the laboratory. These are shown in Section 3.1.2 and Section 3.1.3 respectively. The results for the percentage of air voids used for the compaction curves were shown from Table A2.1 to Table A2.10, and the percentage of air voids for the testing specimens were depicted from Table A2.11.

3.2.4 Determination of the Bulk Specific Gravity, G_{mb}

Determination of the bulk specific gravity follows American Standard ASTM D2726-00. As set out in the standard, a specimen that has been cooled down at room temperature is first

weighed for the dry mass, denoted as A. The specimen is then submerged in water to record its mass in water, denoted as C. Finally, the wet specimen is taken out of the water and its surface is wiped with a piece of cloth to remove the surface water, and its mass, denoted as B, is recoded.

To determine the bulk specific gravity, Equation 5 is used.

$$G_{mb} = \frac{A}{B - C} \qquad \text{Equation 5}$$

Where G_{mb} = Bulk specific gravity

A = Mass of dry specimen in air (g)

B = Mass of the saturated surface dry specimen in air (g)

C = Mass of the specimen in water (g)

The bulk specific gravity for all the specimens prepared for the purpose of the compaction curves, the factorial experiment, and the complex modulus are shown in Appendix 2.

3.2.5 Determination of the Maximum Specific Gravity, G_{mm}

Determination of the maximum specific gravity follows Australian standard AS 2891.7.1-1993. This is done using a pycnometer, shown as Figure 3.7. There are two parts to the standard; First part is the determination of the volume of the pycnometer, and the second part is the test itself. The figures mentioned in this section are shown in Appendix 1.

Figure 3.7 A pycnometer used to measure the maximum specific gravity, G_{mm}

The second part of the test started with the inclusion of the sample. Two samples of each mix are to be tested. The weight of each sample is 500 g for AC-10 aggregate gradation, and 750 g for AC-14 aggregate gradation.

First, the sample is left in the oven at 105°C until the mass is constant. The sample must be separated out so that the finer aggregate portions are not larger than 6mm (Figure A1.4). Then the sample is placed into the pycnometer and the mass of the pycnometer, lid and sample is measured and denoted as m_3. Thirdly, water is added to the pycnometer until it reaches certain mark on the side of the pycnometer then the pycnometer was covered with lid and attached to a vacuum pump. Apply as much vacuum as the pycnometer can withstand to remove all air particles trapped within the aggregate particles. Use a mallet and gently tap on the pycnometer to help with the air bubbles removal (Figure A1.5). After no more air bubbles can be

observed, detach the vacuum pump and fill the pycnometer with water at 25°C, and place it in a water bath for no less than one hour. Then top up the pycnometer with water at 25°C, slide on the lid and invert the pycnometer several times until no more bubbles can be observed (Figure A1-6). Take the pycnometer out of the water, wipe the surface of the pycnometer, and measure the mass of the pycnometer, lid, sample and water and denote it as m_4 (Figure A1-7). The maximum specific gravity is determined by Equation 6.

$$G_{mm} = \frac{(m_3 - m_1)\rho_w}{(m_3 - m_1) - (m_4 - m_2)} \qquad \text{Equation 6}$$

Where G_{mm} = maximum specific gravity, tonnes per cubic metre

m_1 = mass of the pycnometer and lid (g)

m_2 = calibrated mass of pycnometer and lid, filled with water at 25°C (g)

m_3 = mass of the pycnometer, lid and test portion (g)

m_4 = mass of the pycnometer, lid, test portion and water (g)

ρ_w = density of water at 25°C (0.997 t/m3)

Since the asphalt mixtures were extracted from three different batches, each of the three batches was tested for their maximum specific gravity, and an average value was determined.

With the determination of all the above parameters, testing samples can then be prepared to the controlled 5% ± 0.5% air voids.

For the determination of the maximum specific gravity given as Equation 6, the measurement for each of the variables and the resulting maximum specific gravity are shown in Table 3.2

and Table 3.3 for each of the three asphalt mixture batches collected from Fulton Hogan. Each batch had two lots of specimen that were tested. The final maximum specific gravity for AC10 and AC14 were 2.407 and 2.469 t/m^3 respectively.

Table 3.2 Maximum specific gravity calculations for aggregate gradation AC10 for each of the three batches of asphalt mix.

		m_1	m_2	m_3	m_4	water density	Max Specific Gravity	Average
First	Spec 1	2984.3	7396.9	3732.2	7843.2	0.997	2.4723	2.4693
	Spec 2	2984.3	7396.9	3732.6	7842.7	0.997	2.4663	
Second	Spec 1	2984.3	7396.9	3732.9	7843	0.997	2.4673	2.4687
	Spec 2	2984.3	7396.9	3732.5	7843.1	0.997	2.4701	
Third	Spec 1	2984.3	7396.9	3732.6	7843.2	0.997	2.4704	2.4684
	Spec 2	2984.3	7396.9	3732.9	7842.9	0.997	2.4665	

Table 3.3 Maximum specific gravity calculations for aggregate gradation AC14 for each of the three batches of asphalt mix.

		m_1	m_2	m_3	m_4	water density	Max Specific Gravity	Average
First	Spec 1	2984.3	7396.9	3485.2	7690.2	0.997	2.4056	2.4069
	Spec 2	2984.3	7396.9	3484.3	7689.9	0.997	2.4082	
Second	Spec 1	2984.3	7396.9	3484.6	7689.8	0.997	2.4050	2.4041
	Spec 2	2984.3	7396.9	3484.7	7689.7	0.997	2.4032	
Third	Spec 1	2984.3	7396.9	3484.6	7689.8	0.997	2.4050	2.4041
	Spec 2	2984.3	7396.9	3484.7	7689.7	0.997	2.4032	

3.2.6 Generating Compaction curves

Compaction curves are generated for the purpose of determining the required number of gyrations (for Gyropac) or numbers of blows (for Marshall Compaction Hammer) for a given air void percentage. Since the compaction energy will depend on the geometry of the specimen (that is the diameter and thickness), the aggregate gradation and the compaction method different compaction curves according to these factors will need to be prepared. These factors are shown in Table 3.4.

Table 3.4 Factors for determining the compaction curves

Diameter (mm)	Thickness (mm)	Compaction Method	Aggregate Gradation
100	40	Gyropac	AC-10
100	40	Gyropac	AC-14
100	40	Marshall Compaction Hammer	AC-10
100	40	Marshall Compaction Hammer	AC-14
100	70	Gyropac	AC-10
100	70	Gyropac	AC-14
100	70	Marshall Compaction Hammer	AC-10
100	70	Marshall Compaction Hammer	AC-14
150	40	Gyropac	AC-10
150	40	Gyropac	AC-14
150	40	Marshall Compaction Hammer	AC-10
150	40	Marshall Compaction Hammer	AC-14
150	70	Gyropac	AC-10
150	70	Gyropac	AC-14

150	70	Marshall Compaction Hammer	AC-10
150	70	Marshall Compaction Hammer	AC-14

In total, sixteen compaction curves will need to be generated. Each curve is defined by three points, and each point consists of two replicates to increase the accuracy of the air voids determination.

Table A2.1 to Table A2.10 in the Appendix showed the percentage air voids given a certain number of blows or gyrations. The percentage air voids were determined by first determining an averaged bulk specific gravity from both replicates. Then substituting the average bulk specific gravity and the maximum theoretical specific gravity into Equation 4 gave the value of the percentage air voids.

Figure A2.1 to Figure A2.8 displayed the compaction curves for the samples with different geometric size and compaction methods. The compaction curves shown as Figure A2.1, A2.3 and A2.4 were required to be adjusted to compensate for experimental errors and the change of compaction temperature.

Note that the compaction curves for the 150mm diameter specimens compacted using the Marshall hammer are not shown. This is due to the fact that with larger diameter specimens, the surface area for the heat to dissipate is much greater than the smaller diameter specimens during compaction. Furthermore, with a manual Modified Marshall hammer, the amount of time taken to compact a specimen will increase, causing greater heat loss and inconsistency in

the percentage of air voids. Therefore trial and error were used to prepare the 150mm diameter Marshall compacted specimens at 5% ± 0.5% air voids.

The next section describes the main investigation of designing an experiment that analyses the interaction of different factors. Supplementary experiments on the comparison of strain from three methods during a resilient modulus test and different modulus comparisons are also included in the next section.

3.3 Design of experiment

The design of the experiment for the investigation of the factors mentioned in Section 2.3 follows a 2^{k-1} one-half fractional factorial experimental design introduced in Section 2.4. This section will elaborate the factorial design in the context relevant to this research.

As mentioned, there are seven factors in consideration for the half factorial design. This resulted in a resolution V design, which means that no main effects and two-factor interactions are aliased with any other main effect, two-factor interactions, three-factor interactions or four-factor interactions, but three-factor interactions are aliased with four-factor interactions. This resulted in sixty-three alias structure, depicted in Table 3.5.

Table 3.5 Alias structure for the one half fractional factorial design

A + BCDEFG	BF + ACDEG	ABG + CDEF	BDF + ACEG
B + ACDEFG	BG + ACDEF	ACD + BEFG	BDG + ACEF
C + ABDEFG	CD + ABEFG	ACE + BDFG	BEF + ACDG
D + ABCEFG	CE + ABDFG	ACF + BDEG	BEG + ACDF
E + ABCDFG	CF + ABDEG	ACG + BDEF	BFG + ACDE
F + ABCDEG	CG + ABDEF	ADE + BCFG	CDE + ABFG
G + ABCDEF	DE + ABCFG	ADF + BCEG	CDF + ABEG
AB + CDEFG	DF + ABCEG	ADG + BCEF	CDG + ABEF
AC + BDEFG	DG + ABCEF	AEF + BCDG	CEF + ABDG
AD + BCEFG	EF + ABCDG	AEG + BCDF	CEG + ABDF
AE + BCDFG	EG + ABCDF	AFG + BCDE	CFG + ABDE
AF + BCDEG	FG + ABCDE	BCD + AEFG	DEF + ABCG
AG + BCDEF	ABC + DEFG	BCE + ADFG	DEG + ABCF
BC + ADEFG	ABD + CEFG	BCF + ADEG	DFG + ABCE
BD + ACEFG	ABE + CDFG	BCG + ADEF	EFG + ABCD
BE + ACDFG	ABF + CDEG	BDE + ACFG	

Using MINITAB®, all seven factors with their high and low levels were inputted, and the number of replicates specified. MINITAB® then generated all the test runs required for the analysis, and once the responses for the test runs were collected and entered into the MINITAB® worksheet, a model was fitted and using the p-value and level of significance of 0.05, the important effects or interactions were identified.

In addition to the main investigation of the interactions of factors affecting resilient modulus, the next two sections describe two supplementary investigations.

3.4 Laboratory Measurements of Complex, Flexural and Resilient modulus relationship

In this part a summary of the experimental tests curried out to measure the complex, flexural, and resilient modulus values is discussed. The relationship between these three parameters is discussed in the next chapter in the analysis part.

3.4.1 Complex modulus test

The complex modulus, also known as the dynamic complex modulus, is determined by applying sinusoidal vertical loads to cylindrical specimens while measuring the deformation (Roberts, 1996). The cylindrical specimen used in this test is similar to the ones used in resilient modulus testing, the main difference being that the height to diameter ratio of the complex modulus testing sample is required to be at least 2. The reason of this high height to diameter ratio is to reduce the effect of friction at both ends of the sample.

Due to this height constraint, a 100 mm diameter specimen will require a height of 200 mm, which is not achievable using normal Gyropac mould. Therefore in this study, a height to diameter ratio of 1 is used on the condition that a friction reducing material, in this case silicone grease, is applied between the specimen and the loading platens to reduce the end effects. Figure 3.8 depicts a typical complex modulus test setup.

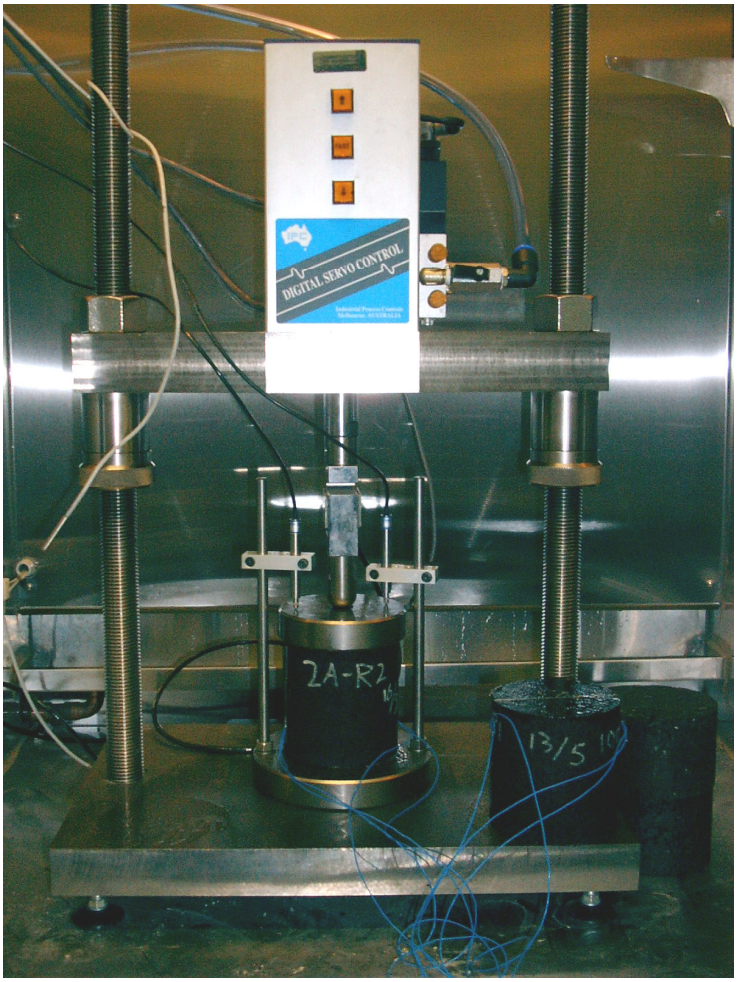

Figure 3.8 The complex modulus test setup

The complex modulus test required that the samples are tested at three different temperatures for three different loading frequencies. The temperatures were 5°C, 25°C and 40°C, and the

frequencies were 16, 4 and 1 hertz. The complex modulus was then calculated by dividing the stress applied to the sample, which was determined by dividing the applied load by the cross-section area, by the strain measured using the average of the two vertical LVDT.

The primary use of the dynamic modulus is to determine the stress-strain relationships in pavement structure under an applied load (Roberts, 1996).

3.4.2 Flexural test

The flexural test is conducted by applying repeated haversine loadings to an asphalt beam. Figure 3.9 shows the asphalt beam samples prepared by compacting a slab of asphalt mix to the same percentage of air voids (5 ± 0.5%) and cutting it into beams. Figure 3.10 shows the cut surfaces of the AC10 and AC14 asphalt beams compacted to the required 5% air voids. Figure 3.11 shows the flexural modulus apparatus in a temperature-controlled cabinet.

Figure 3.9 AC14 asphalt beams

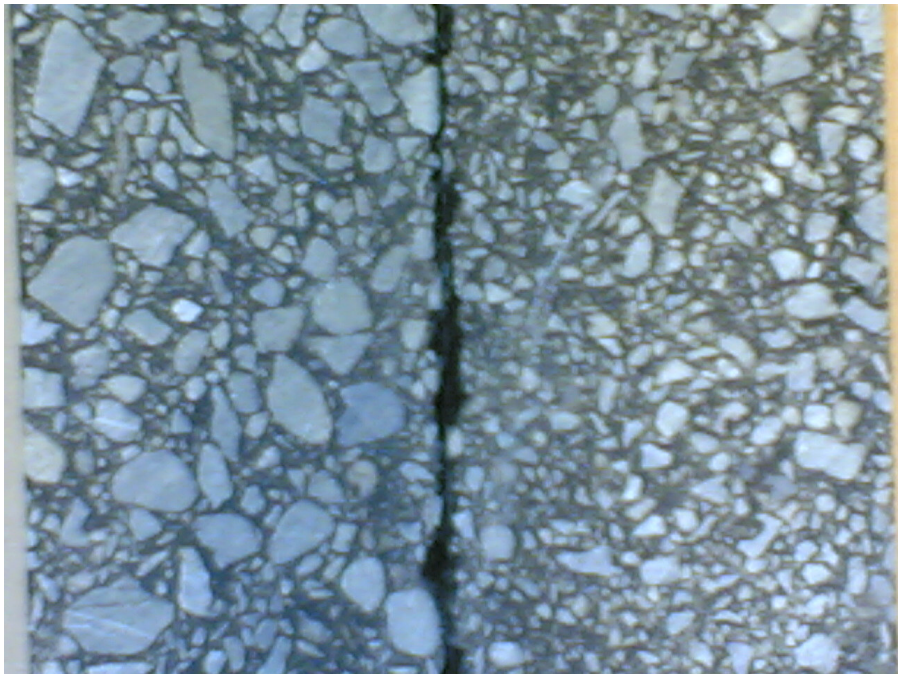

Figure 3.10 Cut surfaces of the asphalt beams, with AC14 on the left and AC10 on the right

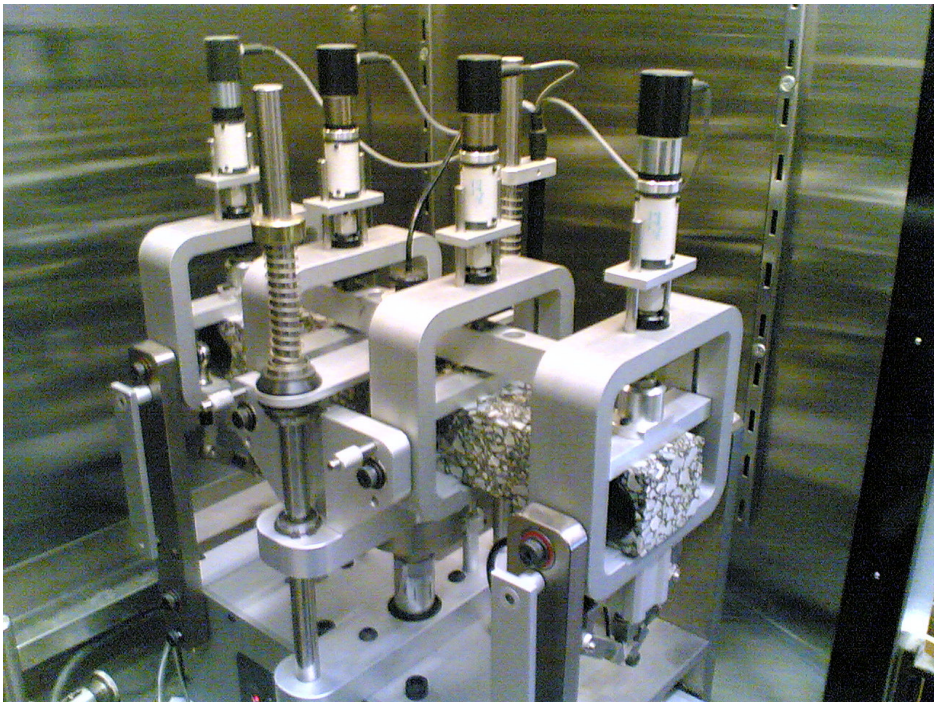

Figure 3.11 Flexural modulus testing apparatus in a temperature-controlled cabinet

The loadings are applied at third points of the beam to ensure that a constant bending moment is produced in the centre of the beam. The deflection as a result of a load is measured at the centre of the beam using an LVDT.

The flexural test can be done either by the constant stress or constant strain mode of loading. In this investigation, the constant strain mode of loading had been chosen. The constant strain of 400 microstrain is recommended in the test method prepared by the Asphalt Research Review Group for Austroads.

To calculate the flexural modulus, first the stress and strain at the outer fibres are calculated after 200 load applications using the basic relationships for stresses and strains in beams. The equations for the stress, strain and the flexural modulus are shown as Equation 7, Equation 8 and Equation 9 respectively.

$$\sigma = \frac{3aP}{bh^2} \qquad \text{Equation 7}$$

$$\varepsilon = \frac{12hd}{3l^2 - 4a^2} \qquad \text{Equation 8}$$

$$E_s = \frac{Pa(3l^2 - 4a^2)}{(48Id)} \qquad \text{Equation 9}$$

Where σ = tensile stress in the outer fibres, psi

ε = tensile strain in the outer fibres, inches/inch

E_s = flexural stiffness modulus, psi

a = distance between support and first applied load, inches

P = total dynamic load with ½ P applied at third points, lbs

b = specimen width, inches

h = specimen height, inches

l = reaction span length, inches

I = moment of inertia of specimen, $inch^4$

d = dynamic deflection of beam at the center, inches

3.4.3 Resilient modulus test

The resilient modulus test had been described in Section 2.2. The test pulse period in the test settings were set to the recommended 3000 ms, which means that the frequency of the test was 1 / (3 s). Therefore in the frequency versus the modulus plot, the resilient modulus is plotted at a frequency of 1/3 Hertz.

Chapter 4

Analysis of the Experimental Results

This section describes all the test results for the main investigation of factorial experimental design. It also presents the comparison of the strain taken from a resilient modulus test using LVDT, the strain measured using strain gauges, and the strain derived from finite element modelling, as well as the determination of the relationship between the resilient modulus, flexural modulus, and complex modulus. These are divided into the subsections as follows.

4.1 Factorial experimental design

In this section, the results of the half factorial design are shown and discussed. Table 4.1 shows the factors that have been considered in the half fractional factorial analysis and the high and low level of the numerical factors, along with the different levels for the categorical factors.

In the analysis, instead of using the results of three replicates, only two other replicates were considered after excluding any outliers. This is to increase the quality of the analysis by eliminating the anomalies. This reduced the number of runs from 192 to 128 ($2 \times 2^{7-1} = 128$). Based on the 192 resilient modulus test results which were analyzed using MINITAB® (MINITAB® Release 14 Statistical Software) and Design Expert Software (Design Expert version 6), Table 4.2 showed the analysis of variance for the different effects. The higher the F value or the lower the P value the higher the significance of the factor.

Figure 4.1 showed the normal probability plot of the standardised effect. Effects that lie on the straight line were depicted as insignificant main effects or interactions, whereas effects lying outside of the straight line were considered as significant. It is clear that the maximum nominal aggregate size is the most important factor affecting the resilient modulus, followed by the load duration, the specimen geometry represented by the thickness and diameter then the interactions between the different factors. This is further verified by the Pareto chart shown as Figure 4.2, which displayed the interactions in terms of significance.

Table 4.1 Factors considered in the factorial analysis

Abbreviation	Factors	Levels		Unit
A	Diameter of specimen	100	150	mm
B	Thickness of specimen	40	70	mm
C	Max nominal aggregate size	10	14	mm
D	Compaction methods	Gyropac	Hammer	Categorical
E	Load form	Triangular	Sinusoidal	Categorical
F	Load duration	100	200	ms
G	Preset strain level	20	60	με

Table 4.2 Analysis of Variance of the significant factors.

Source	Sum of Squares	DF	Mean Square	F Value	P-Value Prob > F
Model	61571729	18	3420652	162.6082	< 0.0001
A	4345352	1	4345352	206.5659	< 0.0001
B	6589358	1	6589358	313.2397	< 0.0001
C	24831866	1	24831866	1180.438	< 0.0001
D	1095940	1	1095940	52.09794	< 0.0001
F	10507674	1	10507674	499.5055	< 0.0001
G	192355	1	192355	9.144022	0.0031
AB	2108945	1	2108945	100.2533	< 0.0001
AC	3140645	1	3140645	149.2975	< 0.0001
AD	1443301	1	1443301	68.61048	< 0.0001
BC	1171215	1	1171215	55.6763	< 0.0001
BF	311655.1	1	311655.1	14.81522	0.0002
CD	2690620	1	2690620	127.9046	< 0.0001
CF	188498	1	188498	8.96067	0.0034
ABC	1922761	1	1922761	91.40268	< 0.0001
ABD	456729	1	456729	21.71163	< 0.0001
BCD	334971.1	1	334971.1	15.92359	0.0001
BCF	206885.3	1	206885.3	9.83475	0.0022

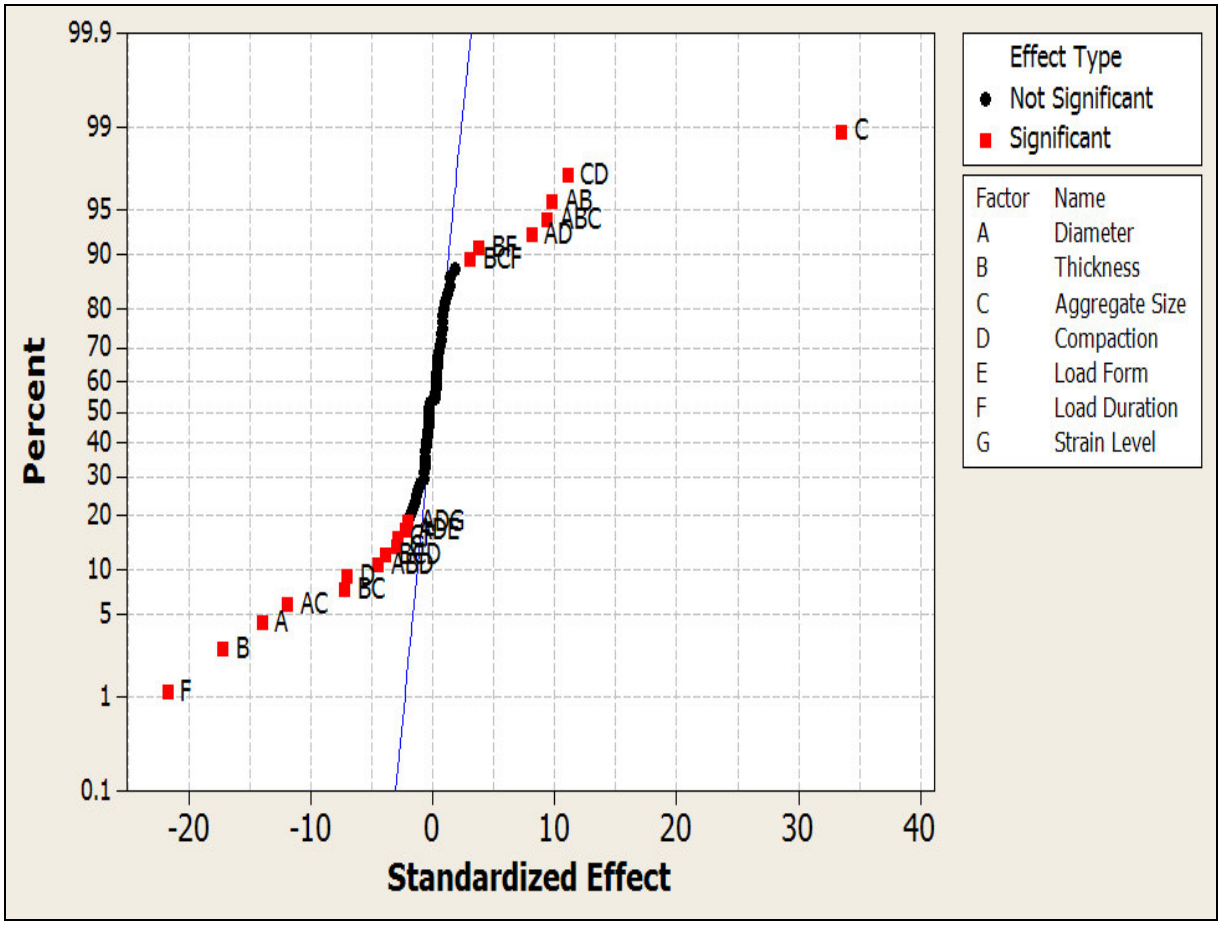

Figure 4.1 Normal probability plot of the standardised effects

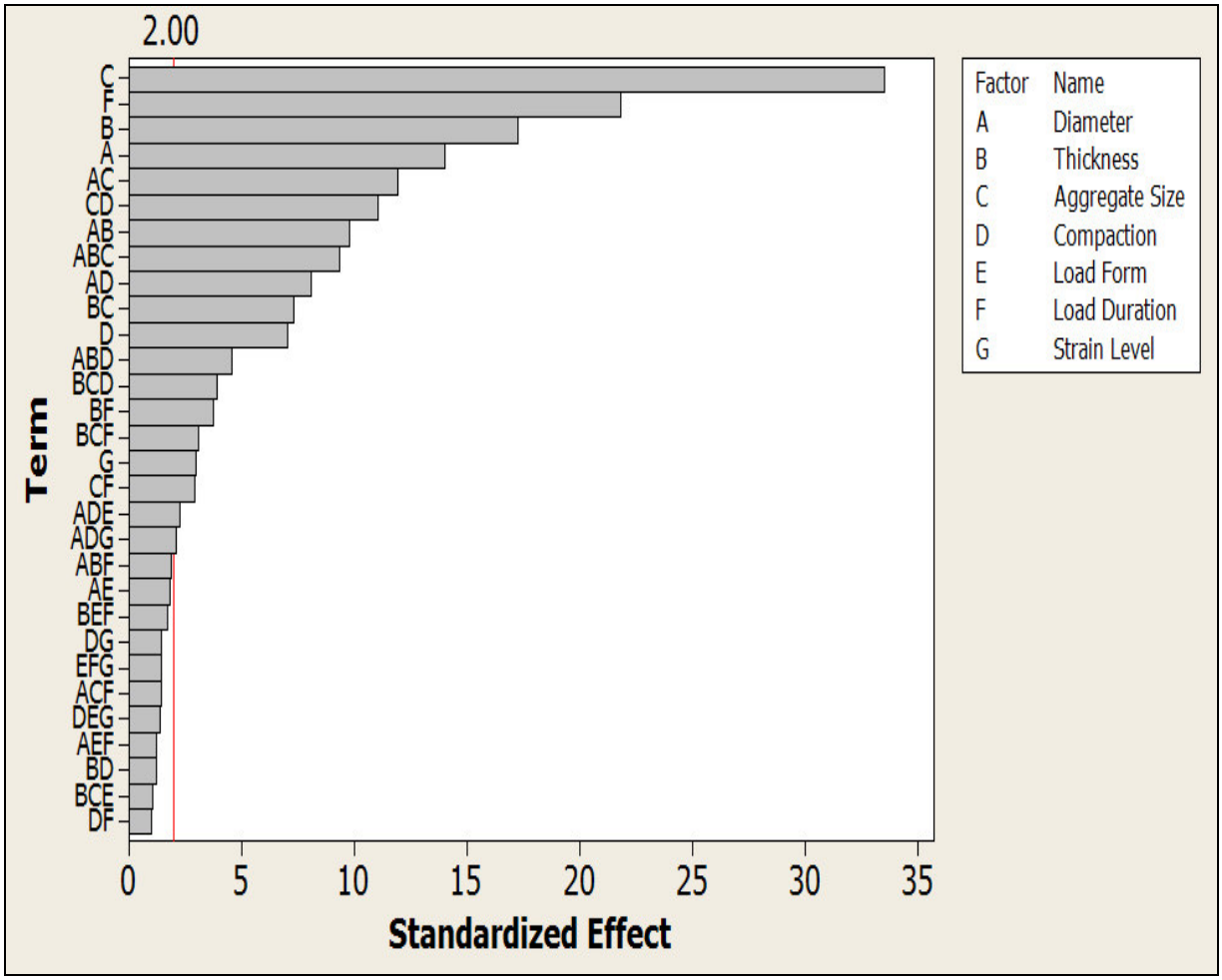

Figure 4.2 Pareto chart which displays the significant interactions at a 0.05 significance level

Now that the significant factors are known, the top main effects and 2-factor interactions can then be discussed.

Figure 4.3 showed the effect of the maximum nominal aggregate size on resilient modulus. It is clear that the coarser the aggregate gradation the higher the resilient modulus of the asphalt mix. This is expected due to the fact that larger aggregates have higher particle to particle contact in the coarser aggregate structure. The analysis of variance shown in Table 4.2 showed that maximum nominal aggregate size has the largest F value, reflecting the importance of the aggregate gradation on the resilient modulus. This is further verified by the Pareto chart shown in Figure 4.2.

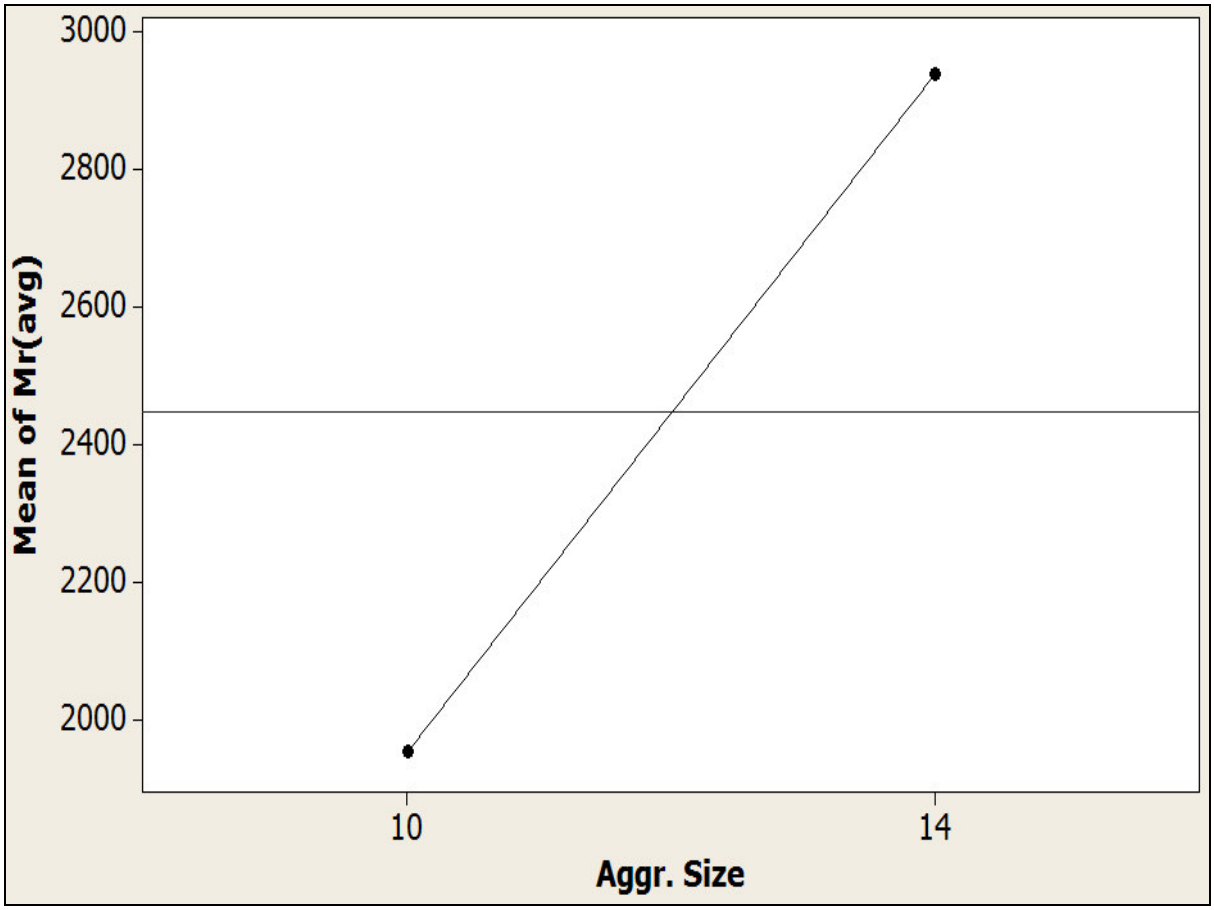

Figure 4.3 Effect of maximum nominal aggregate size on the resilient modulus

Figure 4.4 showed the effect of the load duration on the resilient modulus. It is evident that the longer the load duration the smaller the resilient modulus. This is expected because longer duration meant that the asphalt sample experienced higher strain for a longer period of time, hence reducing the resilient modulus. This effect can be attributed to the viscoelastic nature of bituminous materials which causes these mixes to be rate dependent. It is well known that slow traffic has the most damaging effect on the asphalt pavement causing severe rutting and distortions in the pavement structure. Therefore when measuring the resilient modulus in the laboratory an appropriate load duration should be selected in order to measure a representative resilient modulus for the insitu conditions.

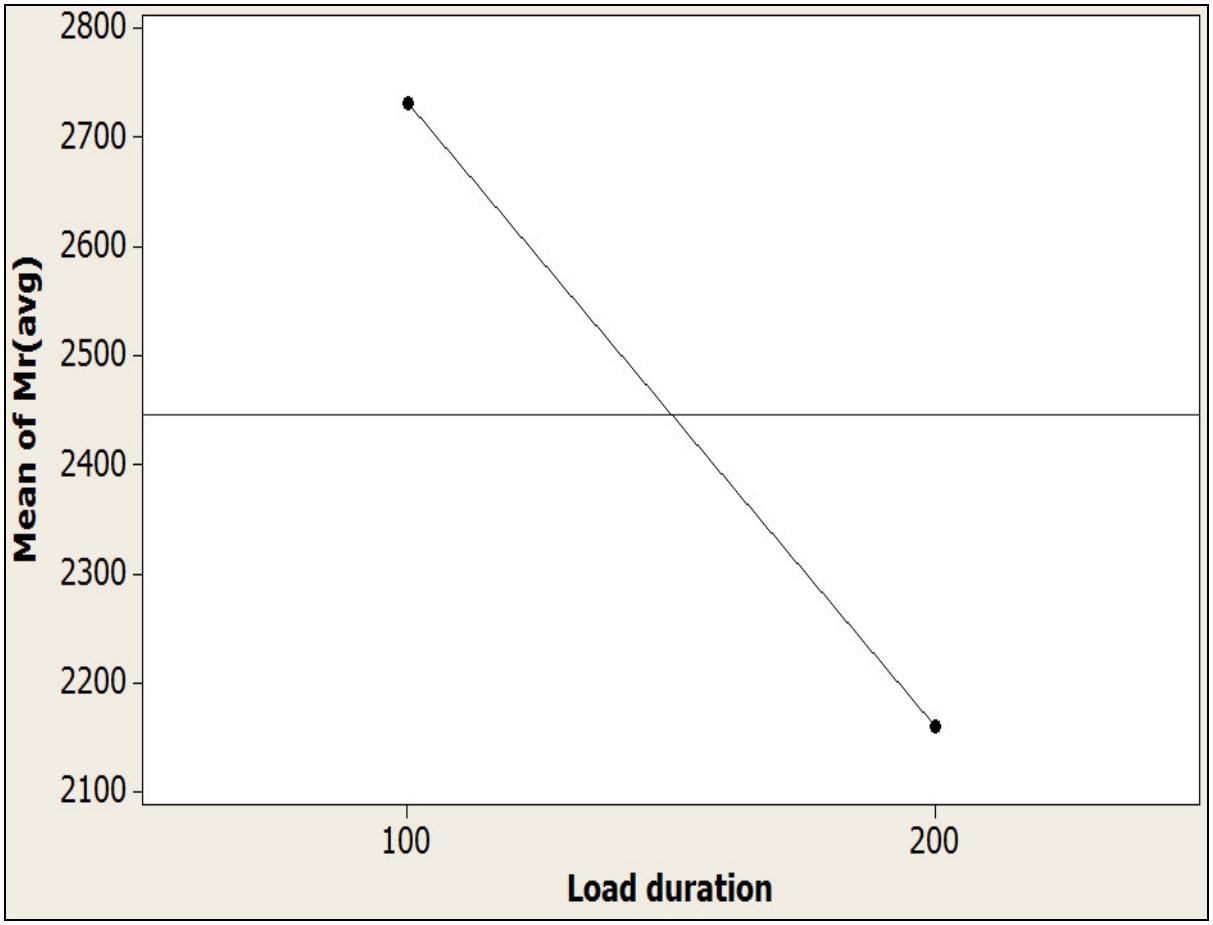

Figure 4.4 Effect of load duration on the resilient modulus

Figure 4.5 and 4.6 showed the effect of specimen thickness and diameter. It is clear that smaller diameter and thinner specimens yield higher resilient modulus than larger diameter and thicker specimens. This effect may be explained by the higher confinement of the aggregate particles in the smaller dimension. In addition for the larger diameter and thicker specimens the probability of having higher percentages of micro-cracks is higher than that in the smaller specimens, therefore the rate of energy release in the larger specimens is higher that that in the smaller specimens. A similar effect of that is noticed in Portland cement specimens as the smaller cylinders always yield a higher strength than that of the larger specimens. Therefore, a representative geometry should be selected in order to have a resilient modulus that matches the actual field conditions.

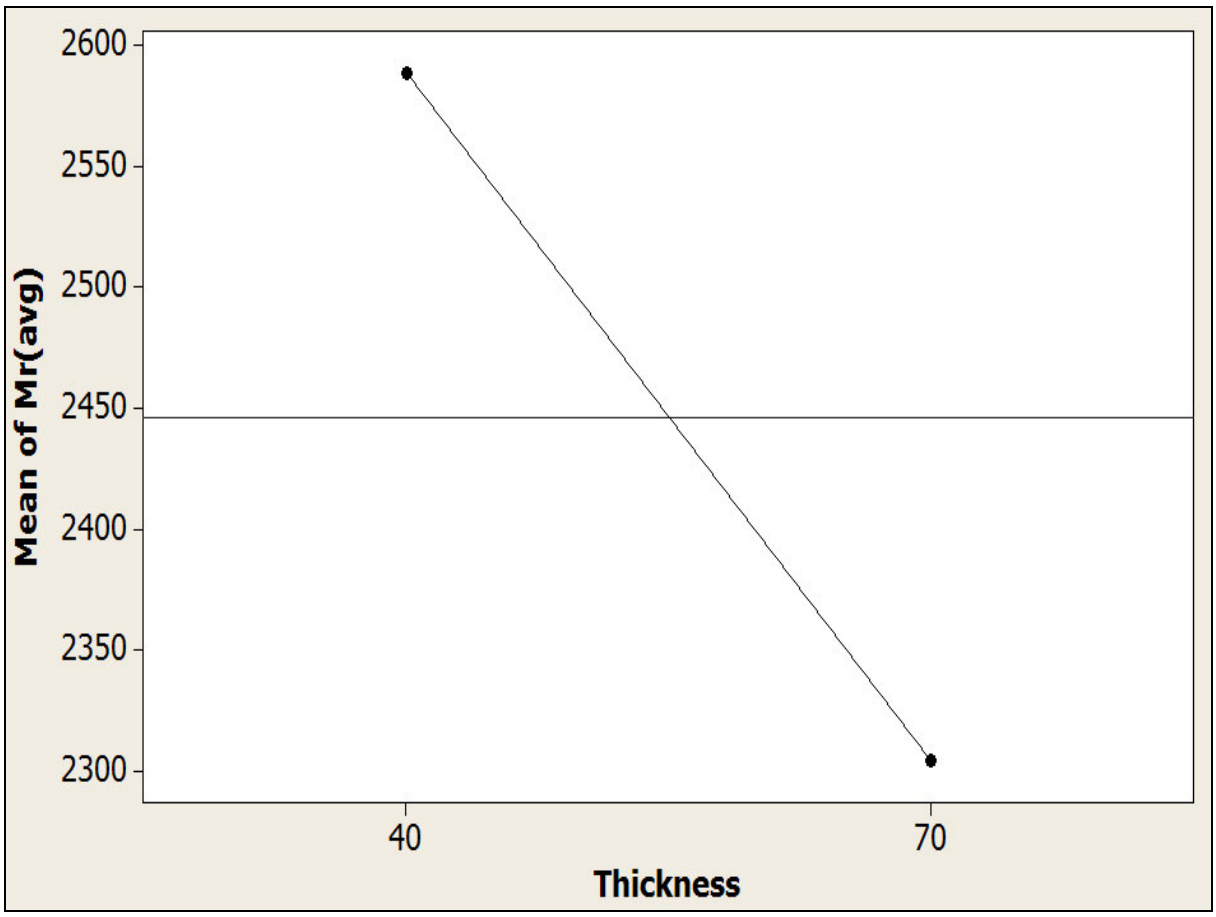

Figure 4.5 Effect of specimen thickness on the resilient modulus

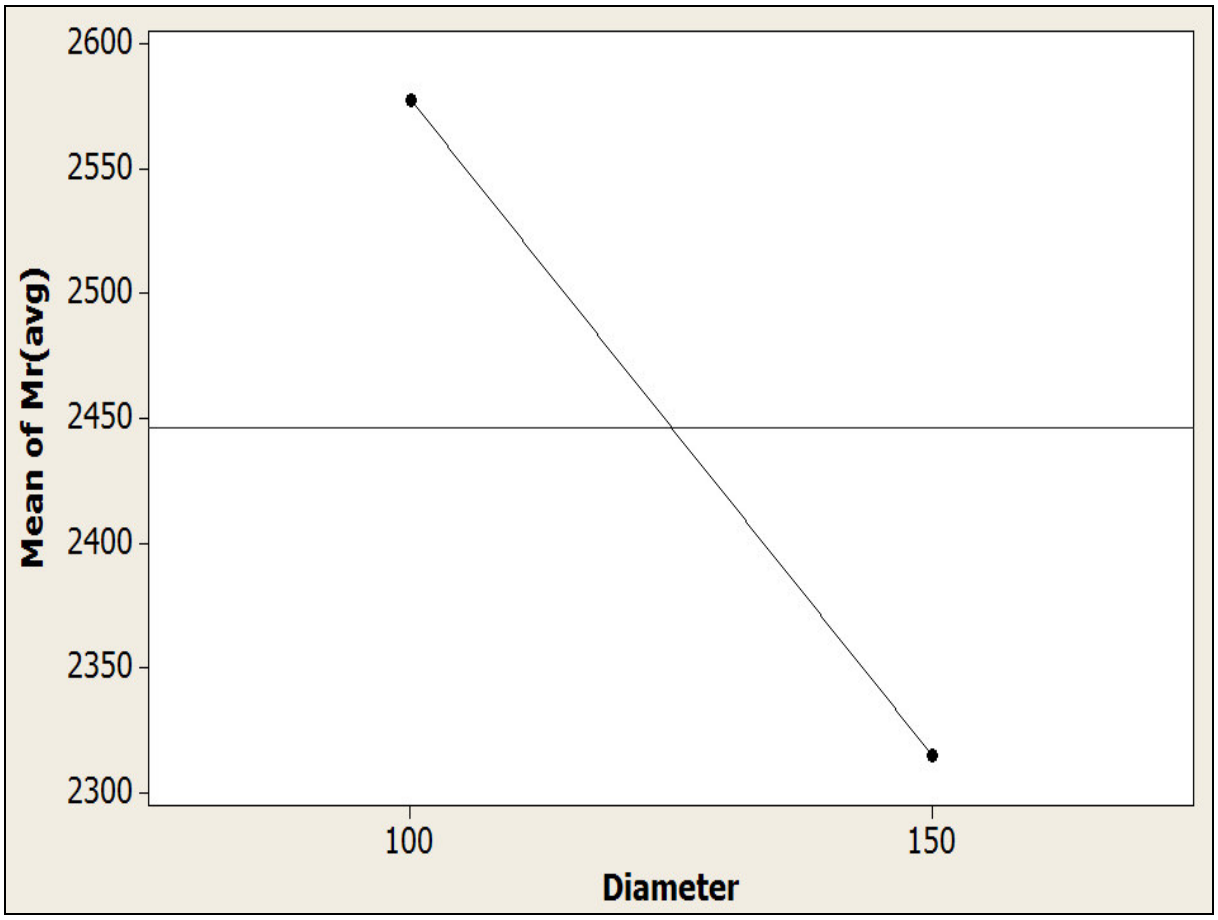

Figure 4.6 Effect of specimen diameter on the resilient modulus

Figure 4.7 displayed the effect of the interaction between the aggregate size and specimen diameter on resilient modulus. It is clear that the effect of coarser gradation is very prominent in the smaller diameter specimen while this effect is less in the larger diameter specimen. This means that using the smaller 100mm diameter mould in the laboratory is very sensitive to the aggregate gradation compared to the 150mm diameter specimens. This is most likely due to the higher degree of confinement in the smaller diameter mould compared to the larger diameter mould.

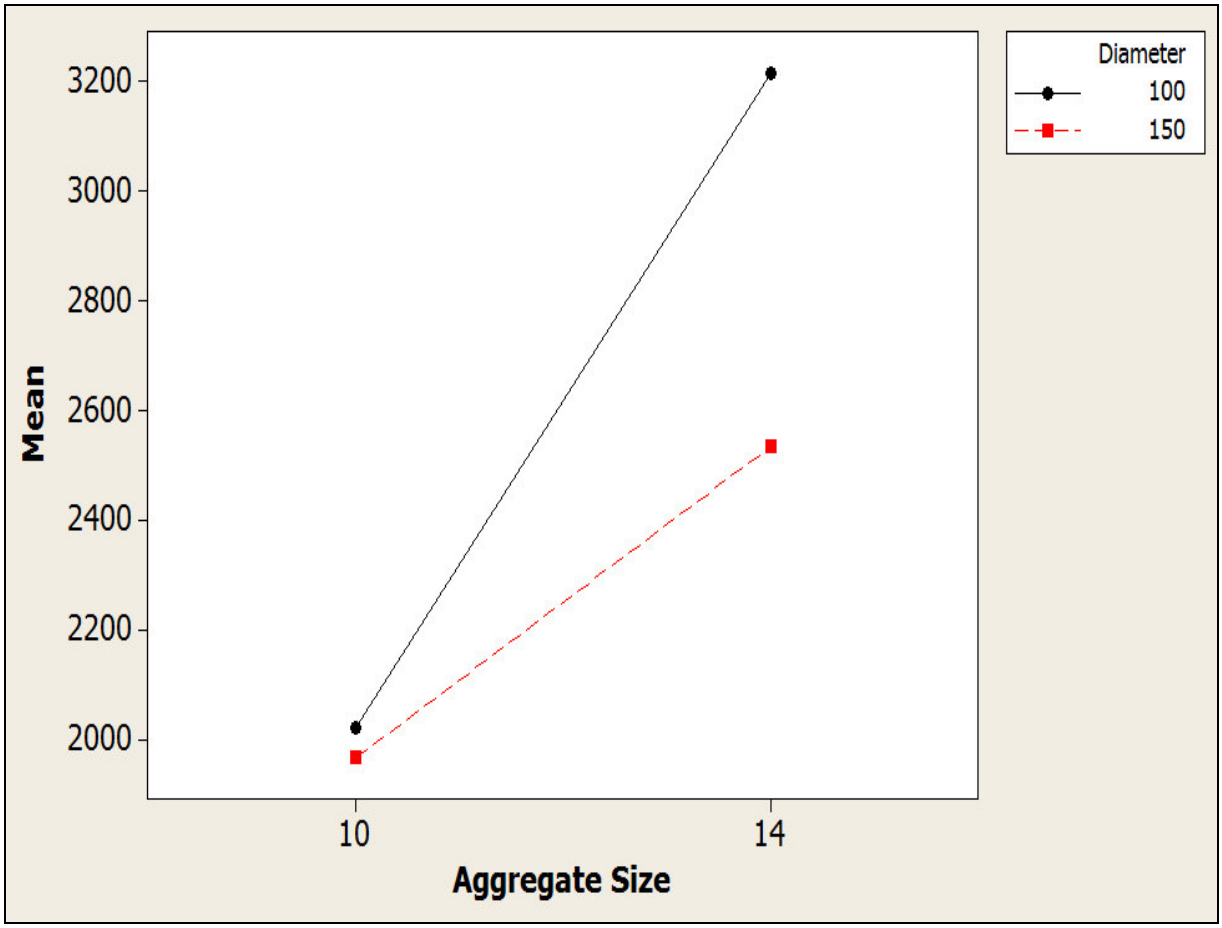

Figure 4.7 Effect of interaction between aggregate size and specimen diameter on the resilient modulus

Figure 4.8 showed the interaction between the aggregate size and compaction method. It is clear that that effect of the compaction method is much larger for the least coarse aggregate gradation than it is for the coarse aggregate gradation. This is probably due to the two different compaction method which yield two different types of aggregate orientation and packing.

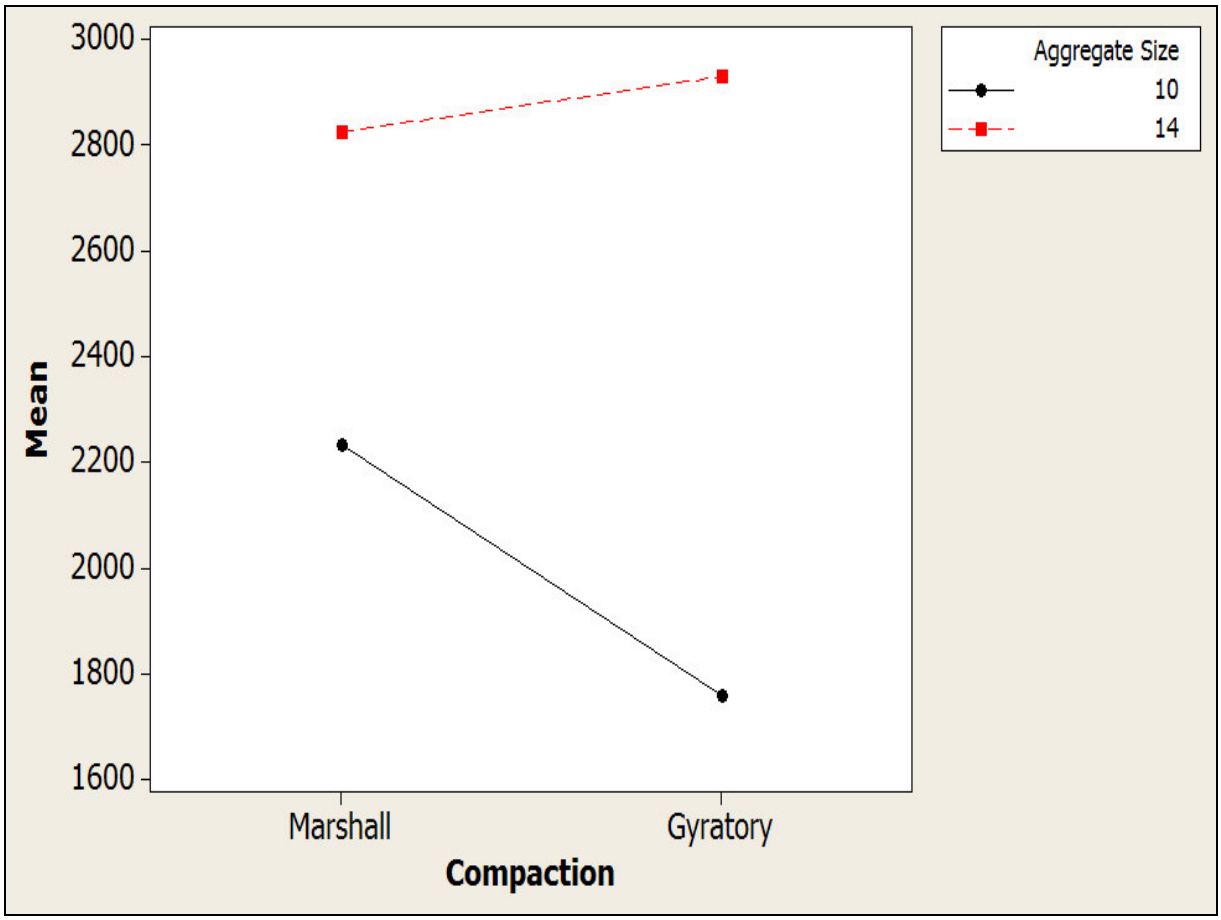

Figure 4.8 Effect of interaction between aggregate size and compaction method on the resilient modulus

Figure 4.9 showed the effect of the interaction between specimen diameter and thickness on the resilient modulus. It is clear that the effect of the diameter is pronounced for the thinner specimen while this effect is minute for the thicker specimen. Notice also that the thickness has a significant effect on the smaller diameter specimen while this effect is not much on the larger diameter specimen.

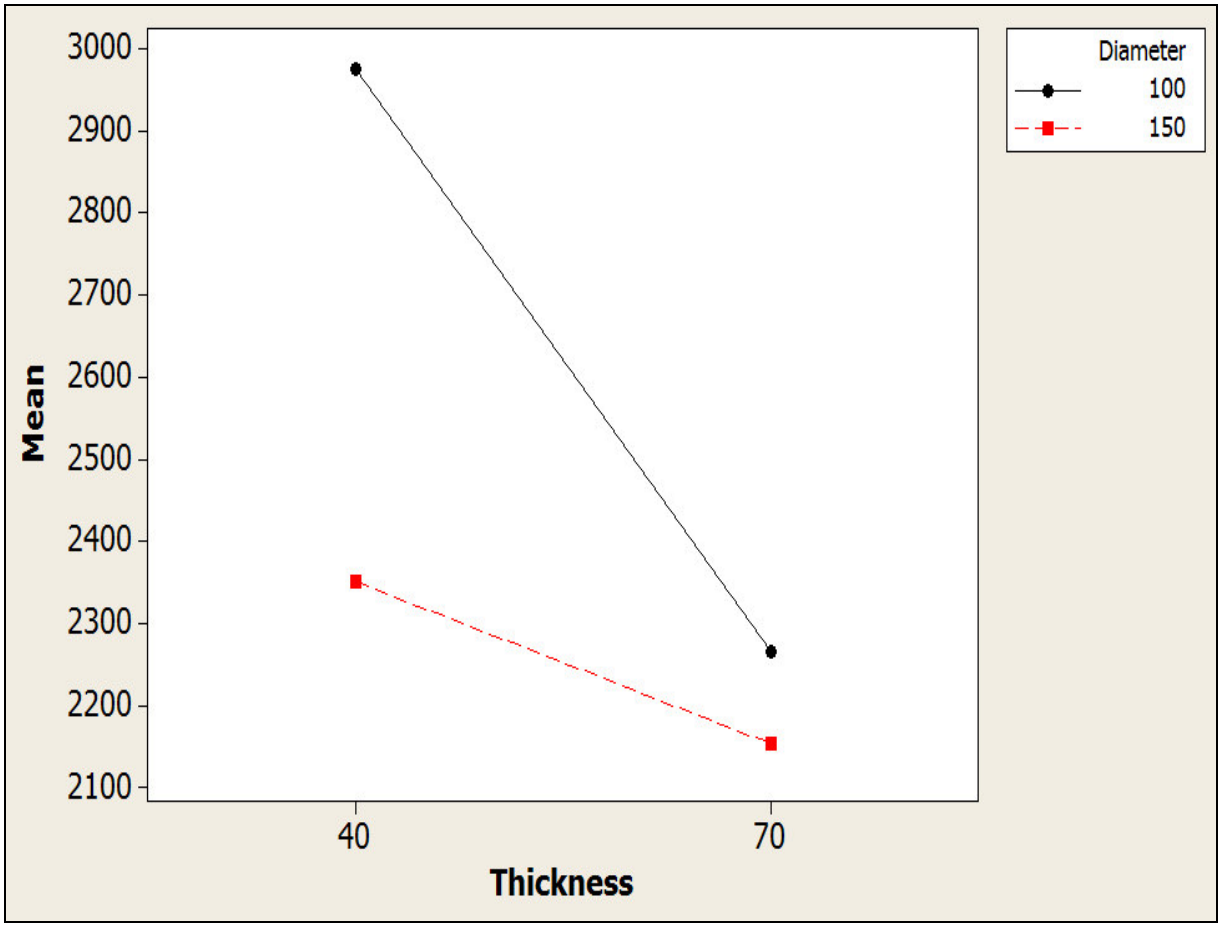

Figure 4.9 Effect of interaction between aggregate size and compaction method on the resilient modulus

Figure 4.10 shows the 3-way interaction between the specimen diameter, thickness and aggregate size. It is clear that the smallest dimension cylindrical specimen with coarser aggregate gradation has the highest resilient modulus. This could be the result of the confinement that occurred during compaction of a small-sized sample, with the strong aggregate interlock resulted from aggregate contact by using 14mm aggregate size. The lowest resilient modulus occurred when the diameter, thickness and aggregate size were 150mm, 70mm and 10mm respectively. This again could be attributed to the less confinement effect compared to smaller samples and to the high probability of the existence of micro-cracks which will lead to the reduction of resilient modulus. The smaller 10mm aggregate size also meant that there was less aggregate contact hence lower aggregate interlocking strength, resulting in a lower resilient modulus.

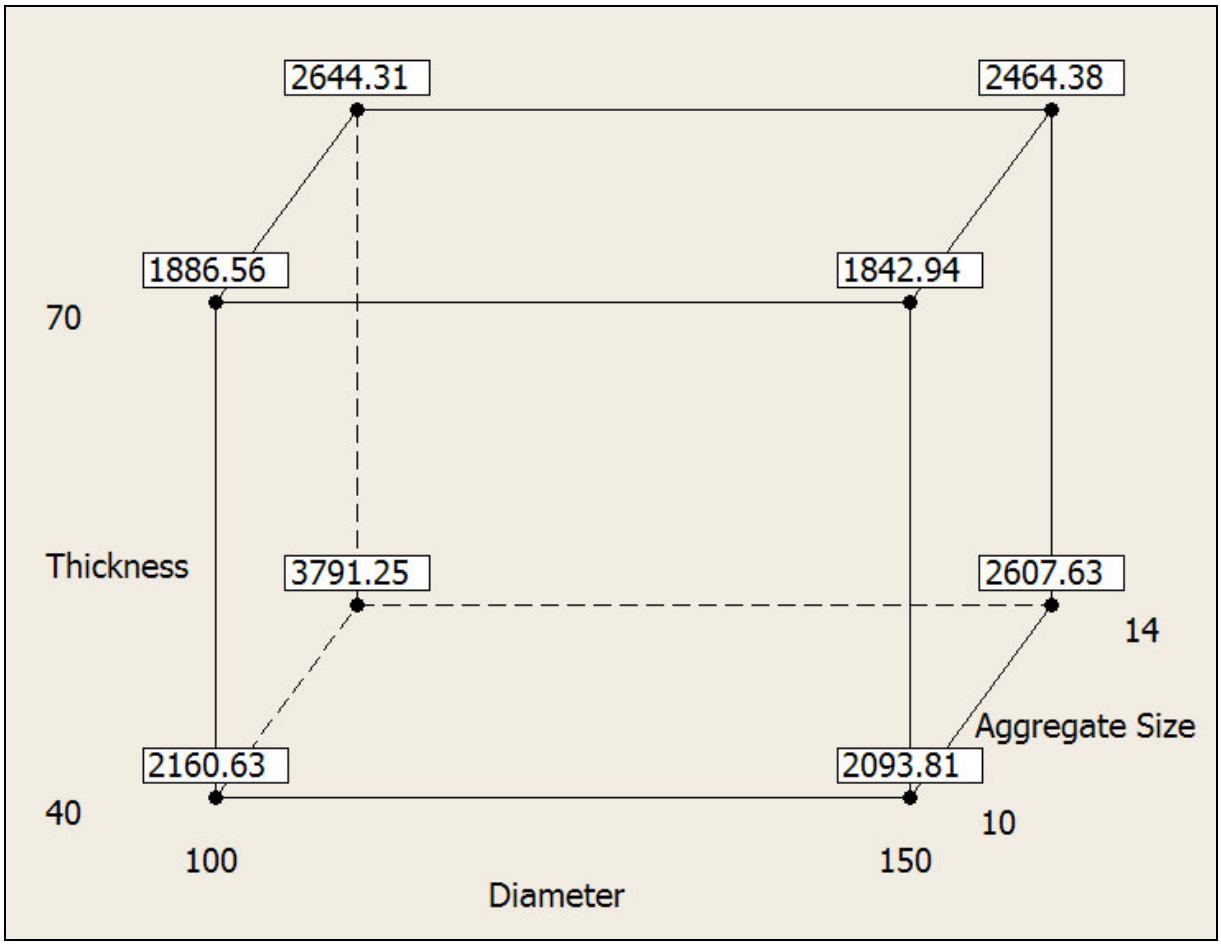

Figure 4.10 Cube plot of the 3-way interaction of specimen diameter, thickness and aggregate size

Figure 4.11 shows the effect of the interaction between specimen diameter and compaction method on the resilient modulus. It is obvious that the effect of the compaction method is marked for the smaller diameter specimen while this effect is very small for the larger diameter specimen.

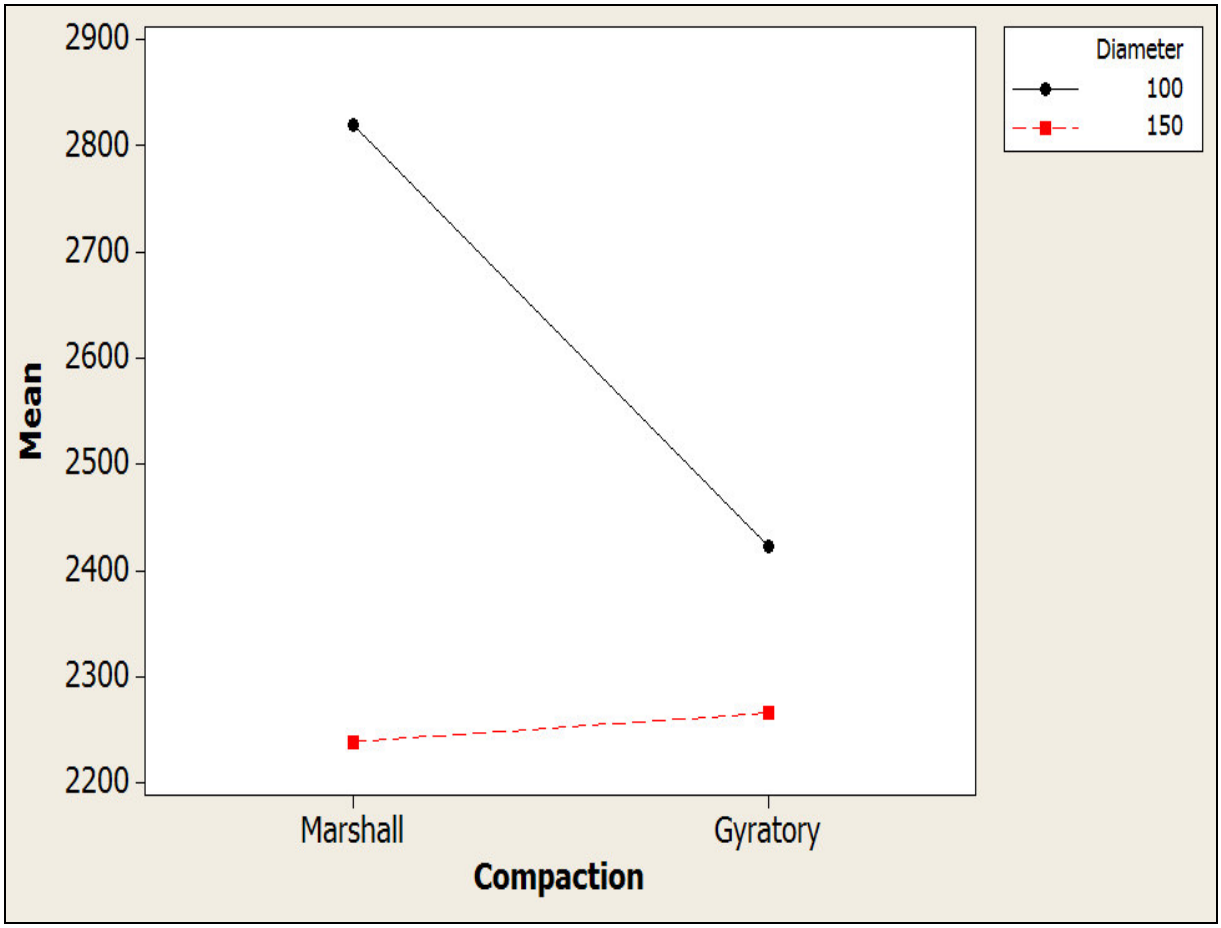

Figure 4.11 Effect of interaction between specimen diameter and compaction method on the resilient modulus

Figure 4.12 shows the interaction between the specimen thickness and aggregate size. It is obvious that the coarser gradation is providing slightly higher effect on the resilient modulus for the thin specimens (40 mm) and this effect is reduced for the thick specimens (70 mm).

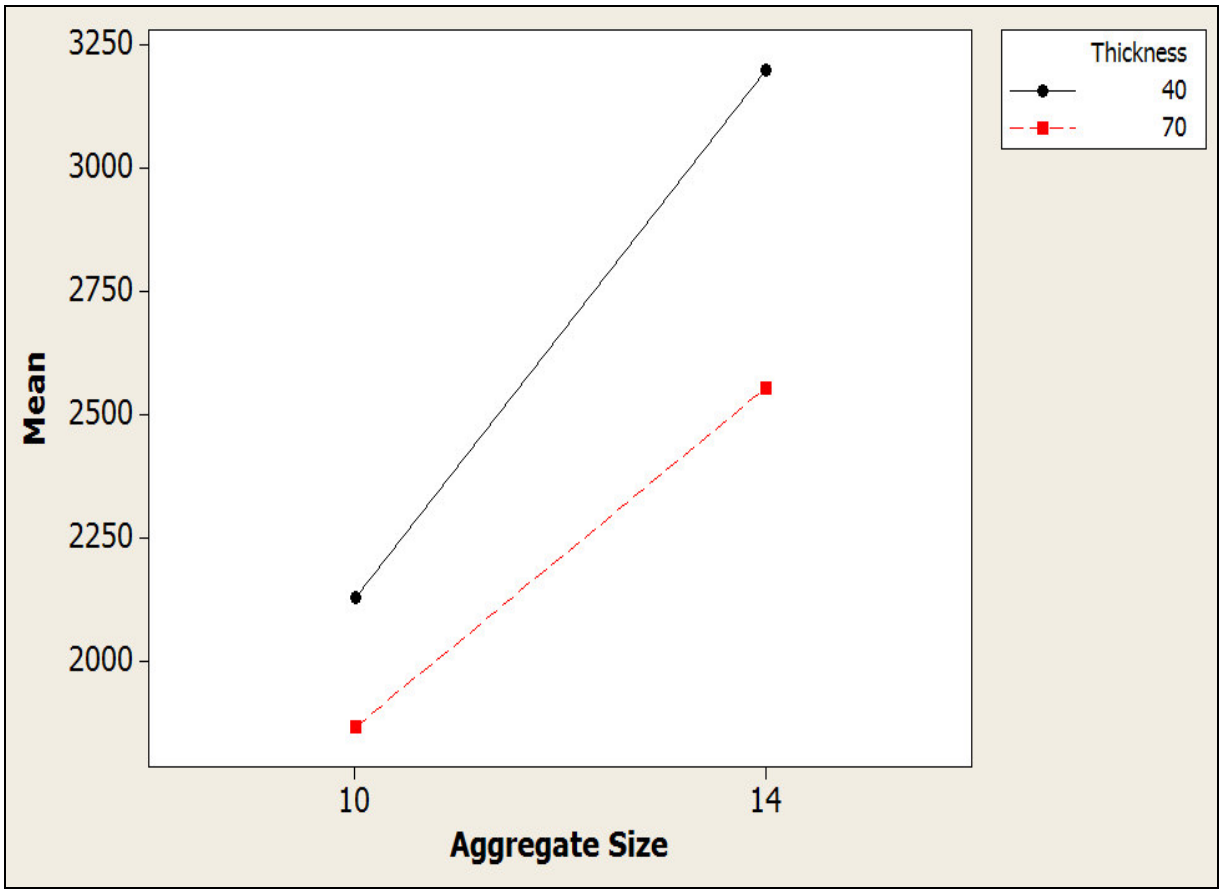

Figure 4.12 Effect of interaction between specimen thickness and aggregate size on the resilient modulus

Figure 4.13 shows the effect of the compaction method on the resilient modulus. It is evident that Marshall hammer produces specimens with a slightly higher resilient modulus than Gyropac. This could be due to the dynamic nature of Marshall hammer compaction and the different aggregate orientation and packing.

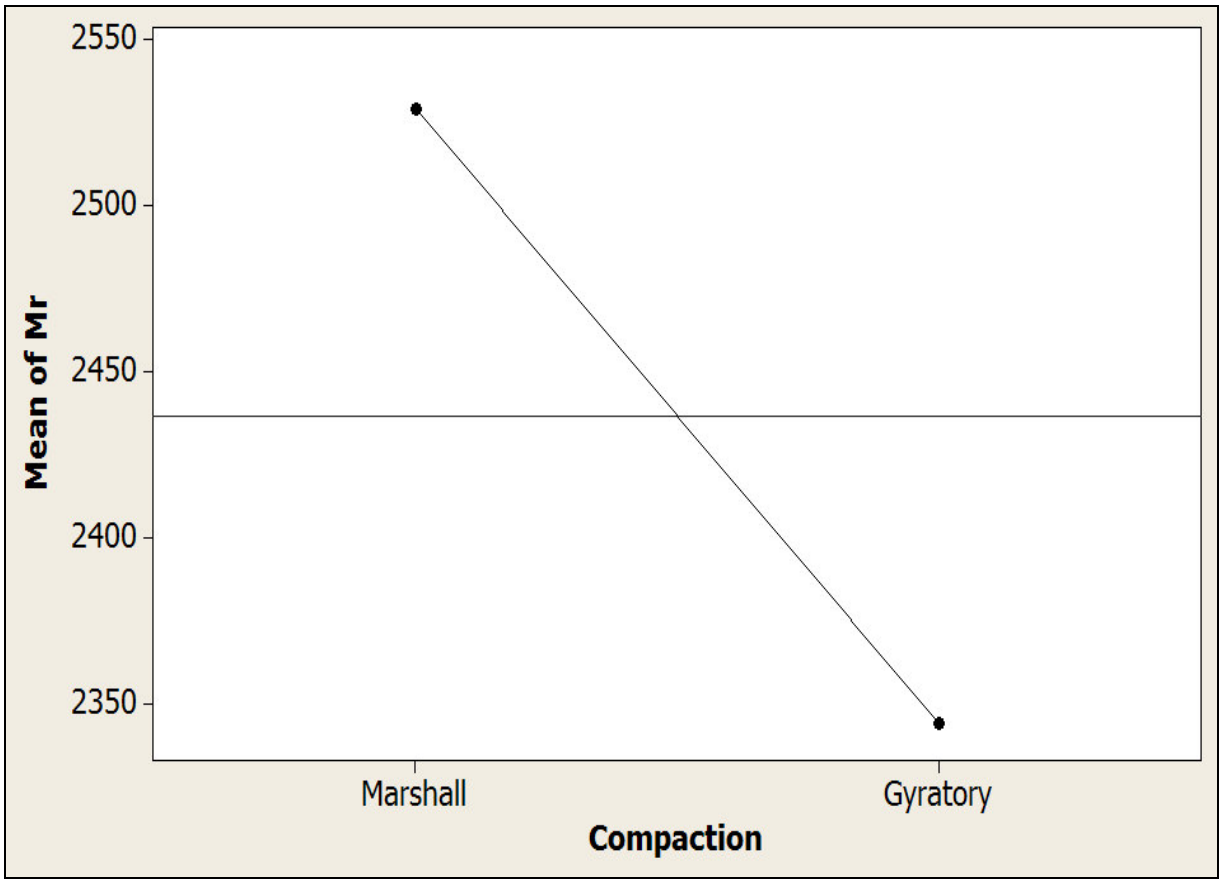

Figure 4.13: Effect of compaction method on the resilient modulus

Resilient Modulus Comparisons for Moulded and Cored Specimens

For some of the plots in the previous section, the degree of confinement for samples in different mould sizes led to samples with different resilient modulus. To determine the significance of the degree of confinement, three cylindrical samples of AC10 and three samples of AC14 which were cored from slabs were tested for their resilient modulus. These results were compared with samples prepared from moulds, and shown in Table 4.3.

For AC10 specimens the moulded samples had resilient modulus approximately 2.35 times larger than the cored samples. For the AC14 specimens this ratio is approximately two. This means that moulded samples do in fact have a much larger resilient modulus than cored samples.

Table 4.3 Comparison of the cored and moulded samples

	Cored samples				Moulded samples		
	1	2	3	**Average**	1	2	**Average**
AC10	796	838	960	**865**	1979	2094	**2037**
AC14	1171	1304	1451	**1309**	2824	2711	**2768**

The main effects and interactions plots in this section described the effect of one or more factors affecting resilient modulus. Through this it was learnt that proper measures are in place to create the best possible representative of resilient modulus for the insitu conditions.

The next two sections described the supplementary experiment on strain comparison and modulus comparison.

4.2 Strain Comparison

In this investigation, the comparison of the maximum tensile strain across the horizontal diametral of a sample either calculated or measured by means of closed form equations, the strain gauge and finite element modelling (FEM) is conducted. This is to investigate the accuracy of the widely used closed form equations shown as Equation 10 and Equation 11 below, and the accuracy of the FEM prediction, compared to the strain measured using a strain gauge.

$$\sigma_X = \frac{2P}{\pi dt} \qquad \text{Equation 10}$$

$$\varepsilon_p = \frac{\sigma_X (1+3\upsilon)}{S} 1000 \qquad \text{Equation 11}$$

Where σ_x = Maximum tensile stress (kPa)

P = Peak load (kN)

d = Diameter of specimen (m)

t = Thickness of specimen (m)

S = Stiffness modulus (MPa)

ε_p = Maximum tensile strain (micro strain)

The overview of this part of the research is that two cylindrical samples with thicknesses of 40mm and 70mm respectively were loaded diametrically to obtain two responses; the first is the maximum tensile strain read by the strain gauge, and the second is the peak load and stiffness modulus obtained by the testing software. The former was done by attaching two strain gauges on both flat face of the cylindrical specimen across the horizontal diametral, and the response recorded using a laptop. The latter was recorded and used in the closed form equations to calculate the maximum tensile stress and hence the maximum tensile strain. A replicate for each thickness was prepared and tested as well in order to generate a more accurate averaged result. To obtain maximum tensile strain that were comparable, the load and the stiffness modulus were kept at 750N and 1500MPa respectively.

The finite element modelling part of this investigation was completed using ABAQUS. The complete steps undertaken to create the model with the appropriate loadings and to view the response are shown in Appendix 1.

A half cylindrical model, shown in Figure 4.14, was used to model the actual cylindrical sample due to its simplicity in analysis. Two boundary conditions were specified; first was the strip of area fully constraint under the half cylinder to approximate the bottom platen during testing, and second was the flat area on the side that was constraint in all but the downward direction. The Poisson ratio and Young's modulus for the model were inputted as 0.4 and

1500MPa. Due to the contact area between the top platen and the sample the loading was converted to a pressure by dividing the load of 750N by the contact area, and the pressure was applied across the top strip area in the downward direction.

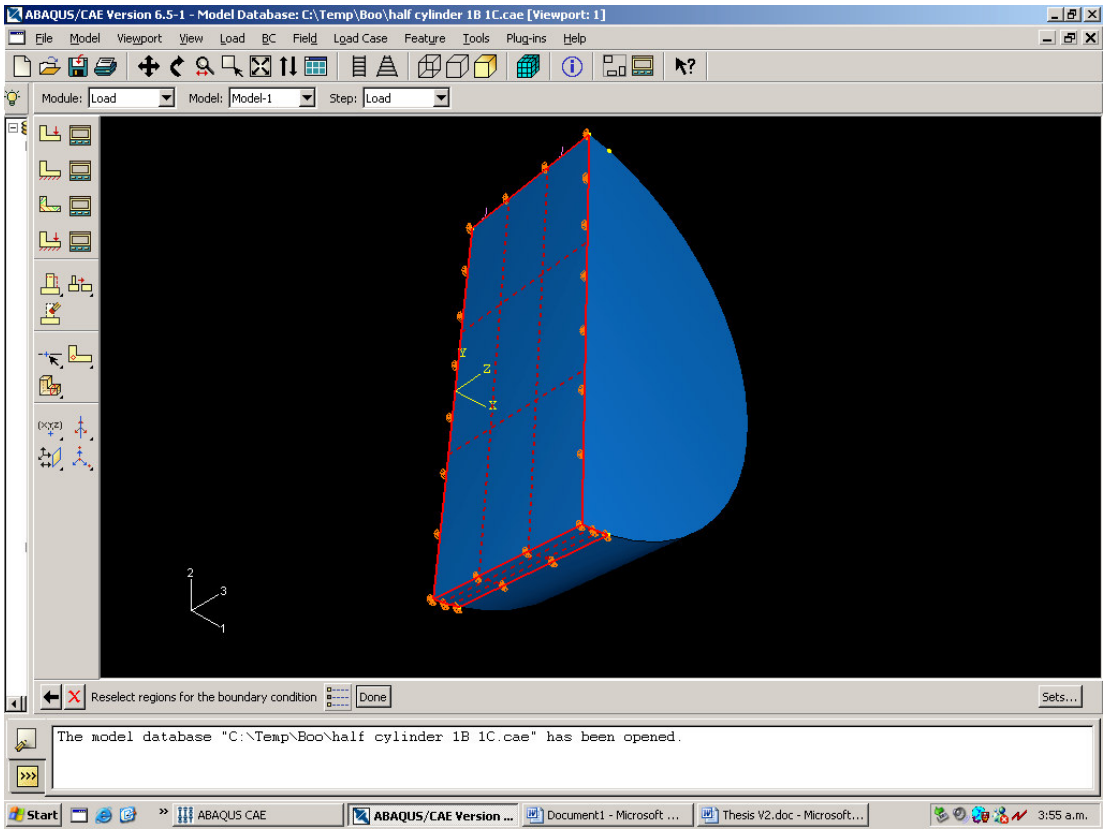

Figure 4.14 Half cylindrical model representation of the cylindrical sample, with the boundary conditions highlighted in red

The model was subjected to a static analysis and the maximum tensile strain was determined. This is done for model of a range of thicknesses between 40mm and 70mm.

The strain measured or predicted using the closed form equations, FEM and strain gages are plotted in Figure 4.15. The measurements of bulk specific gravity and air voids for the samples used in this investigation are included in Appendix 2.

Referring to all three trends, it can be seen that there is a high degree of variability among all three strain calculation and measurement.

As mentioned, the recommended thickness for 100mm diameter specimen is 50mm. Looking at Figure 4.15, at 50mm the closed form solution and the FEM predicted strain are approximately 50 microstrain and 100 microstrain more than the actual strain measured by the strain gage respectively.

Table 4.3 shows the percentage differences of FEM prediction and closed form solutions relative to the strain gage measurement for sample thicknesses varying from 40mm to 70mm. Note that the smallest percentage difference is 25.8%, and this occurred at 40mm and 70mm sample thicknesses. FEM predicted strain that was closer to the measured strain for the 40mm thick specimen and closed form solution predicted strain closer to the measured strain for the 70mm thick specimen.

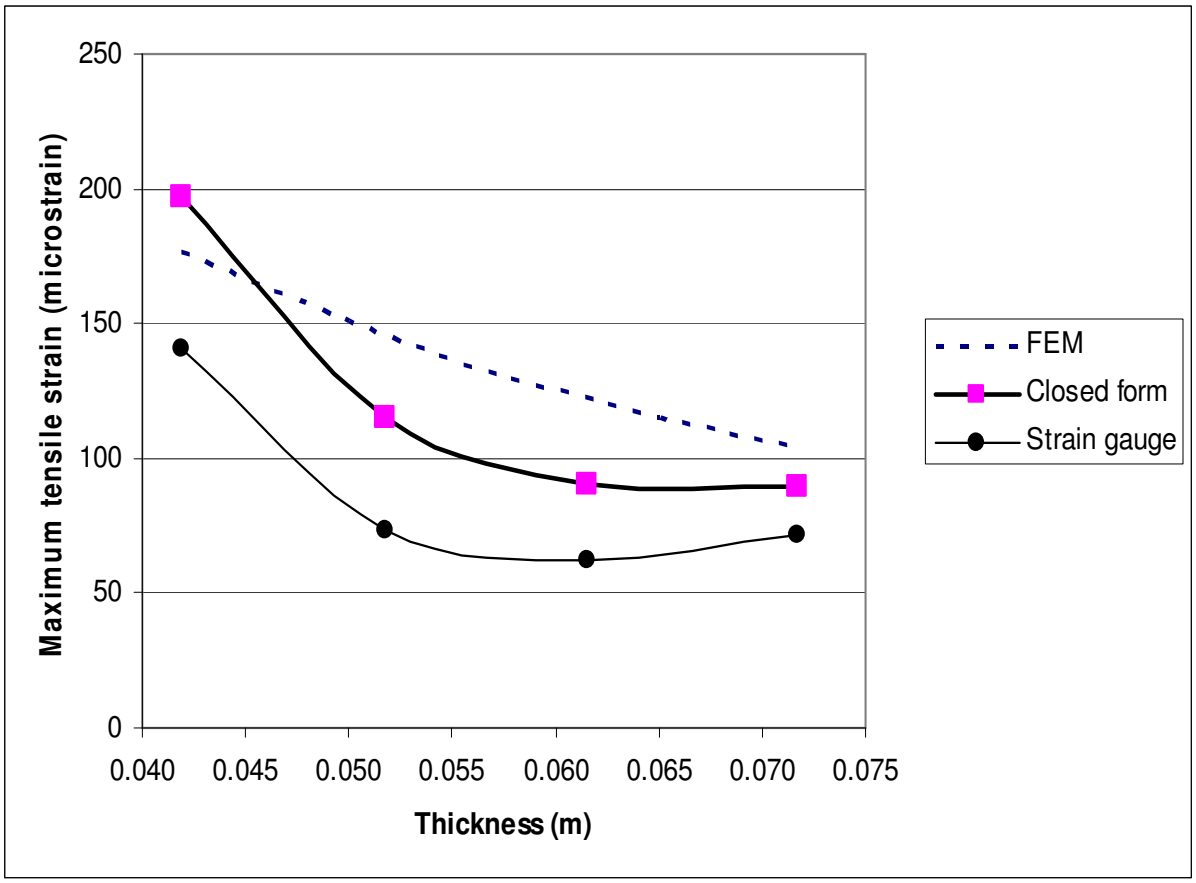

Figure 4.15 Comparison plot of the three strain derived from closed form equations, FEM and strain gages

Table 4.4 Percentage error of closed form solution and FEM compared with strain gage measurement

	Percentage Difference							
	0.0419m thick		0.0518m thick		0.0615m thick		0.072mm thick	
	Closed form	FEM	Closed form	FEM	Closed form	FEM	Closed form	FEM
Strain gauge	39.96%	25.82%	58.28%	106.39%	45.64%	100.79%	25.84%	46.05%

This investigation suggested that although the percentage difference relative to the measured strain, the closed form equation is still a more accurate method than FEM. However, according to Figure 4.15, the closed form equations are more accurate only for specimens with thicknesses greater than 55mm.

4.3 Modulus Comparison

In this part of the investigation the dynamic complex modulus, flexural modulus, and resilient modulus were determined and compared for AC10 and AC14 samples according to their respective standards, provided that the air voids percentage is about 5%. This is done to see if there was any relationship between these three moduli.

To allow comparable moduli, all three modulus tests were tested at loading frequencies of 1, 4 and 16 Hz for asphalt specimens prepared using AC10 and AC14 aggregate gradation. Figure 4.16 and 4.17 illustrated the plots for AC10 and AC14 respectively.

It was observed that for AC10 all three moduli were almost parallel to each other, or translated in the upwards vertical direction. The dynamic modulus was found to be a factor of 1.26 times that of the resilient modulus, and the flexural modulus was found to be a factor of 1.17 times that of the resilient modulus.

Looking at Figure 4.17 for AC14 it could be observed that there is no obvious pattern. All three moduli responded differently to different loading frequencies. The chart shown is not as simplistic as the one for AC10.

This part of the research showed that it is possible to predict either three of the modulus given that only one is known for smaller maximum nominal aggregate size.

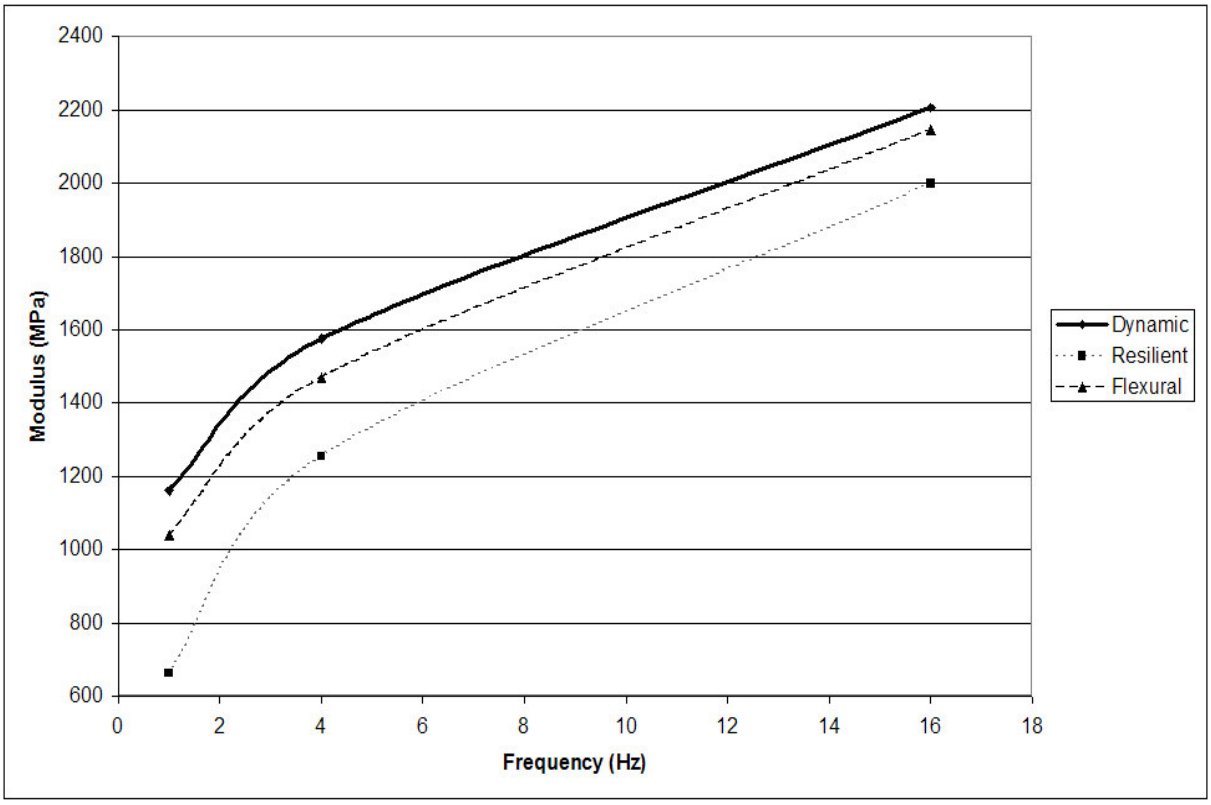

Figure 4.16 Modulus comparison for AC10 aggregate gradation

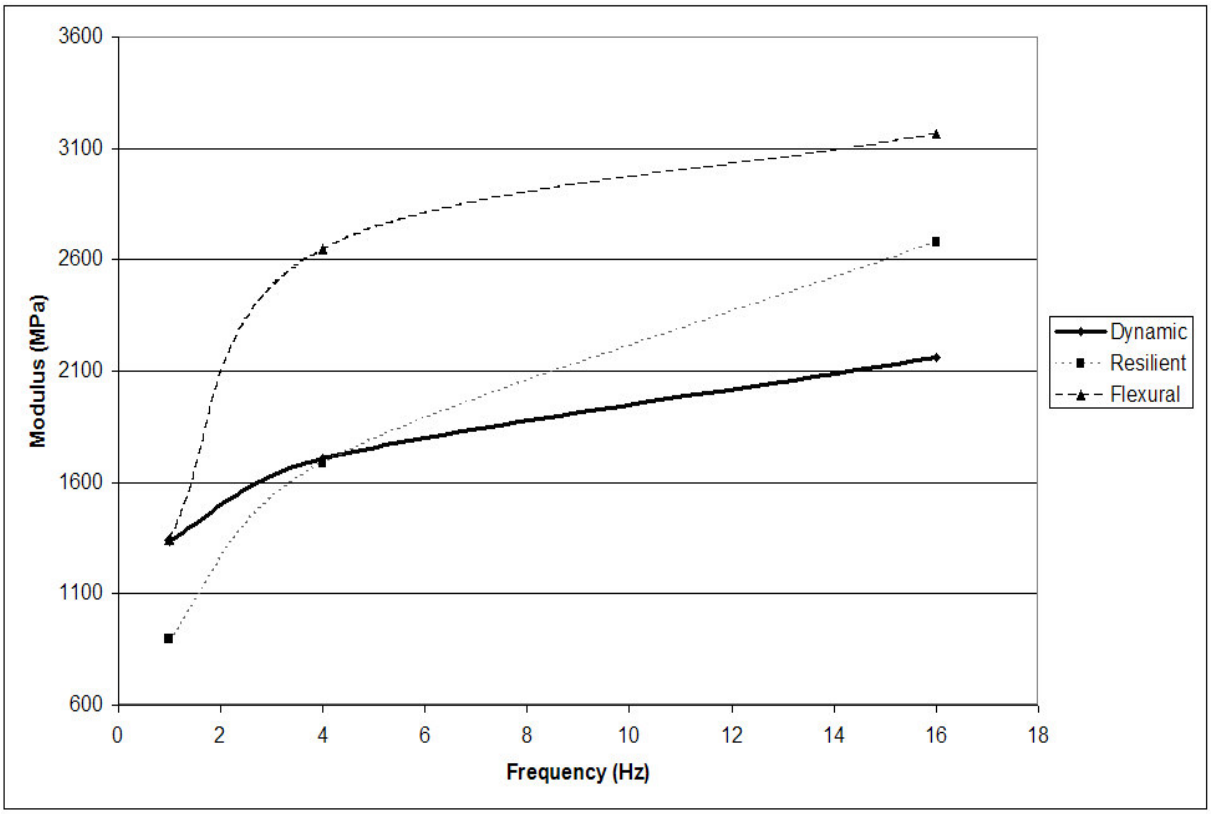

Figure 4.17 Modulus comparison for AC14 aggregate gradation

Chapter 5

Conclusions and Recommendations

The results of the 2k-1 half factorial experimental design of the factors affecting the resilient modulus of a cylindrical sample subjected to a resilient modulus test by indirect tensile method had shown that not only most of the individual factors were influential, the interaction between these factors were also critical. It was found that the maximum nominal aggregate size was the most significant factor influencing the resilient modulus, followed by load duration, specimen thickness, and specimen diameter. The most significant 2-level interaction was the diameter-aggregate size interaction, and the most significant 3-level interactions was the diameter-thickness-aggregate size interaction. This means that the geometry of the specimen size for a resilient modulus test is critical for it to be a representative of insitu condition.

Another finding for the investigation was that the effect of the confinement during compaction for 100mm diameter and 40mm thick specimens were large. This highlights the needs to find a suitable geometry for a resilient modulus test with a small confinement effect.

The strain comparison suggested that the closed form equations were indeed a suitable approach to determine maximum horizontal strain during a resilient modulus test.

The modulus comparison suggested that it is possible to predict either resilient, complex and flexural modulus given that only one of them is known for AC10 specimens.

References

Brown, E. R. and C. E. Bassett,1990. Effects of maximum aggregate size on rutting potential and other properties of asphalt-aggregate mixtures. *Transportation Research Record (1259): 107-119.*

Huang, Y.H. 1993. Pavement Analysis and Design, *Prentice Hall Inc*.

Kandhal, P.S and E.R. Brown 1990. Comparative evaluation of 4-inch and 6-inch diameter specimens for testing large stone asphalt mixes. *Serviceability and Durability of Construction Materials – Proceedings of the First Materials Engineering Congress* Part 1, Aug 13-15 1990.

Lim, C.T. and Tan, S.A et al 1995. Specimen size effects on the diametrical mechanical testing of cylindrical asphalt mixes. *Journal of Testing and Evaluation, Volume 23: 436-441.*

Hugo, F. and W.J. Schreuder 1993, Effect of sample length on indirect tensile test parameters. *Proceedings of the Association of Asphalt Paving Technologists Technical Sessions.* Volume 62 page 422-449

Roberts, Kandhal, Brown, Lee and Kennedy 1996, Hot Mix Asphalt materials, mixture design and construction. *NAPA Research and Education Foundation.*

Harvey, J., K. Eriksen, et al 1994. Effects of laboratory specimen preparation on aggregate-asphalt structure, air-void content measurement, and repetitive simple shear test results. Transportation Research Record (1454): 113-122

Fwa, T.F., B.H. Low, et al 1993. Compaction of asphalt mixtures for laboratory testing: Evaluation based on density profile. Journal of Testing and Evaluation, Volume 21: 414-421.

Hartman, A.M, M.D. Gilchrist, et al. 2001. Effect of mixture compaction on indirect tensile stiffness and fatigue. Journal of Transportation Engineering, Volume 127, issue 5, page 370-378.

Button, J.W., D.N. Little, et al 1994. Correlation of selected laboratory compaction methods with field compaction. Transportation Research Record, Volume 1454 page 193-201.

Bonnot, J. 1997. Selection and use of the procedures for laboratory compaction of bituminous mixtures. Performance related test procedures for bituminous mixtures, page 52-73.

Montgomery, D.C. 2001. Design and Analysis of Experiments. John Wiley and Sons Inc

Montgomery, D.C. and G.C. Runger 2003. Applied Statistics and Probability for Engineers, Wiley

Design Expert version 6, State-Ease Inc.2021 East Hennpin Ave., Suite 480, Minneapolis, MN 55413

Appendix 1

Determination of the Compacting Temperature

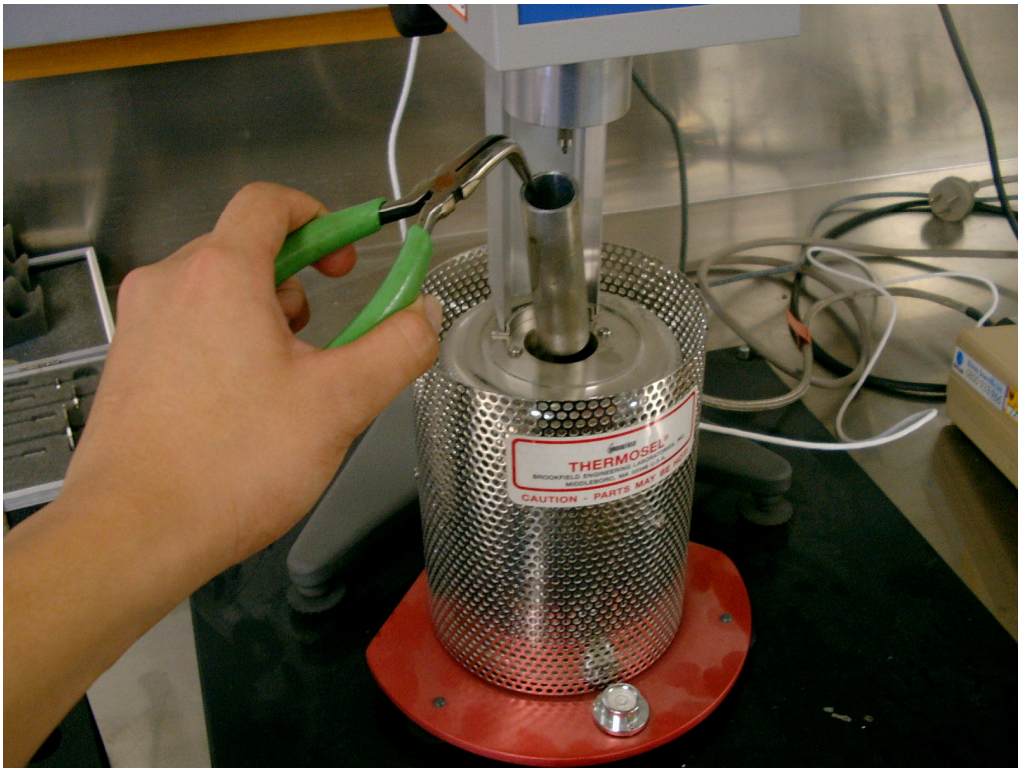

Figure A1.1 Placing the sample container into the thermo-container

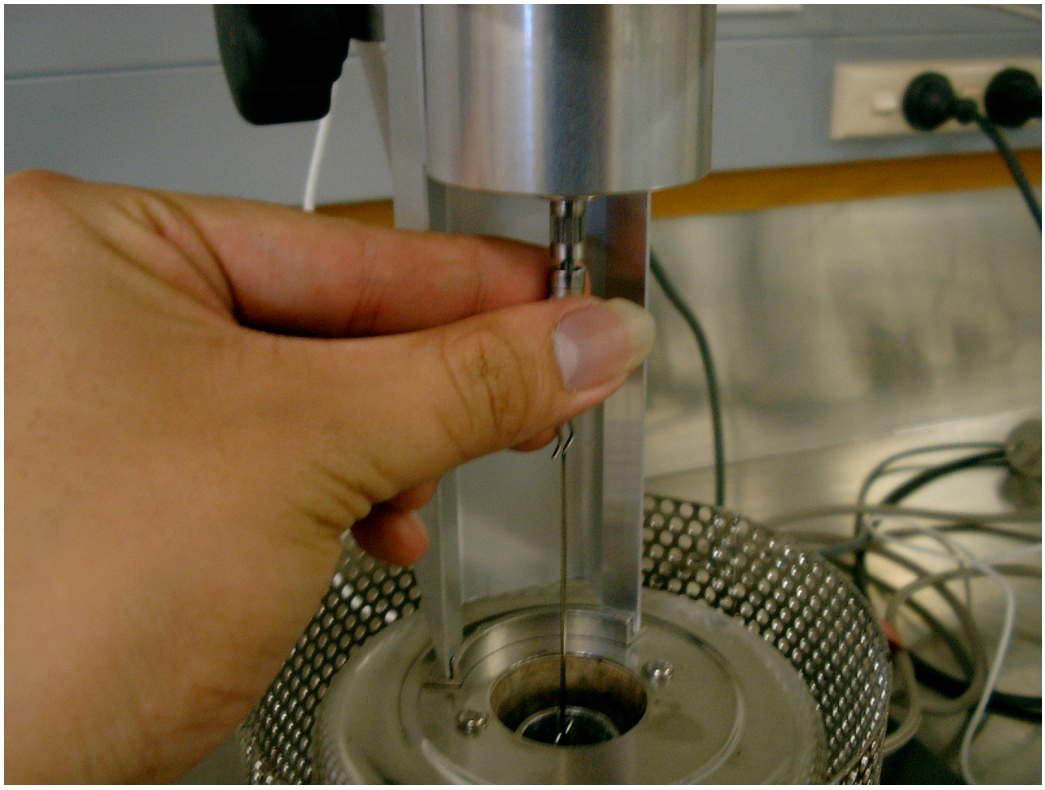

Figure A1.2 Inserting the spindle

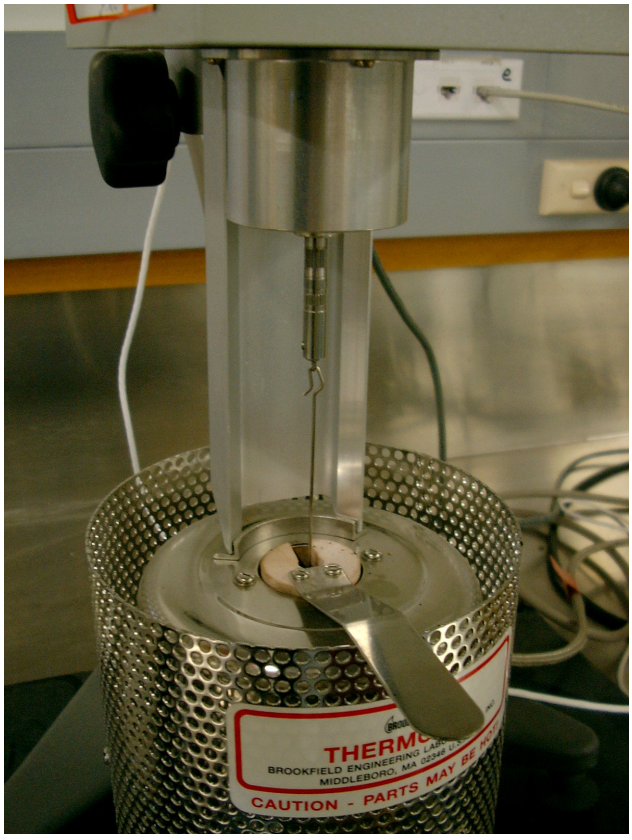

Figure A1.3 Placing the lid to avoid bitumen splashing

Determination of the Maximum Specific Gravity, G_{mm}

Figure A1.4 Sample are separated out so that the finer aggregate portions are not larger than 6mm

Figure A1.5 Using a mallet, gently tap on the pycnometer to help with the air bubbles removal

Figure A1.6 Inverting the pycnometer several times until no more bubbles can be observed

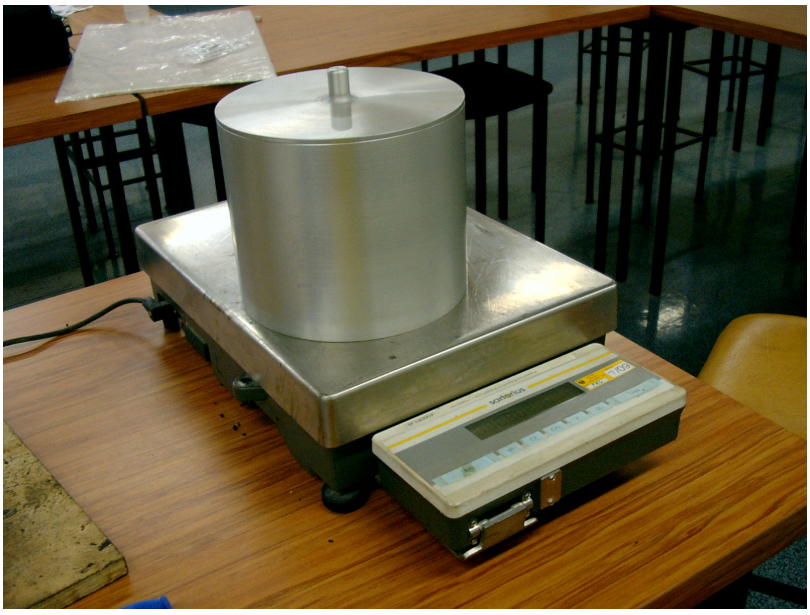

Figure A1.7 Measuring the mass of the pycnometer, lid, sample and water

Using ABAQUS

To make the half cylindrical model, a part of half cylindrical is created by specifying the cross-section of the model as shown in Figure A1.8. After sketching the cross-section, extrude the cross-section by specifying the thickness of the model. The shape of the model is then obtained as Figure A1.9.

To create the area strip where the pressure is applied, first the curved edges are partitioned and the curved face of the model is partitioned according to the partitioned edges (Figure A1.10). Then the material properties of asphalt sample are inputted, creating an asphalt sample section and assigning it to the model.

Boundary conditions were specified in Figure A1.11 as the area highlighted in red. The flat side of the model were constrained in all but the downward direction, and the bottom of the sample was constrained in all direction.

The model now needs to be meshed. Figure A1.12 showed the appearance of the model after the hexagonal meshing. After submitting the model to analysis, the shape of the deformed model can be seen in Figure A1.13. To get a reading for the maximum tensile strain in the middle of the sample, a path highlighted in red was created (Figure A1.14) so that the maximum tensile strain can be plotted along the path (Figure A1.15).

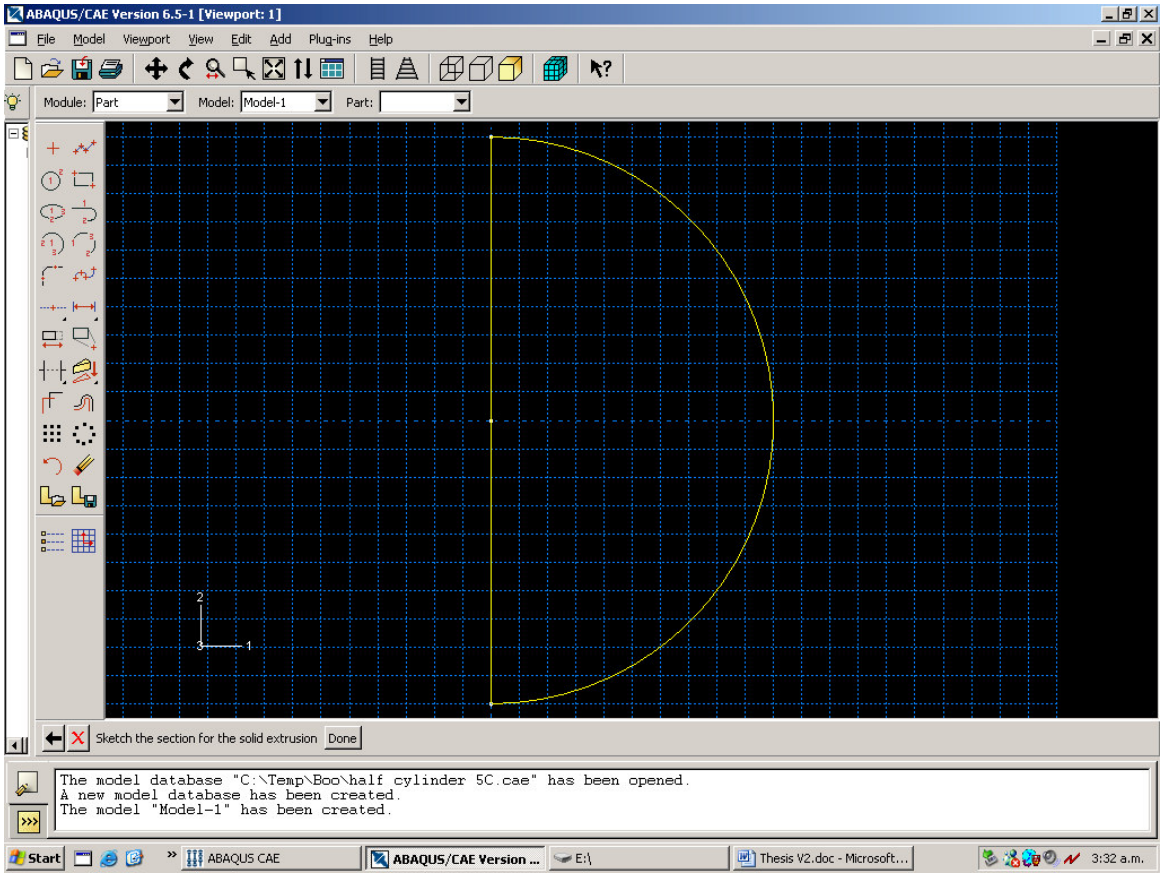

Figure A1.8 Creating the model by first specifying the cross-section of the model

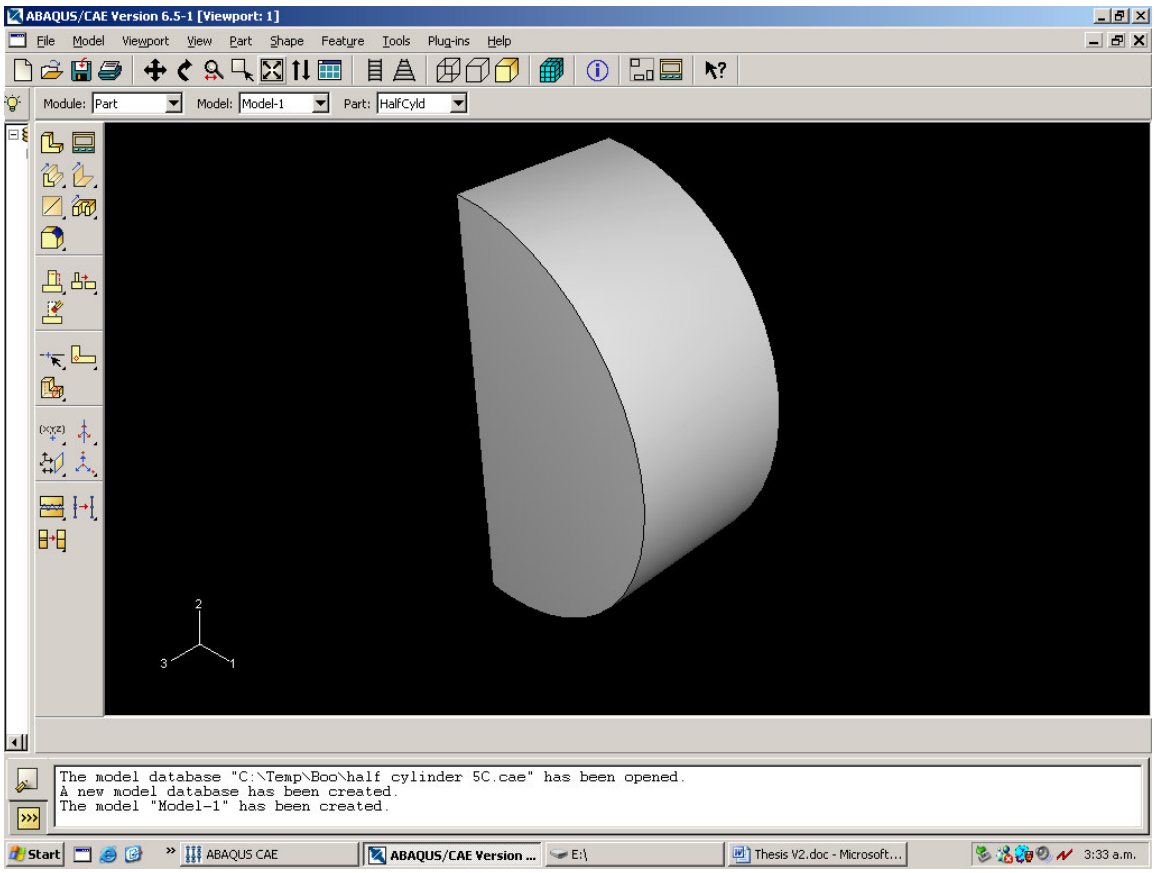

Figure A1.9 Shape of model

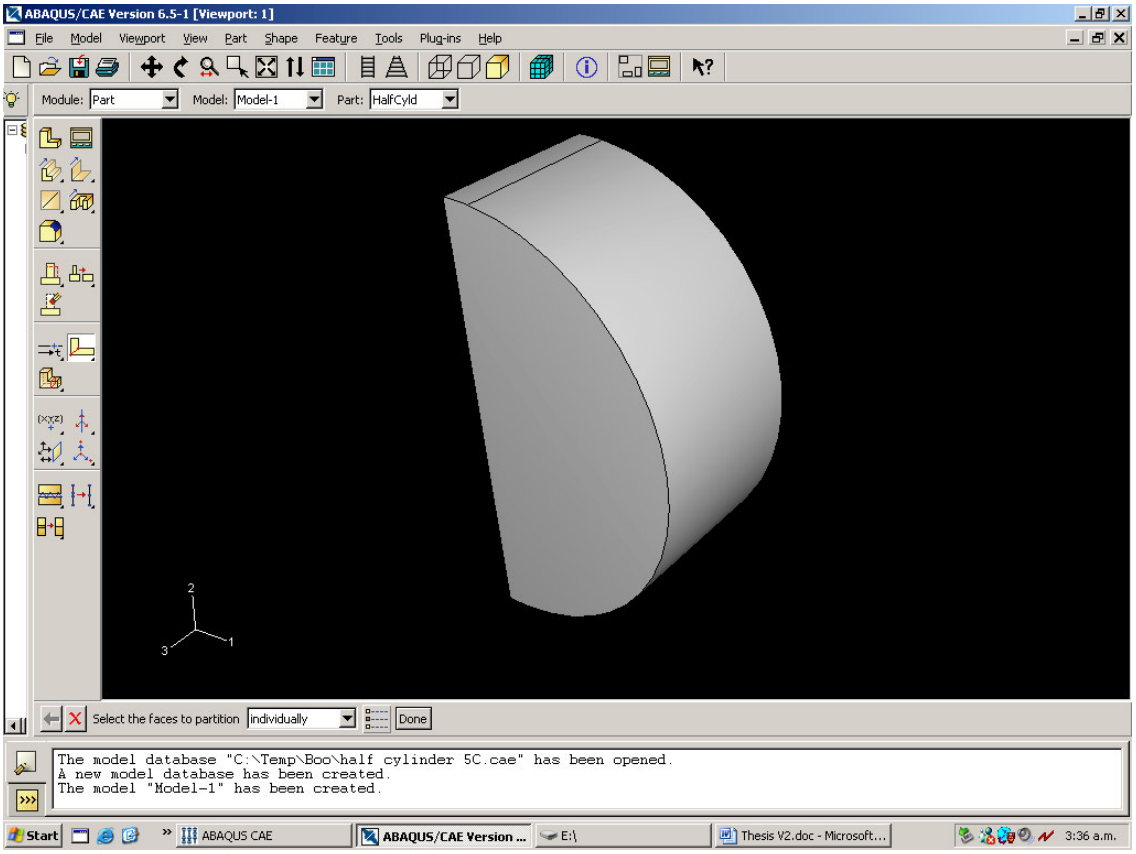

Figure A1.10 Model with partitioned curved face for loading and boundary condition

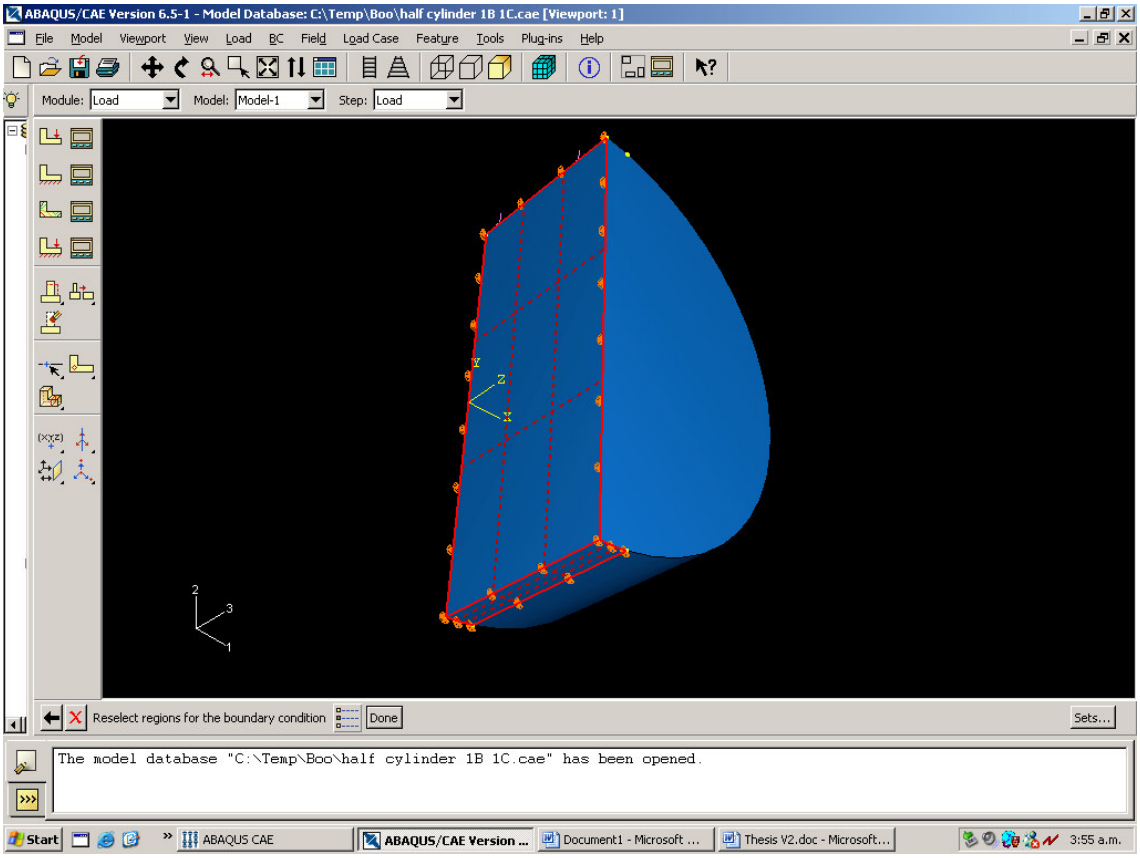

Figure A1.11 Boundary conditions are highlighted in red

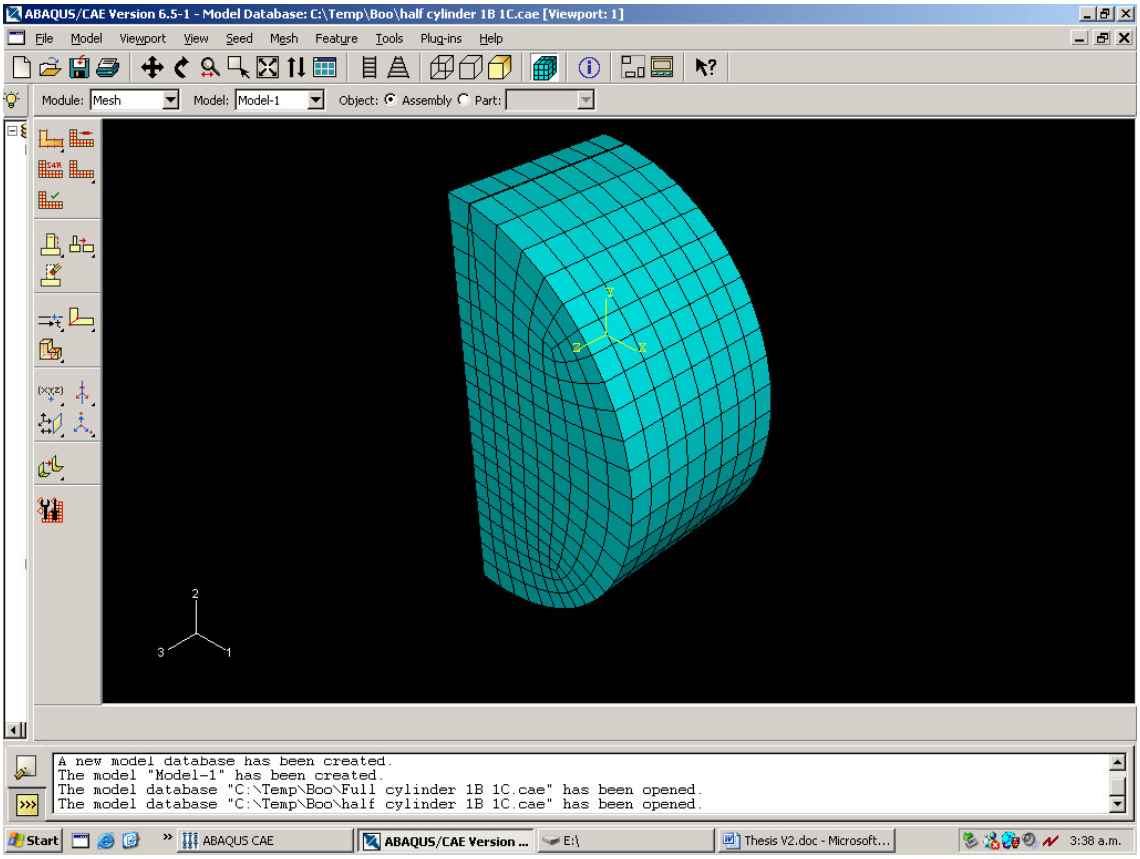

Figure A1.12 Hexagonal meshing of the model

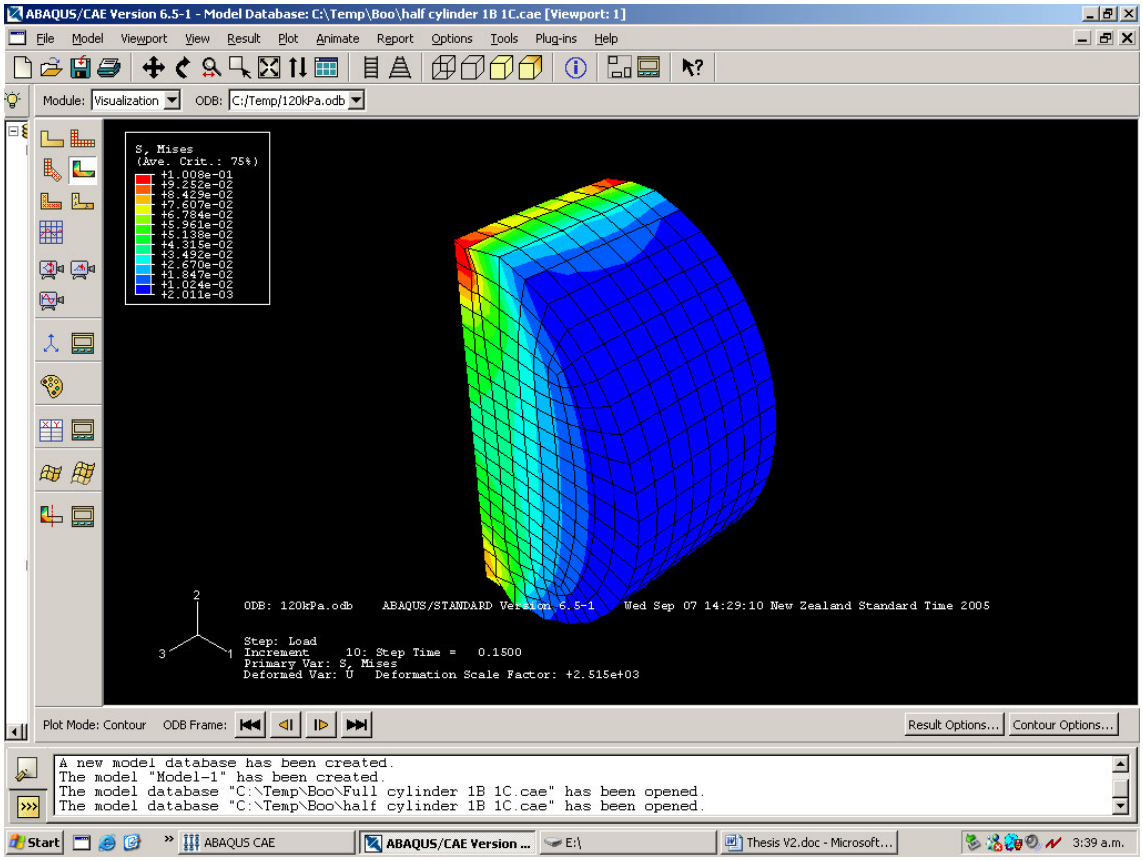

Figure A1.13 Visualisation of the deformed model

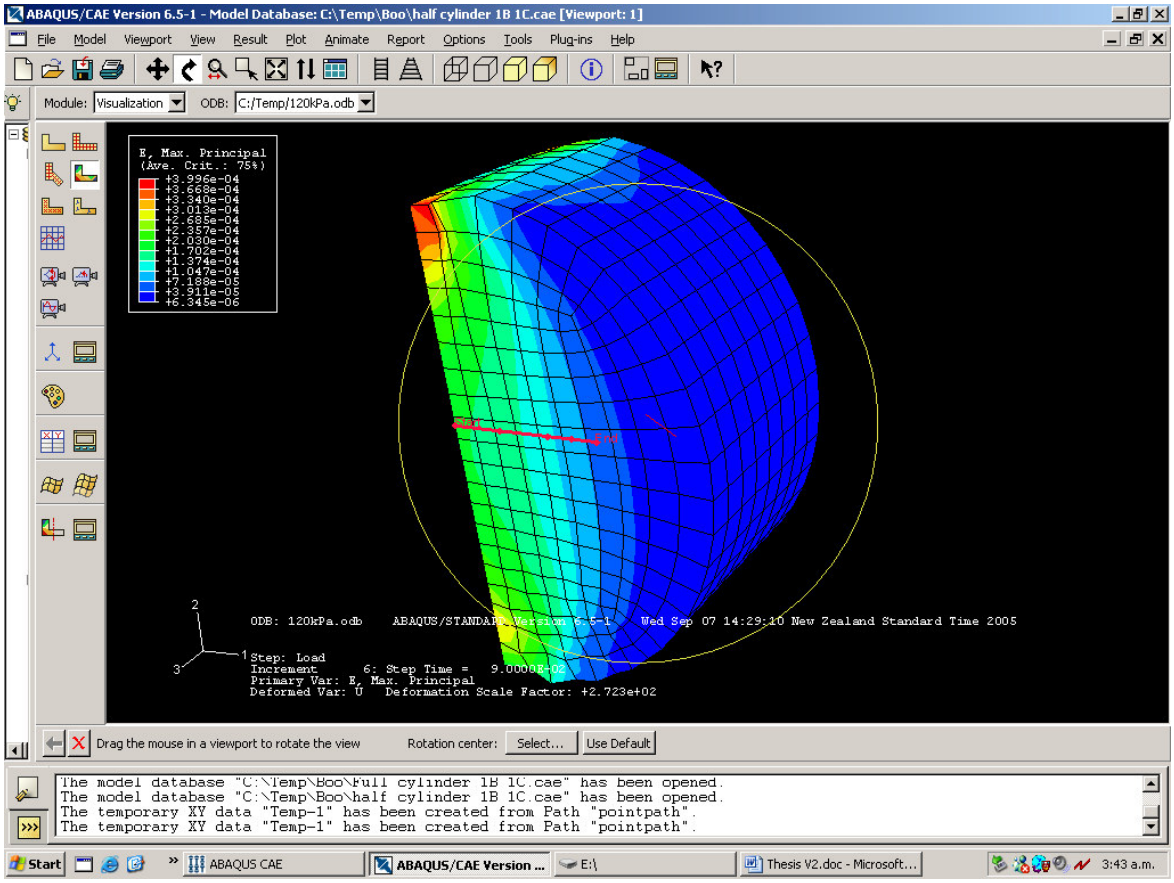

Figure A1.14 Deformed contour displaying the path highlighted in red

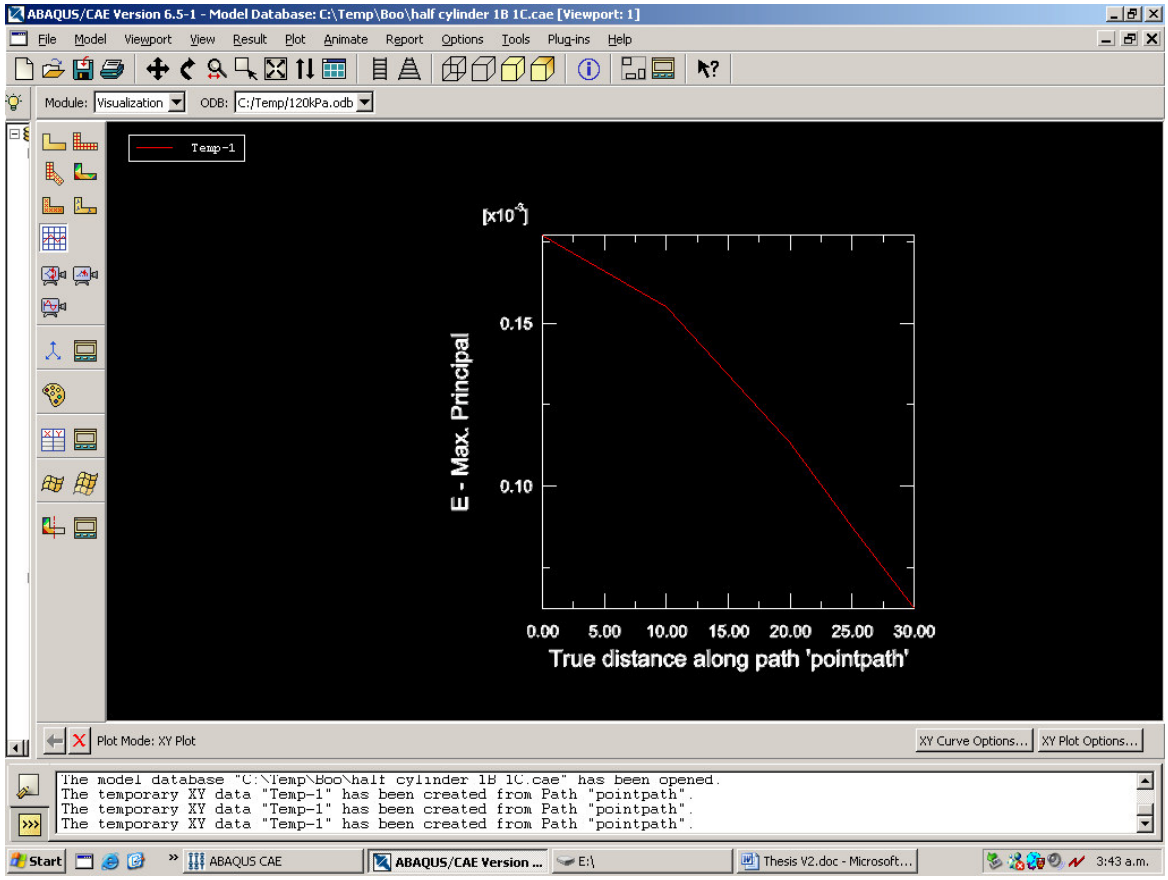

Figure A1.15 Plot showing the maximum tensile strain along the path

Appendix 2

Compaction Curves Results

For 100mm Diameter, 40mm Thick specimens:

Table A2.1 Compaction curve values for AC10 aggregate gradation Gyropac compacted samples

No. of gyrations	Replicate 1							Replicate 2												
	Weight (g)	Comp Temp (°C)	Thickness (mm)	Comp Time	A	B	C	Weight (g)	Comp Temp (°C)	Thickness (mm)	Comp Time	A	B	C	G_{mb1}	G_{mb2}	$G_{mb(avg)}$	G_{mm}	%VA	Adj %VA
50	730	143	68.1	27-Jan	730.64	731.72	403.47	730	144	68.2	27-Jan	731.75	732.8	402.99	2.226	2.219	2.222	2.407	7.67	5.67
100	730	145	67.2	27-Jan	730.63	731.21	408.9	730.2	145	66.8	28-Jan	727.85	728.39	407.73	2.267	2.270	2.268	2.407	5.76	3.76
120	730	145	66.7	28-Jan	726.21	726.92	407.45	730	145	66.7	28-Jan	726.12	726.44	407.66	2.273	2.278	2.275	2.407	5.46	3.46

Table A2.2 Compaction curve values for AC10 aggregate gradation Marshall hammer compacted samples

No. of blows	Replicate 1						Replicate 2											
	Weight (g)	Comp Temp (°C)	Comp Time	A	B	C	Weight	Comp Temp (°C)	Comp Time	A	B	C	G_{mb1}	G_{mb2}	$G_{mb(avg)}$	G_{mm}	%VA	Adj %VA
30	730	144	10-Feb	727.45	727.64	411.4	730.2	145	10-Feb	727.62	727.96	410.54	2.300	2.292	2.296	2.407	4.60	5.00
50	730.3	145	11-Feb	728.28	728.45	417	730.2	145	11-Feb	730.21	730.36	417.02	2.338	2.330	2.334	2.407	3.02	3.42
75	730.2	145	15-Feb	728.94	729.12	420.75	730.1	145	10-Feb	729.02	729.24	420.12	2.364	2.358	2.361	2.407	1.91	2.31

For 100mm Diameter, 40mm Thick specimens:

Table A2.3 Compaction curve values for AC14 aggregate gradation Gyropac compacted samples

No. of gyrations	Replicate 1							Replicate 2											
	Weight (g)	Comp Temp (°C)	Thickness (mm)	Comp Time	A	B	C	Weight (g)	Comp Temp (°C)	Thickness (mm)	Comp Time	A	B	C	G_{mb1}	G_{mb2}	$G_{mb(avg)}$	G_{mm}	%VA
50	743	145	68.5	25-Jan	741.14	742.29	414.37	743	145	68.5	25-Jan	740.79	742.45	415.84	2.260	2.268	2.264	2.469	8.30
100	743	145	67.5	25-Jan	741.98	743.11	419.44	743	145	67.6	26-Jan	740.85	742.22	423.36	2.292	2.323	2.308	2.469	6.52
127	743	145	66.7	30-Mar	743.38	743.8	423.93	743	145	67.8	26-Jan	741.53	742.55	421.43	2.324	2.309	2.324	2.469	5.87

Table A2.4 Compaction curve values for AC14 aggregate gradation Gyropac compacted samples

No. of blows	Replicate 1						Replicate 2										
	Weight (g)	Comp Temp (°C)	Comp Time	A	B	C	Weight	Comp Temp (°C)	Comp Time	A	B	C	G_{mb1}	G_{mb2}	$G_{mb(avg)}$	G_{mm}	%VA
30	743.1	143	2-Jan	741.64	741.97	424.12	742.9	145	2-Feb	741.3	742	424.5	2.333	2.335	2.334	2.469	5.47
50	743.2	143	2-Feb	741.04	741.49	428.21	743	144	2-Feb	741.32	742.32	424.37	2.365	2.332	2.348	2.469	4.88
75	743	143	2-Feb	740.22	740.66	428.02	743.1	144	2-Mar	740.78	741.59	427.64	2.368	2.360	2.364	2.469	4.27

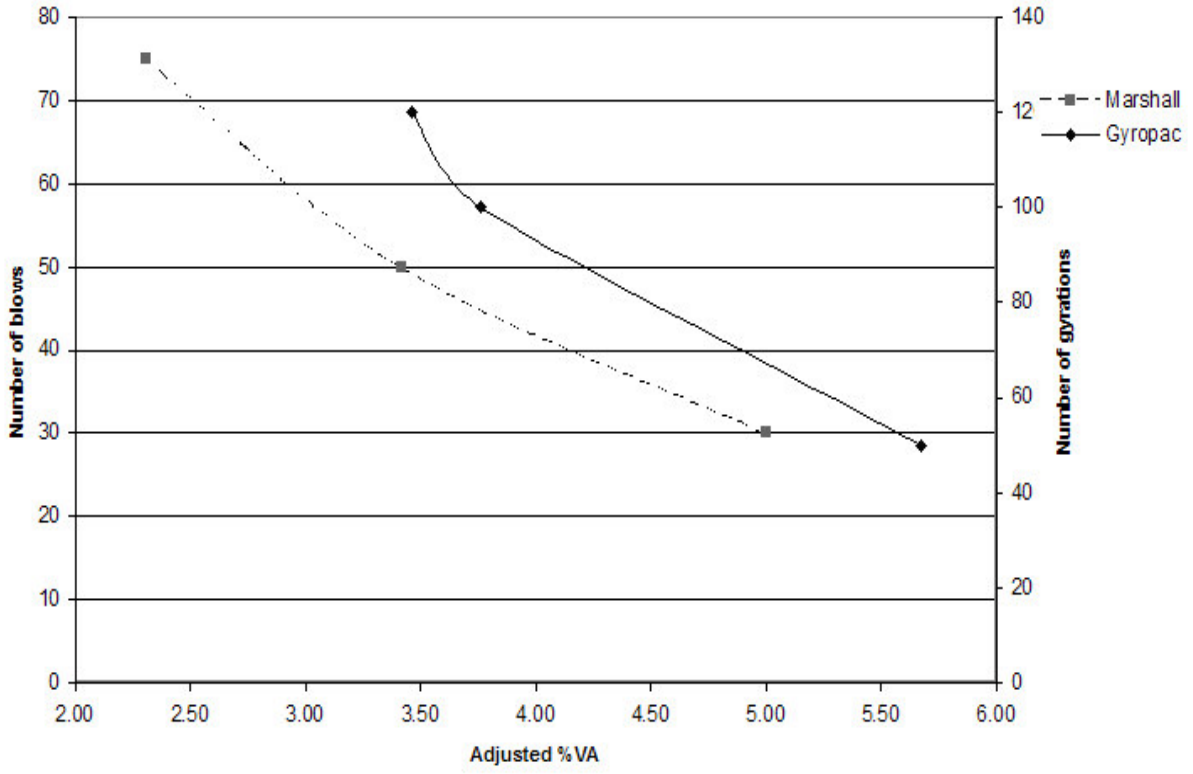

Figure A2.1 Compaction curve as plotted from Table A1.1 and Table A1.2 for Gyropac compacted specimens

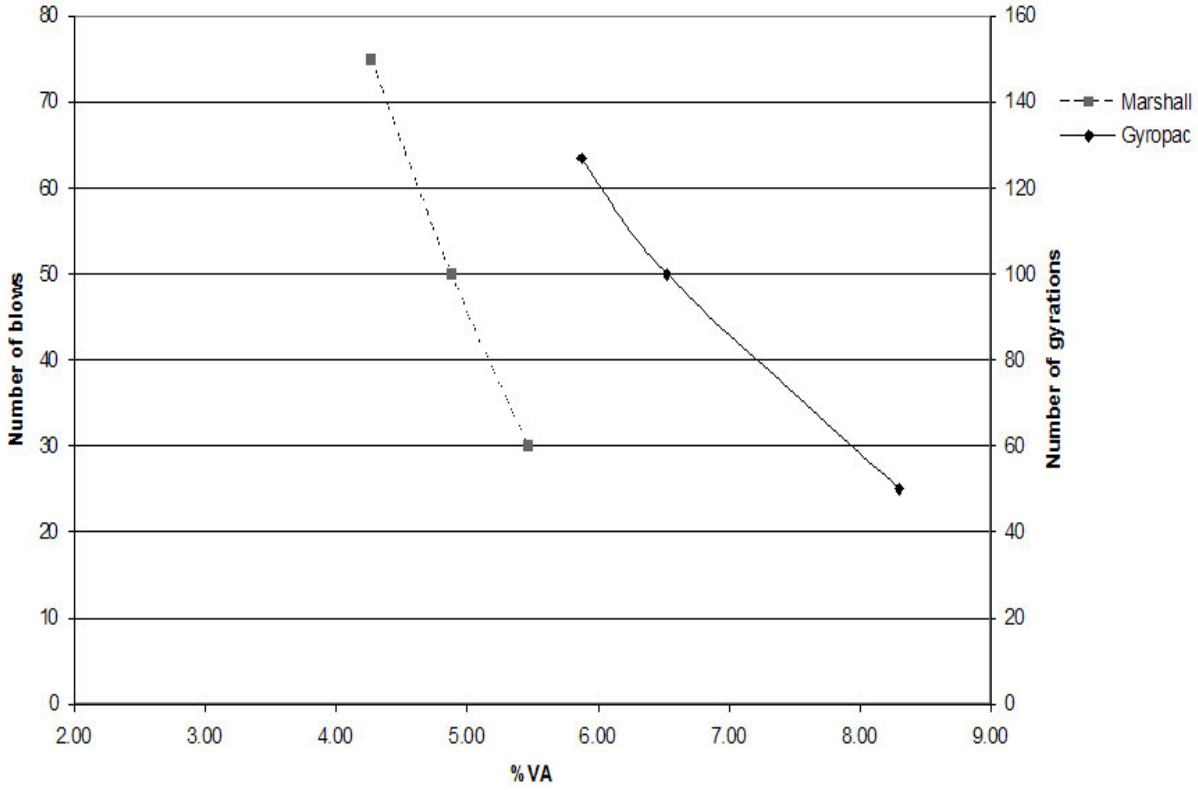

Figure A2.2 Compaction curve as plotted from Table A1.3 and Table A1.4 for Gyropac compacted specimens

For 100mm Diameter, 70mm Thick specimens:

Table A2.5 Compaction curve values for AC10 aggregate gradation Gyropac compacted samples

No. of gyrations	Replicate 1							Replicate 2												
	Weight (g)	Comp Temp (°C)	Thickness (mm)	Comp Time	A	B	C	Weight (g)	Comp Temp (°C)	Thickness (mm)	Comp Time	A	B	C	G_{mb1}	G_{mb2}	$G_{mb(avg)}$	G_{mm}	%VA	Adj %VA
50	1278.2	143	74	27-Jan	1279.86	1281.47	711.3	1278.2	143	73.8	27-Jan	1278.26	1280.59	705.23	2.245	2.222	2.233	2.407	7.22	4.92
100	1278.2	144	71.9	27-Jan	1275.74	1276.4	721	1278.2	144	72	28-Jan	1278.04	1278.69	722.16	2.297	2.296	2.297	2.407	4.58	2.28
120	1278.2	144	71.5	28-Jan	1276.61	1277.04	723.99	1278.1	144	71.8	28-Jan	1277.4	1277.73	724.27	2.308	2.308	2.308	2.407	4.11	1.81

Table A2.6 Compaction curve values for AC10 aggregate gradation Marshall hammer compacted samples

No. of blows	Replicate 1						Replicate 2											
	Weight (g)	Comp Temp (°C)	Comp Time	A	B	C	Weight	Comp Temp (°C)	Comp Time	A	B	C	G_{mb1}	G_{mb2}	$G_{mb(avg)}$	G_{mm}	%VA	Adj %VA
50	1278	145	14-Feb	1274.75	1275.47	709.7	1278	145	15-Feb	1274.28	1274.97	711.25	2.253	2.260	2.257	2.407	6.24	4.24
75	1278	145	14-Feb	1275.95	1276.41	724.04	1278	144	20-Feb	1274.01	1274.56	722	2.310	2.306	2.308	2.407	4.12	2.12
100	1278	45	15-Feb	1276.85	1277.03	731.34	1278.1	144	18-Feb	1275.87	1275.99	732.73	2.340	2.349	2.344	2.407	2.61	0.61

Table A2.7 Compaction curve values for AC14 aggregate gradation Gyropac compacted samples

No. of gyrations	Replicate 1							Replicate 2												
	Weight (g)	Comp Temp (°C)	Thickness (mm)	Comp Time	A	B	C	Weight (g)	Comp Temp (°C)	Thickness (mm)	Comp Time	A	B	C	G_{mb1}	G_{mb2}	$G_{mb(avg)}$	G_{mm}	%VA	Adj %VA
50	1302	142	74	26-Jan	1301.94	1304.3	735.36	1300.3	142	73.8	26-Jan	1300.6	1303.56	738.56	2.288	2.302	2.295	2.469	7.04	5.54
100	1300.2	142	72.9	26-Jan	1300.7	1303	744.97	1300.1	145	72.9	26-Jan	1300.1	1301.29	744.92	2.331	2.337	2.334	2.469	5.48	3.98
120	1300.3	144	71.7	26-Jan	1299.55	1300.15	747.37	1300.2	145	71.9	26-Jan	1298.92	1299.65	744.87	2.351	2.341	2.346	2.469	4.98	3.48

Table A2.8 Compaction curve values for AC14 aggregate gradation Marshall hammer compacted samples

No. of blows	Replicate 1						Replicate 2											
	Weight (g)	Comp Temp (°C)	Comp Time	A	B	C	Weight	Comp Temp (°C)	Comp Time	A	B	C	G_{mb1}	G_{mb2}	$G_{mb(avg)}$	G_{mm}	%VA	Adj %VA
50	1300.1	144	3-Feb	1297.21	1299.18	732.4	1300.1	145	3-Feb	3-Feb	1296.38	1298.54	733.75	2.289	2.295	2.292	2.469	7.17
75	1300	144	4-Feb	1298.02	1300.39	744.79	1300	145	4-Feb	4-Feb	1297.8	1298.86	743.4	2.336	2.336	2.336	2.469	5.37
100	1300	145	4-Feb	1297.3	1298.12	748.87	1300.1	145	4-Feb	4-Feb	1296.33	1297.82	749.3	2.362	2.363	2.363	2.469	4.31

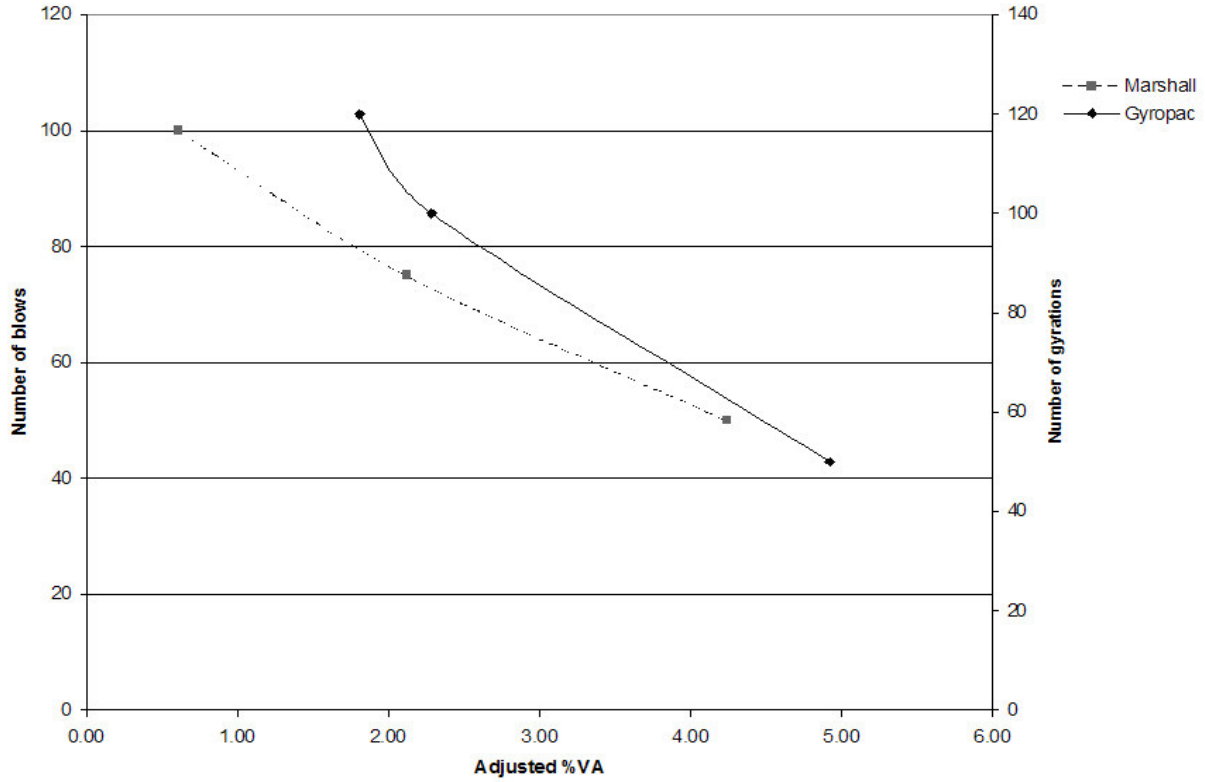

Figure A2.3 Compaction curve as plotted from Table A1.5 and Table A1.6 for Gyropac compacted specimens

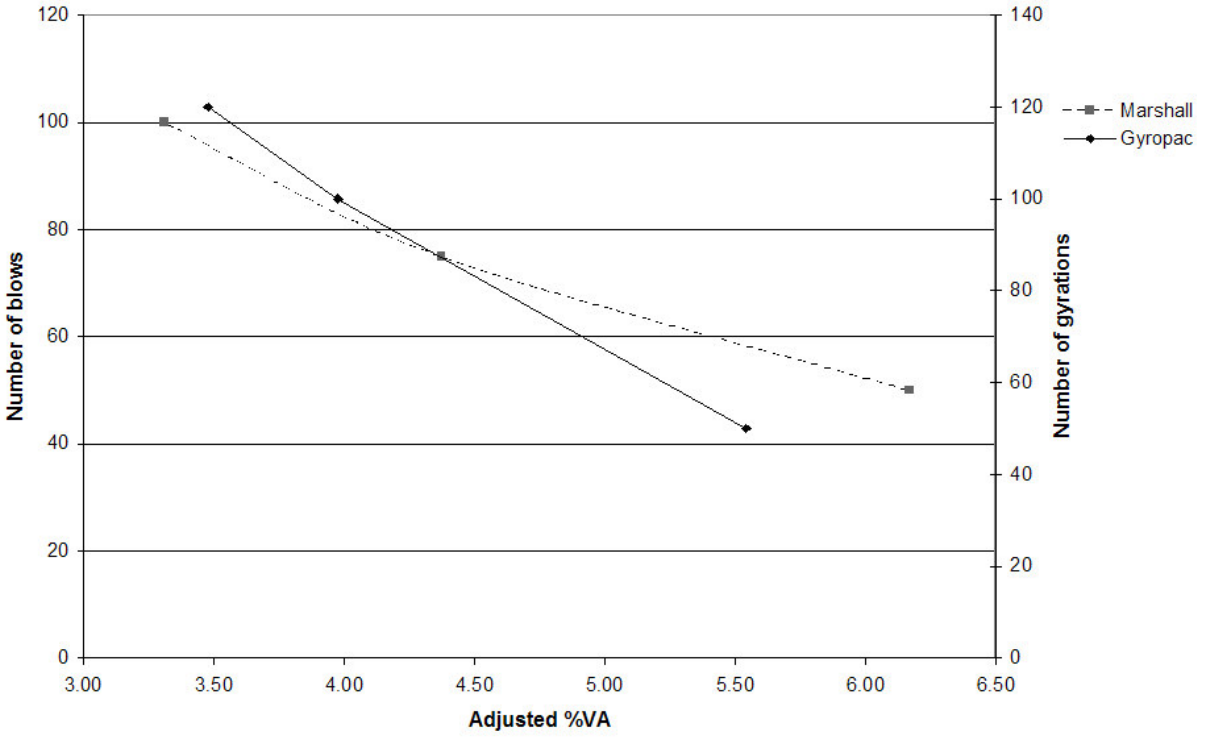

Figure A2.4 Compaction curve as plotted from Table A1.7and Table A1.8 for Gyropac compacted specimens

For 150mm Diameter, 40mm Thick specimens:

Table A2.9 Compaction curve values for AC10 aggregate gradation Gyropac compacted samples

No. of gyrations	Replicate 1							Replicate 2											
	Weight (g)	Comp Temp (°C)	Thickness (mm)	Comp Time	A	B	C	Weight (g)	Comp Temp (°C)	Thickness (mm)	Comp Time	A	B	C	G_{mb1}	G_{mb2}	$G_{mb(avg)}$	G_{mm}	%VA
50	1642.6	145	91.7	11-Feb	1642.23	1646.55	889.05	1642.7	145	91.4	14-Feb	1639.57	1643.55	890.84	2.168	2.178	2.173	2.407	9.72
100	1643	144	88.3	14-Feb	1639.01	1641.38	901.72	1642.1	144	87.9	15-Feb	1639.57	1641.63	902.89	2.216	2.219	2.218	2.407	7.87
120		145		15-Feb	1638.57	1640.81	902.3	1643.1	145	90.4	18-Feb	1639.3	1640.87	908	2.219	2.237	2.228	2.407	7.45
150		144		4-Mar	1639.47	1640.99	910.87								2.245		2.245	2.407	6.71
200		145		7-Mar	1639.41	1640.52	918.68								2.271		2.271	2.407	5.64

Table A2.10 Compaction curve values for AC14 aggregate gradation Gyropac compacted samples

No. of gyrations	Replicate 1							Replicate 2											
	Weight (g)	Comp Temp (°C)	Thickness (mm)	Comp Time	A	B	C	Weight (g)	Comp Temp (°C)	Thickness (mm)	Comp Time	A	B	C	G_{mb1}	G_{mb2}	$G_{mb(avg)}$	G_{mm}	%VA
50	1670	144	91.4	17-Feb	1669.33	1686.58	937.46	1670.2	145	91	17-Feb	1667.44	1680.2	935.3	2.228	2.238	2.233	2.469	9.75
100	1670	145	91.2	17-Feb	1668.61	1677.14	932.53	1670	144	88.6	21-Feb	1666.06	1670.63	933	2.241	2.259	2.250	2.469	8.88
120	1670.3	144	88.6	21-Feb	1665.54	1672.87	928.89	1670.1	145	89.3	23-Feb	1666.67	1673.03	925.9	2.239	2.231	2.235	2.469	9.49
150		145	88.4	6-Mar	1665.14	1668.61	934.89								2.269		2.269	2.469	8.08
210		145	88.1	8-Mar	1668.19	1671.2	938.75								2.278		2.278	2.469	7.75

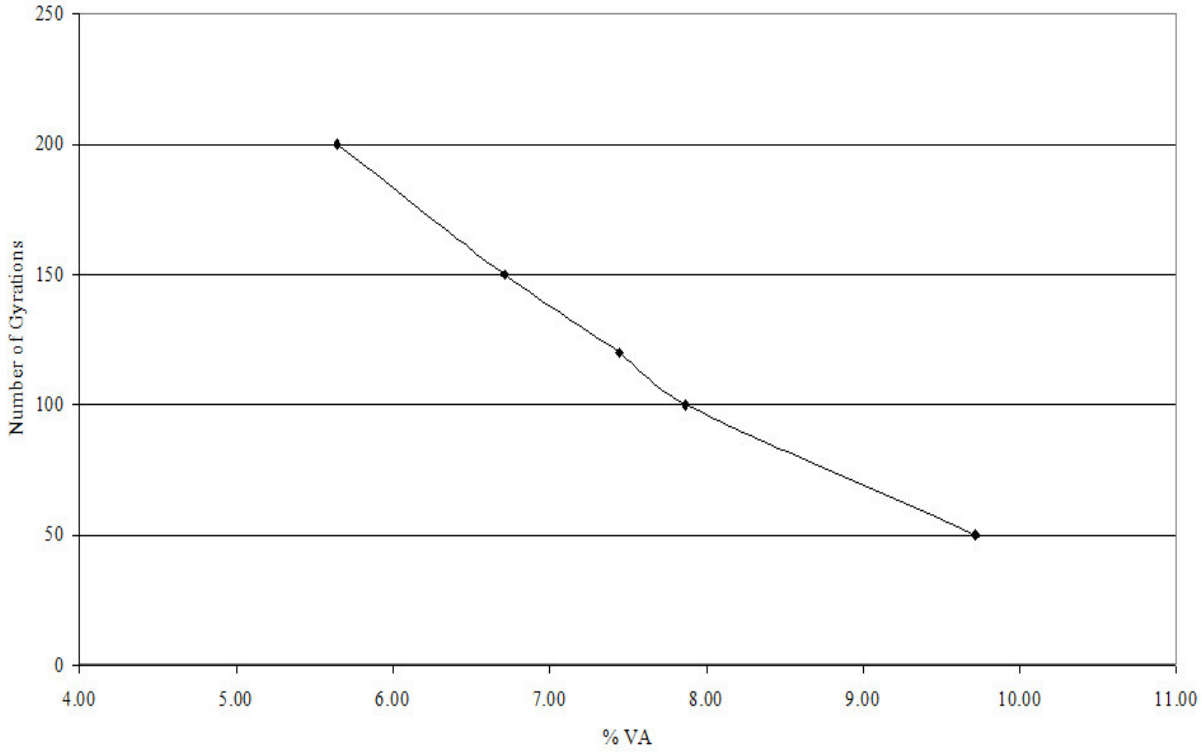

Figure A2.5 Compaction curve as plotted from Table A1.7 for Gyropac compacted specimens

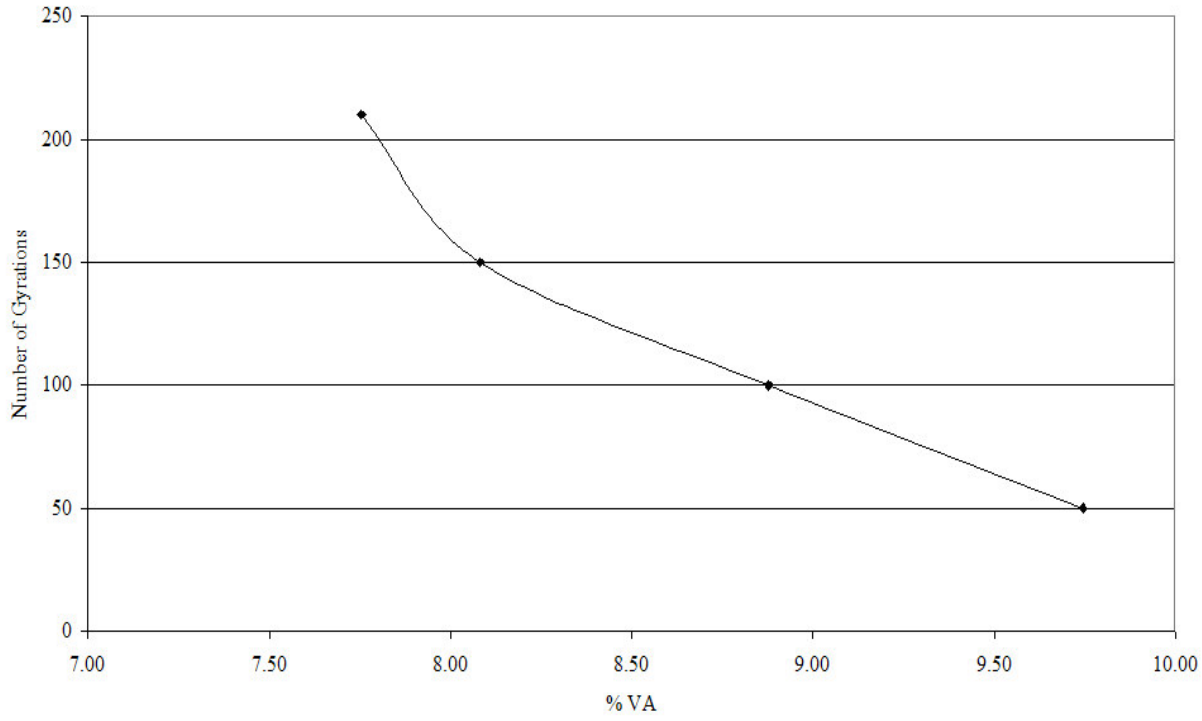

Figure A2.6 Compaction curve as plotted from Table A1.8 for Gyropac compacted specimens

For 150mm Diameter, 70mm Thick specimens:

Table A2.11 Compaction curve values for AC10 aggregate gradation Gyropac compacted samples

No. of gyrations	Replicate 1							Replicate 2											
	Weight (g)	Comp Temp (°C)	Thickness (mm)	Comp Time	A	B	C	Weight (g)	Comp Temp (°C)	Thickness (mm)	Comp Time	A	B	C	G_{mb1}	G_{mb2}	$G_{mb(avg)}$	G_{mm}	%VA
50	2875	144	94.8	10-Feb	2878.54	2883.2	1585.97	2875.2	145	95	10-Feb	2868.97	2873.99	1586.29	2.219	2.228	2.223	2.407	7.62
100	2875	145	93.7	10-Feb	2870.32	2873.9	1603.14	2875.3	144	93.4	10-Feb	2869.73	2872.9	1599.35	2.259	2.253	2.256	2.407	6.27
120	2874.5	142	93	15-Feb	2870.56	2873.08	1608.03	2875	144	94.5	18-Feb	2869.56	2871.6	1610.75	2.269	2.276	2.273	2.407	5.59
140	2875	145	94.6	4-Mar	2870.3	2871.96	1612.94								2.280		2.280	2.407	5.29

Table A2.12 Compaction curve values for AC14 aggregate gradation Gyropac compacted samples

No. of gyrations	Replicate 1							Replicate 2											
	Weight (g)	Comp Temp (°C)	Thickness (mm)	Comp Time	A	B	C	Weight (g)	Comp Temp (°C)	Thickness (mm)	Comp Time	A	B	C	G_{mb1}	G_{mb2}	$G_{mb(avg)}$	G_{mm}	%VA
50	2925	145	97.7	17-Feb	2921.3	2933.06	1637.4	2924.7	144	95.4	22-Feb	2919.67	2929.1	1629.45	2.255	2.247	2.251	2.469	8.85
100	2925.1	145	94.2	22-Feb	2919.35	2928.11	1649.35	2925.2	144	96.4	22-Feb	2922.31	2929.58	1645.5	2.283	2.276	2.279	2.469	7.68
150	2925	145	93.6	6-Mar	2921.24	2926.57	1658.99								2.305		2.305	2.469	6.66
200	2925	145	92.6	7-Mar	2918.09	2921.15	1673.75								2.339		2.339	2.469	5.25

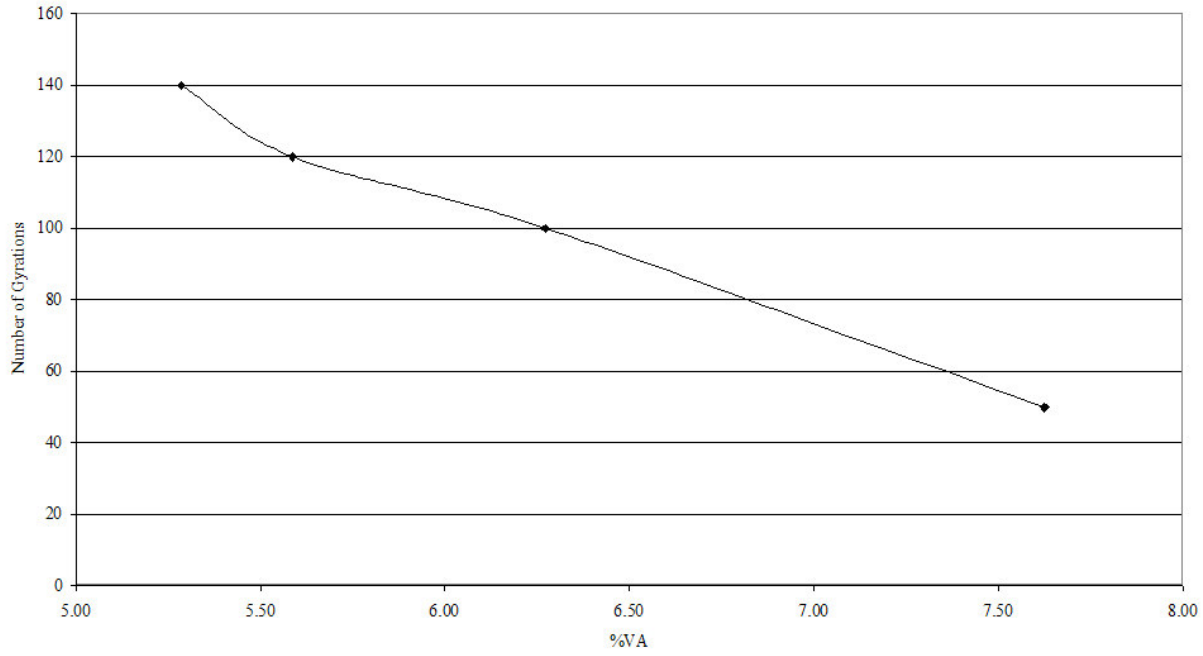

Figure A2.7 Compaction curve as plotted from Table A1.9 for Gyropac compacted specimens

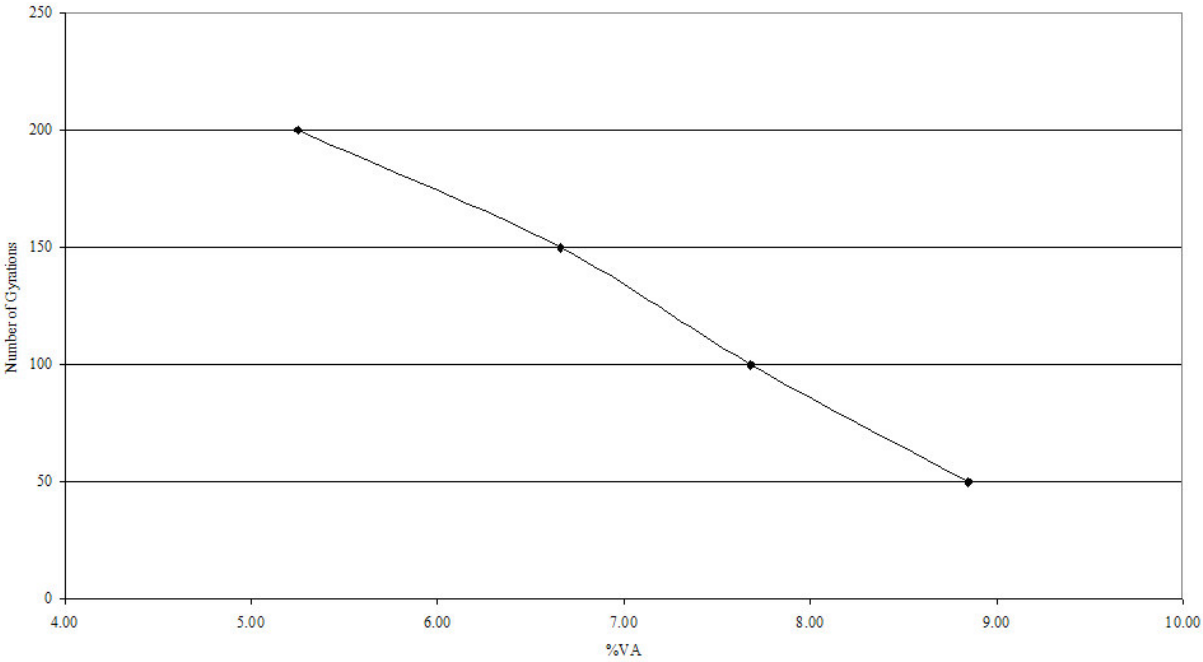

Figure A2.8 Compaction curve as plotted from Table A1.10 for Gyropac compacted specimens

Specimen properties for Factorial Experimental Design

Table A2.13 Specimen properties for factorial experimental design

Diameter (mm)	Height (mm)	Specimen weight (g)	Aggr. Size	Compaction	Gyrations /Blows	Specimen #	Actual Height (mm)	Compaction Temp	Date of preparation
100	40	730.11	AC-10	Gyropac	70G	1b	66.8	145	31-Mar
100	40	730.11	AC-10	Gyropac	60G	1a	66.9	145	7-Apr
100	40	730.11	AC-10	Gyropac	70G	1c	66.7	145	31-Mar
100	70	1277.69	AC-10	Gyropac	50G	5b	72.1	145	31-Mar
100	70	1277.69	AC-10	Gyropac	40G	5a	72.2	145	7-Apr
100	70	1277.69	AC-10	Gyropac	55G	5c	72.3	145	8-Apr
100	40	742.99	AC-14	Gyropac	150G	3b	66	145	31-Mar
100	40	742.99	AC-14	Gyropac	150G	3a	86.7	145	30-Mar
100	70	1300.23	AC-14	Gyropac	60G	7b	72.1	145	5-Apr
100	70	1300.23	AC-14	Gyropac	60G	7a	72.2	144	5-Apr
100	40	742.99	AC-14	Gyropac	110G	3c	66.7	144	30-Mar
100	70	1300.23	AC-14	Gyropac	80G	7c	72.2	145	8-Apr
100	40	730.11	AC-10	Hammer	30B	2a		145	16-Mar
100	70	1277.69	AC-10	Hammer	45B	6a		145	21-Mar
100	70	1300.23	AC-14	Hammer	70B	8a		145	16-Mar
100	40	742.99	AC-14	Hammer	45B	4a		145	17-Mar
100	40	742.99	AC-14	Hammer	48B	4c		145	21-Mar
100	40	730.11	AC-10	Hammer	30B	2c		145	6-Mar
100	70	1300.23	AC-14	Hammer	78B	8c		145	8-Mar
100	70	1277.69	AC-10	Hammer	42B	6c		145	23-Mar
100	40	730.11	AC-10	Hammer	30B	2b		145	21-Mar
100	70	1277.69	AC-10	Hammer	42B	6b		145	23-Mar
100	40	742.99	AC-14	Hammer	48B	4b		145	21-Mar
100	70	1300.23	AC-14	Hammer	70B	8b		145	17-Mar

Specimen #	A	B	C	Gmb	Gmm	VA%
1b	729.49	729.68	411.35	2.29	2.41	4.79
1a	728.16	728.68	408.55	2.27	2.41	5.50
1c	729.70	730.03	412.44	2.30	2.41	4.54
5b	1277.11	1277.95	716.48	2.27	2.41	5.50
5a	1274.96	1275.61	720.35	2.30	2.41	4.61
5c	1276.28	1277.28	720.80	2.29	2.41	4.72
3b	740.80	741.29	425.60	2.35	2.47	4.96
3a	742.87	743.35	427.13	2.35	2.47	4.85
7b	1297.51	1298.74	745.40	2.34	2.47	5.03
7a	1299.21	1299.67	743.30	2.34	2.47	5.42
3c	743.38	743.99	425.35	2.33	2.47	5.51
7c	1299.15	1300.64	743.88	2.33	2.47	5.49
2a	725.86	726.35	408.88	2.29	2.41	5.01
6a	1276.03	1276.43	721.22	2.30	2.41	4.52
8a	1299.45	1300.99	746.74	2.34	2.47	5.04
4a	742.54	743.00	424.80	2.33	2.47	5.49
4c	741.22	741.66	425.50	2.34	2.47	5.04
2c	727.31	727.65	409.66	2.29	2.41	4.98
8c	1297.88	1298.40	747.65	2.36	2.47	4.55
6c	1274.23	1274.76	715.70	2.28	2.41	5.31
2b	728.69	729.14	409.34	2.28	2.41	5.34
6b	1273.87	1274.43	715.25	2.28	2.41	5.36
4b	741.05	741.58	425.02	2.34	2.47	5.19
8b	1300.28	1301.00	744.33	2.34	2.47	5.39

150	40	1642.74	AC-10	Gyropac	230G	9a	86.7	143	16-Mar
150	40	1642.74	AC-10	Gyropac	320G	9b	86.7	145	23-Mar
150	40	1642.74	AC-10	Gyropac	250G	9c	86.7	145	23-Mar
150	40	1671.72	AC-14	Gyropac	600G@160°C	11a	86.6	160	23-Mar
150	40	1671.72	AC-14	Gyropac	400G@160°C	11b	87	160	14-Mar
150	40	1671.72	AC-14	Gyropac	600G@160°C	11c	86.5	160	23-Mar
150	70	2874.79	AC-10	Gyropac	145G	13a	92.3	145	21-Mar
150	70	2874.79	AC-10	Gyropac	140G	13b	94.6	145	4-Mar
150	70	2874.79	AC-10	Gyropac	150G	13c	92.2	145	21-Mar
150	70	2925.51	AC-14	Gyropac	210G	15a	92.2	144	16-Mar
150	70	2925.51	AC-14	Gyropac	220G	15b	92.7	145	21-Mar
150	70	2925.51	AC-14	Gyropac	200G	15c	92.6	145	7-Mar
150	40	1642.74	AC-10	Hammer	37B	10a		145	21-May
150	40	1642.74	AC-10	Hammer	37B	10b		145	26-May
150	40	1642.74	AC-10	Hammer	35b	10c		145	2-Jun
150	40	1671.72	AC-14	Hammer	80B	12a		145	22-May
150	40	1671.72	AC-14	Hammer	77B	12b		145	2-Jun
150	40	1671.72	AC-14	Hammer	68B	12c		145	8-Jun
150	70	2874.79	AC-10	Hammer	45B	14a		145	20-May
150	70	2874.79	AC-10	Hammer	45B	14b		145	22-May
150	70	2874.79	AC-10	Hammer	48B	14c		145	29-May
150	70	2925.51	AC-14	Hammer	73B	16a		145	30-May
150	70	2925.51	AC-14	Hammer	73B	16b		145	3-Jun
150	70	2925.51	AC-14	Hammer	73B	16c		145	7-Jun

9a	1639.28	1640.44	924.10	2.29	2.41	4.93
9b	1640.11	1641.11	920.24	2.28	2.41	5.48
9c	1638.69	1639.70	920.75	2.28	2.41	5.31
11a	1673.35	1674.00	956.62	2.33	2.47	5.53
11b	1666.53	1668.06	955.76	2.34	2.47	5.24
11c	1669.52	1671.44	955.85	2.33	2.47	5.51
13a	2868.88	2870.25	1615.02	2.29	2.41	5.05
13b	2870.30	2871.96	1612.94	2.28	2.41	5.29
13c	2867.62	2869.07	1620.38	2.30	2.41	4.59
15a	2919.19	2922.50	1681.41	2.35	2.47	4.73
15b	2916.06	2919.66	1670.00	2.33	2.47	5.49
15c	2918.09	2921.15	1673.75	2.34	2.47	5.25
10a	1639.50	1640.26	925.10	2.29	2.41	4.76
10b	1639.00	1639.84	925.00	2.29	2.41	4.74
10c	1639.21	1640.69	920.84	2.28	2.41	5.39
12a	1670.10	1670.90	961.56	2.35	2.47	4.64
12b	1669.50	1670.95	962.90	2.36	2.47	4.50
12c	1670.07	1671.41	959.07	2.34	2.47	5.04
14a	2867.86	2869.45	1613.08	2.28	2.41	5.17
14b	2868.86	2870.49	1609.32	2.27	2.41	5.49
14c	2869.54	2871.27	1613.15	2.28	2.41	5.24
16a	2923.43	2925.33	1679.05	2.35	2.47	4.99
16b	2923.39	2925.73	1678.48	2.34	2.47	5.07
16c	2922.50	2924.96	1678.00	2.34	2.47	5.07

Specimen properties for the Strain Comparison investigation

Table A2.14 Specimen properties for strain comparison samples prepared in laboratory

					Max Stress (kPa)		Stiffness Modulus (MPa)				Strain gauge (microstrain)	
	Pulse	Peak Load (kN)	Diameter (m)	Thickness (m)	Readings	Average	Readings	Average	Density	Closed form (microstrain)	Readings	Average
1B	1	0.7502	0.1	0.0419	113.98	114.2	1545	1180.2	2.292	212.80	145.97	143.40
	2	0.7531	0.1	0.0419	114.42		1276				142.30	
	3	0.7531	0.1	0.0419	114.42		1132				144.14	
	4	0.7502	0.1	0.0419	113.98		1013				143.22	
	5	0.7502	0.1	0.0419	113.98		935				141.38	
1C	1	0.7502	0.1	0.0419	113.98	113.7	1764	1383.8	2.298	180.78	138.53	137.81
	2	0.7443	0.1	0.0419	113.09		1488				137.62	
	3	0.7560	0.1	0.0419	114.87		1357				137.62	
	4	0.7443	0.1	0.0419	113.09		1184				136.71	
	5	0.7473	0.1	0.0419	113.54		1126				138.54	
2A	1	0.7473	0.1	0.0518	91.84	91.2	1991	1601.4	2.298	125.28	75.35	74.50
	2	0.7414	0.1	0.0518	91.12		1700				74.64	
	3	0.7414	0.1	0.0518	91.12		1514				73.94	
	4	0.7414	0.1	0.0518	91.12		1442				73.94	
	5	0.7385	0.1	0.0518	90.76		1360				74.64	
2B	1	0.7443	0.1	0.0518	91.47	91.0	2314	1891.4	2.298	105.90	73.32	71.55
	2	0.7414	0.1	0.0518	91.12		2036				71.91	
	3	0.7385	0.1	0.0518	90.76		1825				71.91	
	4	0.7385	0.1	0.0518	90.76		1683				69.09	
	5	0.7414	0.1	0.0518	91.12		1599				-	

3A	1	0.759	0.1	0.0615	78.57	78.0	2275	1879	2.296	91.28	64.20	63.78
	2	0.7531	0.1	0.0615	77.96		1972				64.20	
	3	0.7531	0.1	0.0615	77.96		1800				63.50	
	4	0.7502	0.1	0.0615	77.66		1722				64.20	
	5	0.7502	0.1	0.0615	77.66		1626				62.79	
3B	1	0.7473	0.1	0.0615	77.36	76.9	2253	1875	2.296	90.27	59.89	60.87
	2	0.7443	0.1	0.0615	77.05		2009				61.30	
	3	0.7385	0.1	0.0615	76.45		1800				62.00	
	4	0.7473	0.1	0.0615	77.36		1696				60.59	
	5	0.7385	0.1	0.0615	76.45		1617				60.59	
5A	1	0.7473	0.1	0.0716	66.44	66.3	2022	1638.4	2.296	89.07	77.11	77.11
	2	0.7443	0.1	0.0716	66.18		1774				78.03	
	3	0.7502	0.1	0.0716	66.70		1597				76.19	
	4	0.7443	0.1	0.0716	66.18		1449				77.11	
	5	0.7443	0.1	0.0716	66.18		1350				77.11	
5C	1	0.7531	0.1	0.0719	66.68	66.6	1996	1613	2.293	90.88	66.99	65.89
	2	0.7502	0.1	0.0719	66.42		1741				65.16	
	3	0.7531	0.1	0.0719	66.68		1555				66.08	
	4	0.7560	0.1	0.0719	66.94		1440				65.16	
	5	0.7502	0.1	0.0719	66.42		1333				66.08	

Table A2.15 Strain results using FEM

Thickness	Load (kN)	Elastic Modulus (MPa)	Pressure (KPa)	FEM microstrain
0.042	0.749	1500	1.3558	176.909
0.050	0.749	1500	1.1361	150.721
0.055	0.749	1500	1.0328	136.458
0.060	0.749	1500	0.9468	125.144
0.065	0.749	1500	0.8739	114.995
0.072	0.749	1500	0.7934	104.429

Specimen properties for the Modulus Comparison investigation

Table A2.16 Properties for specimens used in Modulus comparison

	Diameter (mm)	Height (mm)	Specimen weight (g)	Aggr. Size	Compaction	Gyrations	Specimen #	Actual Height (mm)	Compaction Temp	Date of preparation
Mr test	100	65	1186.42	AC-10	Gyropac	45G	1A-R1	67.3	145	10-May
	100	65	1186.42	AC-10	Gyropac	50G	1A-R2	67.3	145	10-May
	100	65	1207.35	AC-14	Gyropac	75G	1B-R1	67.3	145	10-May
	100	65	1207.35	AC-14	Gyropac	75G	1B-R2	67.3	145	12-May
Complex	100	100	1825.27	AC-10	Gyropac	65G	2A-R1	103	145	13-May
	100	100	1825.27	AC-10	Gyropac	60G	2A-R2	103	144	16-May
	100	100	1857.47	AC-14	Gyropac	100G	2B-R1	102.9	145	12-May
	100	100	1857.47	AC-14	Gyropac	70G	2B-R2	103.1	145	13-May

Table A2.17 Percentage air voids determination for specimens used in Modulus comparison

Specimen #	A	B	C	Gmb	Gmm	VA%
1A-R1	1182.86	1183.43	666.41	2.288	2.407	4.95
1A-R2	1184.69	1186.61	671.2	2.299	2.407	4.51
1B-R1	1205.29	1206.33	692.18	2.344	2.469	5.05
1B-R2	1205.51	1206.69	690.18	2.334	2.469	5.47
2A-R1	1822.68	1824.14	1029.2	2.293	2.407	4.74
2A-R2	1822.57	1823.43	1029.25	2.295	2.407	4.66
2B-R1	1851.8	1852.94	1064.68	2.349	2.469	4.85
2B-R2	1852.26	1853.97	1063.94	2.345	2.469	5.04